D I S S E R T A T I O N

Exploring the molecular basis of the gating machinery of TRPC3 ion channel complex

submitted by

BSc MSc

Barbora SVOBODOVA

for the Academic Degree of

Doctor of Philosophy

(PhD)

at the

Medical University of Graz

Gottfried Schatz Research Center for Cell Signaling, Metabolism and Aging

Biophysics

under the Supervision of

Univ.-Prof. Mag. pharm. Dr. rer. nat. Klaus GROSCHNER

2019

Statutory declaration

I hereby declare that this thesis is my own original work and that I have fully acknowledged by name all of those individuals and organisations that have contributed to the research for this thesis. Due acknowledgement has been made in the text to all other material used. Throughout this thesis and in all related publications I followed the “Standards of Good Scientific Practice and Ombuds Committee at the Medical University of Graz”.

In Graz, 31. 07. 2019
Barbora Svobodova

Disclosure

The content of this thesis has been published in a peer-reviewed journals. For reused figures the permission of re-print has been given with the Open-Access-Publication agreements of the publishing group as specified below.

The thesis is based on the following publications:

A. Svobodova B, Lichtenegger M, Platzer D, Di Giuro CML, de la Cruz GG, Glasnov T, Schreibmayer W, Groschner K. A single point mutation in the TRPC3 lipid-recognition window generates supersensitivity to benzimidazole channel activators, Cell Calcium 2019; 79:27-34
B. de La Cruz GG, Svobodova B, Lichtenegger M, Tiapko O, Groschner K, Glasnov T. Intensified Microwave-Assisted N-Acylation Procedure - Synthesis and Activity Evaluation of TRPC3 Channel Agonists with a 1,3-Dihydro-2H-benzo[d]imidazol-2-one Core. Synlett. 2017; 28 (6)
C. Lichtenegger M, Tiapko O, Svobodova B, Stockner T, Glasnov TN, Schreibmayer W, Platzer D, de la Cruz GG, Krenn S, Schober R, Shrestha N, Schindl R, Romanin C, Groschner K. An optically controlled probe identifies lipid-gating fenestrations within the TRPC3 channel. Nat Chem Biol. 2018; 14(4):396–404

All co-authors gave their consent to re-use the data communicated within the publications. Lichtenegger M performed single channel (SI) electrophysiology experiments shown in Figures 11-16. The load of whole cell patch clamp recordings displayed in Figures 8B and 10 was equally shared with Lichtenegger M. Platzer D generated the Mathlab routine for SI data analysis. Schreibmayer W rationalized for SI analysis and troubleshooting. De la Cruz GG synthetized the benzimidazole compounds. Di Giuro CML helped to analyse calcium imaging data shown in Figure 20.

Journal of Cell Calcium is part of Elsevier publishing which allows the authors to reuse published data for the purpose of dissertation any time after publication (for more information visit the journal's website for rights and permission statements https://www.elsevier.com/about/our-business/policies/copyright#Author-rights).

Acknowledgements

The scientific work of the PhD fellow, Barbora Svobodova, was funded from the Austrian Science Fund FWF (W1226-B18) at the Medical University of Graz through the PhD Program “Doctoral College Metabolic and Cardiovascular Disease (DK-MCD)”.

This creation if is a result of more than a 4-year struggle and is definitely not a solo piece! Therefore, I would like to thank all the people who helped me one way or another on my doctoral journey. Spatial limitation will not allow me to list the precise contribution of all the following people so with my deepest gratitude for their assistance I will only list their names. As the following thanks are dedicated to them particularly I am convinced each and every one of them knows why.

My thanks belong to Niroj Shrestha, Thomas Stockner, Gebhard Schratter, Patrick Wiedner, Bernadett Bacsa, Wolfgang Schreibmayer, Mike Poteser, Markéta Bebarová, Chintan Koyani, Lisha Joshi, Toma Glasnov, Elli and the Hills, Gerhard Prossliner, Brigitte Pelzmann, Karin Osibow, Michaela Lichtenegger and my dearest family and friends at home for keeping their sanity at times I lost mine;-).

I would like to express very special thanks to Cristiana M. L. Di Giuro, who went above and beyond to support me, keep me on track and make me finish the doctoral degree. I will always appreciate her for her high scientific standards and admire her for the person of the purest heart she is!

Table of Contents

List of Abbreviations

AD	Alzheimer's disease
AR	ankyrin repeats
ATP	adenosine trisphosphate
BC	bundle-crossing gate
BDNF	brain-derived neurotrophic factor
BI-2	GSK analogue, TRPC3 channel agonist
BTDM	2-(benzo [d][1,3] dioxol-5-ylamino) thiazol- 4-yl)((3 S,5 R)-3,5-dimethylpiperidin-1-yl) methanone, TRPC6 channel blocker
CaM	calmodulin
CCh	carbachol, muscarinic receptor agonist
CD	cytosolic domain
CIRB	calmodulin/inositol trisphosphate receptor binding domain
CRAC	Ca^{2+}-release activated Ca^{2+} channel/current
DAG	diacylglycerol
EC_{50}	half maximal effective concentration
ECD	extracellular domain
EM	electron microscopy
ER/SR	endoplasmic/sarcoplasmic reticulum
FSGS	familial focal segmental glomerulosclerosis
GPCR	G-protein coupled receptor
GSK	GSK1702934A, TRPC3/6 channels agonist
HEK293	human embryonic kidney cells
HH	horizontal helix in the C-terminus of TRPC3
IP_3	inositol-1,4,5-trisphosphate
IP_3R	inositol trisphosphate receptor
LD	linker domain, part of cytosolic N-terminus of TRPC3
LFW	LFW motif, amino acid sequence in the P-loop of TRP channels vital for their function
N	number of activated channels in the membrane patch of single channel recordings
OAG	1-oleoyl-2-acetyl-sn-glycerol, DAG analogue

p.d.f.	probability density function
PDB	Protein Data Bank
PIP_2	phosphatidylinositol-4,5-bisphosphate
PKD2	TRPP-like protein constituting an ion channel
PLC	phospholipase C
P-loop	pore-loop, forming the SF of TRP channels
PM	plasma membrane
ROC	receptor-operated current
RR	ruthenium red, TRPC channel inward current blocker
RTK	receptor tyrosine kinase
S1-6	transmembrane helices 1-6
SAG	1-stearoyl-2-arachidonoyl glycerol, DAG analogue
SEM	standard error of the mean
SF	selectivity filter
SOCE	store-operated Ca^{2+} entry
STIM1	stromal interaction molecule 1
TIRF	total internal reflection fluorescent microscopy
TMD	transmembrane domain
TRAAK	two pore domain potassium channel
TRP	transient receptor potential
TRPA	ankyrin subfamily of transient receptor potential channels
TRPC	canonical subfamily of transient receptor potential channels
TRPM	melastatin subfamily of transient receptor potential channels
TRPML	mucolipin subfamily of transient receptor potential channels
TRPN	NompC-like subfamily of transient receptor potential channels
TRPP	polycystin subfamily of transient receptor potential channels
TRPV	vanilloid subfamily of transient receptor potential channels
UTP	uridin-5'-trisphosphate
VH	vertical helix in the C-terminus of TRPC3
WT	wild type
YFP	yellow fluorescent protein

List of Figures

1. Abstract

TRPC proteins form unique class of cationic channels able to sense, integrate and relay multiple cellular signals. Despite constituting predominantly non-selective channels, their physiological relevance has been clearly linked with cellular Ca^{2+}-dependent processes and their impact on membrane potentials in excitable cells. Recognition of their involvement in an increasing number of pathological states and diseases such as cardiac hypertrophy, arrhythmias, epilepsy, cerebellar ataxia, Huntington's and Alzheimer's disease, etc. calls for means of therapeutic intervention. Effective pharmacological control however requires detailed molecular information on the channel's gating mechanism.

The present study aims to identify and further describe the molecular elements of TRPC3 channel gating by physiological lipid stimuli and a recently discovered synthetic direct TRPC3/6 channel agonist, GSK1702934A (abb. GSK). Using site directed mutagenesis we identified a conserved glycine at position 652 in the S6 of TRPC3 that dramatically influences both activation modes of the channel. Our electrophysiological analysis showed strong reduction in response in $TRPC3_{G652A}$ channels to physiological stimulation via PLC pathway. $TRPC3_{G652A}$ also exhibited altered potency profile of exogenously administered lipids and various GSK structural analogues (benzimidazoles) in comparison to WT TRPC3 channels. Interestingly, the stimulation with benzimidazole compounds resulted in enhanced currents via $TRPC3_{G652A}$ channels. We proved that neither increased potency of benzimidazoles to $TRPC3_{G652A}$ channels or a modified pore architecture are responsible for that observation. Inspection of the gating properties at the single channel level further revealed a unique, long-lived open state in benzimidazole stimulated $TRPC3_{G652A}$ channels. Moreover, $TRPC3_{G652A}$ channels lacked PLC/diacylglycerol mediated cross-desensitization to GSK activation as usually observed for WT TRPC3 channels. Lack of desensitization in $TRPC3_{G652A}$ channels allowed for large benzimidazole-induced Ca^{2+} signals in conditions that fully desensitized WT TRPC3 channels.

Collectively our data suggest, supported by the recent high-resolution cryo-EM based TRPC3 structure, that lipid and possibly also benzimidazole agonists share the recognition site localized to a lateral window between 2 adjacent TRPC3 subunits as well as certain common features of the TRPC3 gating machinery.

2. Zusammenfassung

TRPC-Proteine bilden eine Gruppe von Kationen-leitenden Ionenkanälen, die eine Vielzahl zellulärer Signale erfassen, integrieren und weiterleiten können. Obwohl sie überwiegend eine geringe Selektivität aufweisen, spielen sie eine physiologisch relevante Rolle bei Ca^{2+}-abhängigen zellulären Prozessen und beeinflussen das Membranpotential erregbarer Zellen. Mittlerweile weiß man, dass TRPC-Ionenkanäle bei einer Reihe von pathologischen Zuständen und Krankheiten (kardiale Hypertrophie und Arrhythmien, Epilepsie, Kleinhirnataxie, Huntington- und Alzheimer-Krankheit usw.) eine wichtige Rolle spielen, was die Notwendigkeit therapeutischer Interventionen erkennen lässt. Eine wirksame pharmakologische Kontrolle erfordert jedoch detaillierte Informationen über die Funktionsweise des Kanalproteins auf molekularer Ebene.

Das Ziel dieser Studie war es, die für das Öffnen und Schließen der TRPC3-Kanäle verantwortlichen Proteinabschnitte unter Verwendung von physiologischen Lipidstimuli und eines kürzlich entdeckten synthetischen TRPC3/6-Agonisten, GSK1702934A (GSK) zu identifizieren und zu beschreiben. Mit Hilfe ortsspezifischer Mutagenese konnte ein konserviertes Glycin an Position 652 im Transmembranabschnitt S6 für ein verändertes Aktivierungsverhalten des Kanals verantwortlich gemacht werden. Im Vergleich zu WT-TRPC3-Kanälen zeigten $TRPC3_{G652A}$-Kanäle eine stark verringerte Reaktion auf die physiologische Stimulation über den PLC-Weg sowie ein verändertes Wirkprofil exogen verabreichter Lipide und verschiedener GSK-Strukturanaloga (Benzimidazole). Interessanterweise lösten Benzimidazolverbindungen größere Ionenströme über $TRPC3_{G652A}$-Kanäle aus, jedoch war weder eine erhöhte Wirksamkeit von Benzimidazolen noch eine modifizierte Porenarchitektur der $TRPC3_{G652A}$-Kanäle dafür verantwortlich. Einzelkanaluntersuchungen ergaben einen langlebigen Offen-Zustand in Benzimidazol-stimulierten $TRPC3_{G652A}$-Kanälen. Darüber hinaus fehlte den $TRPC3_{G652A}$-Kanälen eine für WT-TRPC3-Kanäle beobachtete PLC/Diacylglycerin-vermittelte Kreuzdesensibilisierung zur GSK-Aktivierung, was große Benzimidazol-induzierte Ca^{2+}-Signale zur Folge hatte.

Zusammenfassend lässt sich festhalten, dass sich Lipide und möglicherweise auch Benzimidazol-Agonisten sowohl die Erkennungsstelle am TRPC3-Kanal teilen, wie auch deren Öffnen und Schließen ähnlich beeinflussen.

3. Introduction

3.1. Transient receptor potential (TRP) ion channel family

TRP proteins represent a wide family of non-selective cation channels that are expressed in variety of eukaryotic organisms, including mammals and humans. The initial protein, giving name to the entire ion channel family and marking the starting point of TRP channel research, was discovered in late 1980's in *Drosophila melanogaster* mediating the neuro-optical light response. Thereafter, many homologs were discovered and subdivided into seven subfamilies (Figure 1) based on their amino acid sequence and topological similarities: TRPC (canonical), TRPV (vanilloid), TRPM (melastatin), TRPA (ankyrin), TRPP (polycystin), TRPML (mucolipin), and TRPN (NOMPC) (1,2).

TRP proteins are expressed in excitable and non-excitable cells of various tissue types. Although they are predominantly non-selective ion channels they have received particular attention in the scientific community due to their ability to permeate Ca^{2+} ions, representing an important second messenger. Apart from participation in Ca^{2+} signaling pathways, TRP channels are also involved in biological processes that are associated with change in membrane potential as a result of extensive transmembrane ion transport such as action potentials in neuronal and muscle cells.

Figure 1: Phylogenetic tree of TRP channels

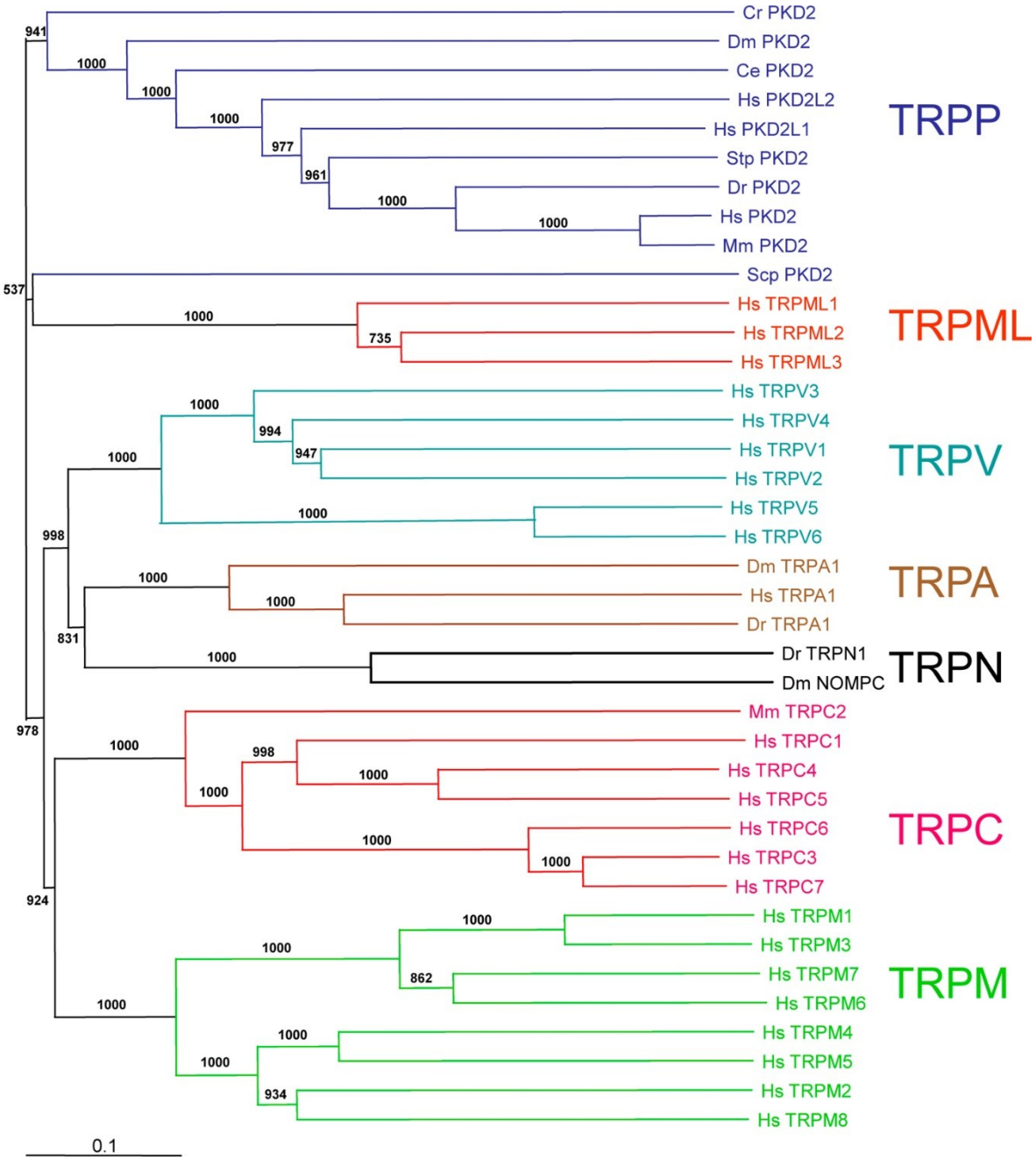

Phylogenetic tree of PKD2 from different species and other TRP channels adapted from Montell (1). The protein sequences were aligned using Clustal X (1.81). The tree was built by the neighbour-joining method in the Clustal X (1.81) package and viewed with TreeView (Page, R.D. 1996. *Comput. Appl. Biosci*. 12:357–358). The bootstrap numbers were derived from 1,000 trials. The seven subgroups of TRP channels are marked by different colors. The species abbreviations are as follows: Ce, *Caenorhabditis elegans*; Cr, *Chlamydomonas reinhardtii*; Dm, *Drosophila melanogaster*; Dr, *Danio rerio*; Hs, *Homo sapiens*; Mm, *Mus musculus*;

Scp, *Schizosaccharomyces pombe*; Stp, *Strongylocentrotus purpuratus*. The accession numbers of the proteins in the tree are as follows: Chlamydomonas_PKD2 (EF446617); Homo_PKD2 (NP_000288); Mus_PKD2(NP_032887); Caenorhabditis_PKD2 (NP_502838); Drosophila_PKD2 (NP_609561); Danio_PKD2 (NP_001002310); Homo_PKD2L1 (Q9P0L9); Homo_PKD2L2 (AAH44581.1); Strongylocentrotus_PKD2 (AAP35006.1); Schizosaccharomyces_PKD2 (CAA91950.1); Homo_TRPV1 (Q8NER1T); Homo_TRPA1 (gi56749685); Homo_TRPML1 (NP_065394.1); Homo_TRPML2 (NP_694991.2); Homo_TRPML3 (NP_060768.8); Homo_TRPM1 (NP_002411.3); Danio_TRPN1 (NP_899192.1); Homo_TRPC1 (AAI13954.1); Homo_TRPC3 (EAX05243.1); Homo_TRPC4 (CAI15560.1); Homo_TRPC5 (NP_036603.1); Homo_TRPC7 (CAD70162.1); Homo_TRPC6 (NP_004612.2); Mus_TRPC2 (NP_035774.1); Drosophila_NOMPC (AAF59842.1); Homo_TRPM4 (Q8TD43); Homo_TRPM2 (AAI12343.1); Homo_TRPM3 (CAM22745.1); Homo_TRPM7 (AAH51024.1); Homo_TRPM5 (NP_055370.1); Homo_TRPM8 (AAI26343.1); Homo_TRPM6 (Q9BX84); Homo_TRPV2 (Q9Y5S1); Homo_TRPV3 (NP_659505.1); Homo_TRPV4 (Q9HBA0); Homo_TRPV5 (NP_062815.2); Homo_TRPV6 (Q9H1D0); Drosophila_TRPA1 (NP_648263.1); Danio_TRPA1 (AAV37177.1). The figure was reused with permission from Huang et al. (3).

3.2. TRPC subfamily

The 7 members of the canonical subfamily of TRP channel (abbreviated as TRPC) are closely related to the first discovered *Drosophila* TRP. According to the similarities in mode of activation and shared sequence homology the canonical TRPC channel family was subdivided in following clusters: TRPC3/6/7; TRPC4/5 and TRPC1, standing alone for its distinctive features. *Trpc2* was not assigned to either of the clusters of TRPCs because it is a pseudogene in humans.

3.3. Role of native TRPC channels in various tissues

TRPC proteins are most prominently expressed in the brain, olfactory neurons, peripheral nervous system (4–6) , various cell types in the heart, lungs (7,8) (especially lung vasculature (9,10)), kidneys (11–13), smooth muscle cells (14,15) or intestinal pacemaker cells (16).

Generally speaking, TRPC channels participate in cellular functions regulating and directing the intracellular, spatial and temporal Ca^{2+} distribution. Such Ca^{2+} signals drive processes like exocytosis, gene transcription, proliferation, differentiation, fine-tuning of membrane excitability, etc. which ultimately decide the cellular fate. The role of certain TRPCs has been demonstrated as particularly important during embryonic or fetal development (e.g. TRPC5 in the brain (13,14)). In a later stage of development, functions of these TRPC members may subside or contribute to other cellular processes.

3.3.1. Physiological roles

There are two reasons which make physiological relevance of TRPC channels in the tissue hard to decipher: First, TRPC channels act as extremely versatile sensing complexes responding to various range of stimuli like pH, intracellular and extracellular ligands, Ca^{2+} concentration, oxidative stress, mechanical stimuli (17–19), voltage, etc. The observed physiological effect of channel activity is therefore typically a result of integration of all stimuli listed above. Second, the natively occurring channels are predominantly assembled as heterotetramers of various subtypes, therefore the proof of principle with the help of overexpression or knockout studies does not reflect the reality.

For illustration of the physiological role of some TRPC members in vivo a few examples are listed below: TRPC4 has been implicated in regulation of neurite outgrowth and neuronal exocytosis (22). TRPC5 is engaged in proper function of amygdala as well as fear-related behaviour (23). It also aids the formation of transient working memory in the entorhinal cortex (24). Despite relatively low TRPC6 expression in the brain, it has been shown to be involved in excitatory synapse formation (25), dendritic outgrowth (26), and brain-derived neurotrophic factor (BDNF)-mediated survival of granule cells in the cerebellum (27). Collectively, TRPC1/4/5 have been implicated also in the perception of pain. For instance, knockdown of or blocking TRPC4/5 channels showed increased pain threshold in mice (28,29). While the role of cardiac resident TRPC (1/3/5/6/7) channels under healthy conditions remains elusive, in pathological state their relevance is more clearly defined.

3.3.2. Pathophysiological roles

Several studies showed at the cellular level as well as in animal models that upregulation of TRPC channels in the heart facilitates hypertrophic signaling by providing an extra Ca^{2+} replenishment system (28–30). TRPC3 member belongs to the most spontaneously active channels among the canonical subfamily. As such it contributes considerably to the development of TRPC-dependent arrhythmias (33,34). Elevated intracellular Ca^{2+} results in increased spontaneous Ca^{2+} release from the sarcoplasmic reticulum (SR) or increased Ca^{2+} oscillations and hence in undesired contraction. Another study showed that loss-of-function TRPC4 had a positive impact on recovery after myocardial infarction and cardiac dysfunction in adult mice (31,32). TRPCs have also been implicated in heart failure (33–36).

Appreciable progress has been made recently in defining the contribution of TRPC channels to disease states of the brain. Studies have shown that targeting TRPC1/4/5 channels could serve treatment of central nervous system diseases such as anxiety, memory, epilepsy and addiction (23,40–42). The significance of TRPC channels in neuronal pathophysiology has been recently also shown for Huntington's disease, brain inflammation, high glucose-related neurotoxicity or epilepsy (42–46).

The first well-described TRPC6 related pathology was familial focal segmental glomerulosclerosis (FSGS). Single point mutation of proline 112 to glutamine resulted in overactive TRPC6 channel with enhanced localization at the plasma membrane (48). In accordance with Heeringa et al. there might be other polymorphisms that lead to the same channel phenotype (M132T; (49)). Consistent with TRPC6 involvement in physiology of the brain, TRPC6-dependent pathological states such as neuronal damage in stroke (49,50), Aβ-production in Alzheimer's disease (AD) (52), and human glioma cell proliferation (52,53) have been described.

TRPC7 was identified as the mediator of angiotensin II generated Ca^{2+} signaling leading to apoptosis in rat cardiomyocytes (55). Similarly, heterotetrameric TRPC7/3/4/1 channels were responsible for extracellular ATP/UTP derived depolarizing current in rat cardiomyocytes creating pro-arrhythmic background in early infarct events (56).

3.4. TRPC3 activation pathways

The general consensus in the scientific community nowadays is that TRPC3, as a member of the lipid-gated subset of TRPCs (TRPC3/6/7), is primarily endogenously activated in a receptor-operated (ROC for receptor operated current) manner via activation of G-protein coupled receptors (GPCRs) or receptor tyrosine kinases (RTKs). Mobilized G-proteins trigger phospholipase C (PLC) activation and hydrolysis of phosphatidylinositol-4,5-bisphosphate (PIP_2) into inositol-1,4,5-trisphosphate (IP_3) and diacylglycerol (DAG) follows. DAG then directly interacts with the channel to activate it (Figure 2). It was demonstrated later that supplementing DAG alone is enough to generate TRPC3 current (57). Unlike other TRPCs, TRPC3 displays considerable constitutive activity, not only in exogenous expression systems but also in native tissue (57,58). This observation is possibly tissue specific and therefore should not be understood as a general property of the channel.

Before discovery of the STIM1 and Orai1 proteins and acknowledging them as the major molecular components of store-operated Ca^{2+} entry (SOCE) or Ca^{2+}-release activated current (I_{CRAC}), it was believed TRP channels might be the effector protein executing the SOCE. As soon as evidence was provided that TRPCs failed to generate I_{CRAC}-like current and that STIM1 was an indispensable component of SOCE, TRPC's role in SOCE was acknowledged as less critical. Nevertheless, there is evidence that TRPC1 can mediate SOCE as well as interact with STIM1 and Orai1 proteins (59,60). TRPC3 contribution to SOCE was shown in mouse pancreatic tissue (62). Despite the evidence of SOCE via TRPC channels, their SOCE activity has not been as well defined as for Orai1 channels. TRPCs, unlike Orai1 protein, can operate independently of STIM1 (62,63). TRPC-STIM1 contact is primarily mediated by electrostatic interactions between the cytosolic domains of both proteins, positively charged residues in C-termini of TRPCs and the lysine rich domain at the very end of STIM1 C-terminus (64).

Figure 2: ROC and SOC activation pathways to stimulate TRPC current

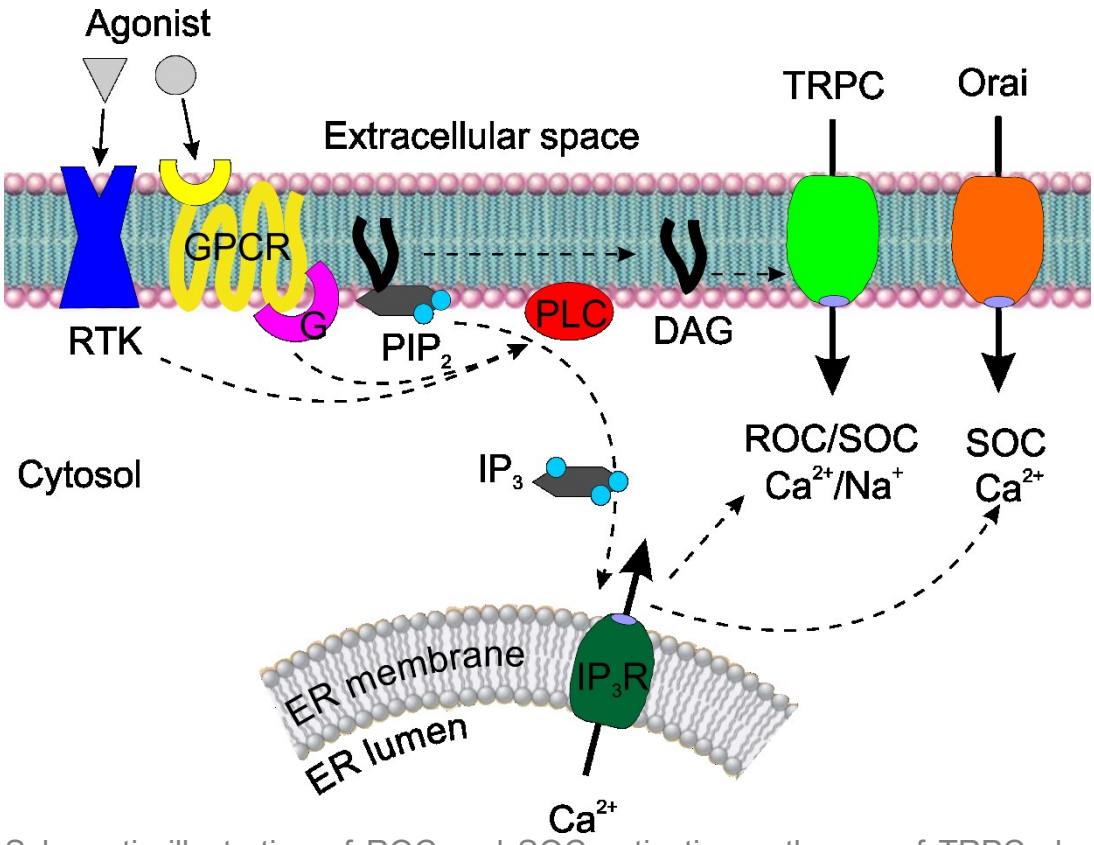

Schematic illustration of ROC and SOC activating pathways of TRPC channels. Extracellular agonist binding to G-protein-coupled receptors (GPCR) or receptors tyrosine kinases (RTK) leads to phospholipase C (PLC) activation. The stimulated PLC hydrolyzes phosphatidylinositol-4,5-bisphosphate (PIP_2) to generate diacylglycerol (DAG) and IP_3. DAG then directly acts to activate TRPC3/6/7 channels while the activated Gα proteins and the drop in PIP_2 levels contribute to TRPC4/5 channels stimulation. At the same time IP_3 triggers Ca^{2+} release from intracellular ER stores activating the SOC pathway.

Of note, the total cellular magnitude of TRPC3 conductance is also proportional to the number of channels available at the plasma membrane and the intracellular channel trafficking and recycling can therefore be considered as a form of activation although some evidence argues otherwise (65). Importantly, TRPC3 channel activity can be modulated by other molecules than DAG, such as products of lipid metabolism, redox compounds, etc. Nevertheless such mode of modulation of TRPC3 activity is not considered as a conventional channel stimulation pathway and hence will not be further discussed (Reviewed in (66)).

3.4.1. Synthetic agonists of lipid-gated TRPC3/6/7 channels

In the past few years, effort has been invested to identify pharmacological tools for the specific therapeutic interventions and to study the physiological relevance of the lipid-gated TRPC channels in tissues. Such purpose requires highly specific and direct TRPC3 ligands. While a considerable number of TRPC3 specific antagonists highly demanded for drug development are available (as listed in (67)), very few TRPC3-specific agonists have been identified for purposes of physiological studies decoding the TRPC role in tissues. The pioneering study initiating the TRPC subtype specific agonist search was the work of Leuner et al. (68). The authors investigate the specificity and potency of several structural hyperforin analogues in activation of TRPC6. The most promising candidate, 2,4-(1-ketohexyl) phloroglucinol (Hyp9 for short), shows no effect in stimulation of TRPC3 or TRPC7 currents, activating specifically TRPC6. The first report of a potent TRPC3/6 activator, GSK1702934A (GSK for short), was introduced by Xu et al. (69). This compound has been successfully used in several studies thereafter (68–71). Using GSK as a template the synthetic chemists, Guedes de la Cruz et al., synthetized several benzimidazole-based GSK structural analogues (72,73). A few of them are the subject of this study and will be discussed in more details later. Lastly, the most recent study employing a high-throughput screening technique identified the best hit from 305 000 compounds, with a chemical structure of a pyrazolopyrimidine skeleton. Based on this promising compound additional structural analogues were produced. The newly designed pyrazolopyrimidine compounds were then probed for activation of TRC3/6/7 channels (67). The set of the new chemicals proved to be potent, direct and fairly selective TRC3/6/7 channels agonists with the largest potency towards TRPC3 (EC_{50} < 20 nM).

3.5. TRPC3 membrane topology

Topology of TRP channels resembles strongly potassium or sodium voltage gated channels. Fully functional channels are composed from 4 homomeric or heteromeric isomers assembled together into a tetramer as has been clearly confirmed by single particle cryo-electron microscopy (EM) (74–80). Each TRPC chain consists of 6 transmembrane domains (TMDs also often referred to as

segments, acronymized S1-S6) with both carboxyl- and amino-termini located in the cytosol (Figure 3).

The short lipid bilayer re-entering loop connecting S5 and S6 forms the selectivity filter (SF) and is hence called the P-loop/pore-loop. The pore helix carries so called ‘LFW’ motif conserved throughout the canonical subfamily of TRPs that is crucial for functionality of the channel. Mutation in this region produce non-conducting channels in a negative-dominant manner (83). The rest of the pore lining is formed by the cytosolic part of S5 and S6 creating the narrowest spot of the pore, so called bundle crossing gate, to prevent ion migration in a closed state. Most of the TRP proteins are highly conserved in the TMD, on the other hand the cytosolic and extracellular domains are fairly different in various subtypes.

The human form of TRPC3 exists in 3 splice variants giving rise to 3 isoforms (Uniprot database nomenclature). Isoform 2 and 3 differ from isoform 1 only by an extra 12 (Isoform 2) / 85 (Isoform 3) amino acids respectively inserted before the start of N-terminus of the protein. For clarity the topological features of TRPC3 discussed further are shared in all 3 isoforms, they might be referred to by different numbers due to the shift originating from prolonged N-termini in isoform 2 and 3.

The N-terminus of TRPC3 starts with 4 ankyrin repeats followed by several horizontal helices preceding the S1. This domain is perfectly positioned for allosteric modulation of TRPC3 activity via cytosolic effector binding. Nevertheless, the PLC-binding region in the N-terminus of TRPC3 was determined to the initial amino acid residues 40-46 respectively (81,82).

S1-S4 helices resemble the voltage sensing domain of voltage-gated K^+ and Na^+ channels and are often referred to as the voltage sensing-like domain. The extracellular loops between S1-S2 carries a potential glycosylation site. Evidence has been provided that the glycosylation state of TRPC3 affects its activity (59). The more glycosylated the channel monomers are, the less constitutive activity the channel exhibits.

The C-terminus of TRPC3, being only approximately half of the length of N-terminus, carries many interaction and regulatory sites (e.g. phosphorylation by PKC (86)) and provides binding platform for regulatory or accessory proteins like immunophilins, calmodulin (CaM), homer, inositol trisphosphate receptor (IP_3R) and most probably other proteins mediating allosteric modulation of the channel or serving as a scaffolding platform for other interactions.

Figure 3: TRPC3 membrane topology

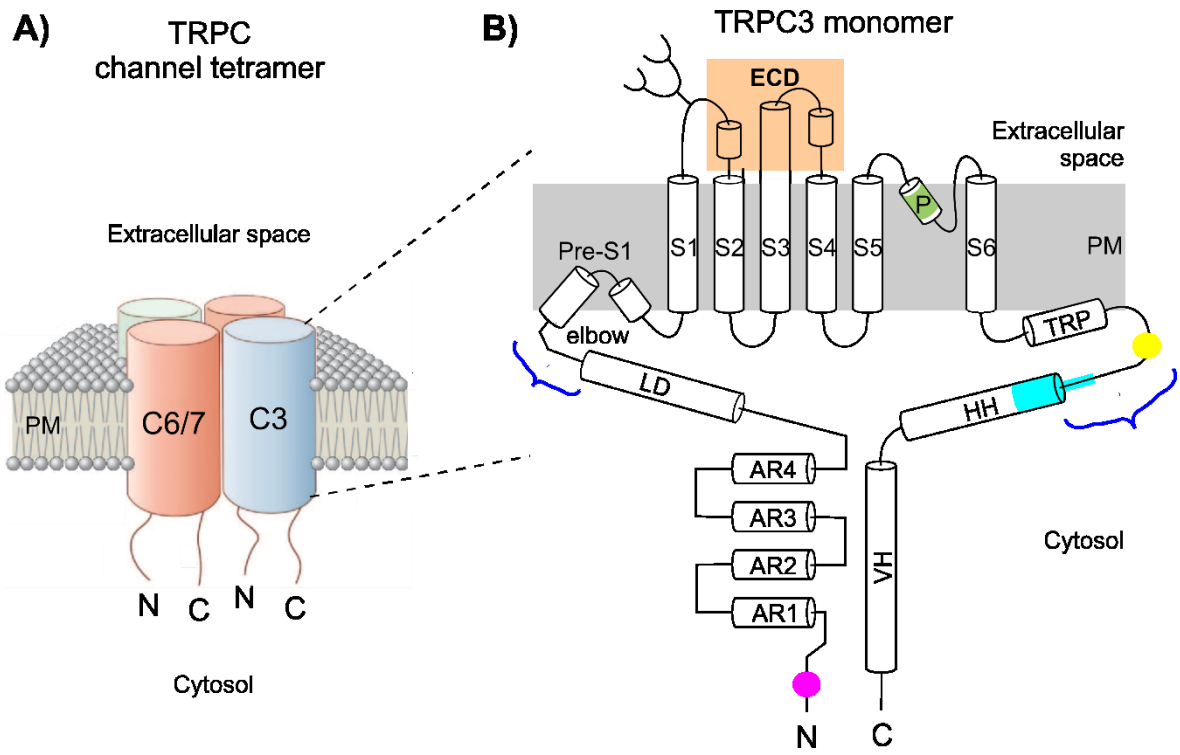

A) Heterotetrameric TRPC channel in the plasma membrane (PM). B) Scheme of TRPC3 monomer topology: AR – ankyrin repeats, LD – linker domain, S1-6 – transmembrane helices, P – pore helix, TRP – TRP box, HH – horizontal helix, VH – vertical helix. Color code: magenta – PLC interaction site, pseudo extracellular domain (ECD) is marked by orange background; green – LFW motif of the pore domain, yellow – PKC phosphorylation site at serine 712 (Isoform 1), cyan – calmodulin / inositol trisphosphate receptor binding domain (CIRB), branching on the S1-S2 linker denotes glycosylation site. Blue curly brackets highlight the regions exposed to intracellular effectors for binding and potential modulation (e.g. immunophilins or other proteins)

In the C-terminus the proline rich region prior to calmodulin / inositol trisphosphate receptor binding (CIRB) domain probably serves as binding platform for immunophilins (87) that catalyse interconversion of proline containing peptide bonds between cis and trans. Immunophilins serve as a target to immunosuppressive drugs. The immunophilin-drug complexes bind calcineurin to inactivate it, preventing Ca^{2+}-dependent response of T-cells (and so their IL-2

release). Immunophilins also work as protein folding chaperons assisting proline-containing peptide bonds that normally do not easily acquire the *trans* conformation common in naturally occurring proteins. During protein folding proline peptide bonds can therefore often become the rate-limiting step of the whole process (88).

3.6. High-resolution molecular structure of TRPC3 ion channel assembly acquired by cryo-EM

The recent technical advance in methods of structural biology, single particle cryo-EM in particular, allowed for solving molecular architecture of many otherwise challenging proteins in higher resolution. Although 2013 brought the first near atomic resolution model of TRPV1 (89), high resolution structures of the canonical TRP subfamily members were first published in the spring of 2018. Thereafter, in a short span of time cryo-EM structures of four TRPCs were available. At this point 3 independent near-atomic models of TRPC3 are published (71,74,75). The full-length protein chain assembled into a four-fold symmetrical homotetramer adopts acorn-shaped structure (Figure 4), especially in the presence of the detergent/lipid ring encompassing the TMD. The ion channel architecture is exclusively composed by α-helices, only the more flexible regions such as parts of the extracellular and intracellular loops or transitions between intracellular helical domains do not acquire highly ordered secondary structure and remain in flexible loop form.

While the past homology models of TRPC3 were sufficient for decent prediction of TMD layout (71,90), structural information on the parts stretching out of the lipid bilayer were the most awaited and are the novel cryo-EM derived information of the highest value.

The cytosolic domain (CD) was the most intriguing architecture information gained from cryo-EM due to its extensive 3D variability within the TRP family. TRPC3 CD resembles the shape of an inverse bell. The C-terminal vertical helices (VH) create the inner lining of a pore within the cytosolic domain using coiled-coil (CC) interactions. The horizontal helix (HH) within CD connects almost perpendicularly to VH (in an 100° angle according to (73)) and via gap provided by unstructured loop continues to the TRP helix. The HH and TRP helix are parallel to

one another and follow the plane of the inner leaflet of the lipid bilayer creating an ideal sliding platform. Moving to the N-terminal part of CD we can see the linker domain (LD) prior to TMD filling up the gap created by TRP box and HH. The very N-terminal end is formed by 4 ankyrin repeats creating an outer circumference enclosing the pore-like structure of C-terminal CC VHs.

The transition between CD and TMD is accommodated by the pre-S1 elbow helices on the N-terminal end and by TRP helix stretching to a predicted re-entrant on the C-terminal end (76).

As rightfully stated by Fan C. and co-authors, the uniqueness of TRPC3 member making it stand out from its close TRPC relatives is given by the atypical pseudo extracellular domain (ECD). The exeptionally long S3 helix extends considerably far into the extracellular space forming the pseudo ECD together with the S1-S2 and S3-S4 loops. The S1-S2 linker carries a glycosylation at asparagine 404 (Isoform 1) which is in agreement with previous results. The impact of this extraordinary pseudo ECD might be hidden in the multiple cavities that are found within its molecular architecture. The authors propose they may serve as potential regulatory binding sites for small molecules such as toxins or drugs.

Figure 4: High-resolution molecular model of TRPC3 channel complex

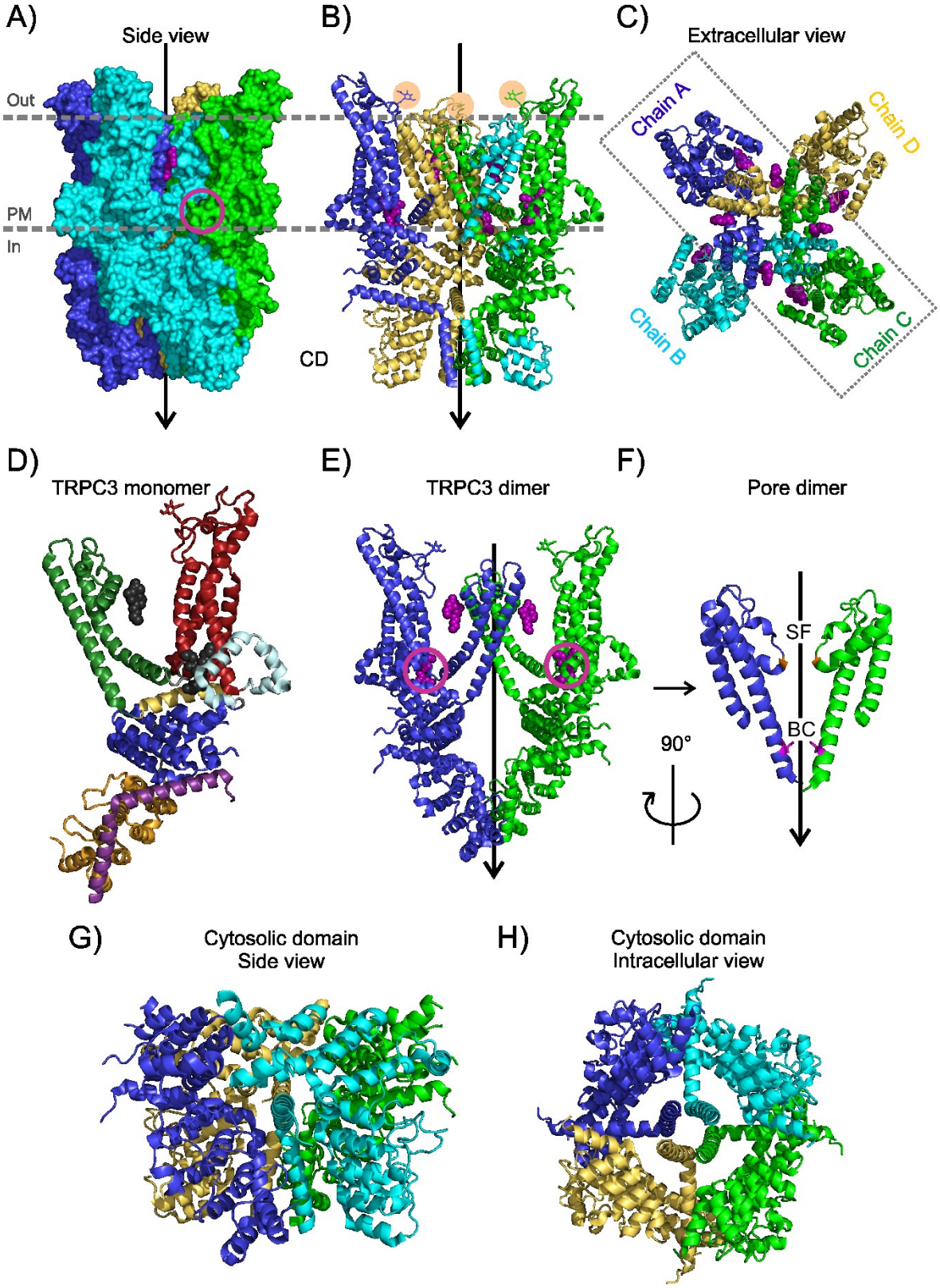

A) Side view of the surface representation of the TRPC3 tetramer architecture resembling an inverse bell-shape/acorn shape (based on cryo-EM structure by Fan et al. (76)). The complex is coloured by chain. Lipid 2 bound in its pocket is depicted in purple spheres, lipid 1 wedged into the cavity behind the pre-S1 elbow is denoted by a purple circle (since it is not visible in this configuration). Arrow represents the intracellular flow of ions. CD stands for cytosolic domain. B) Cartoon representation of the TRPC3 tetramer shown in A). Extracellular glycosylation sites are highlighted by sand-coloured circles. For simplicity some parts of the chain A coloured in dark blue and chain B in cyan were omitted. C) Extracellular view of the pore mouth. Notice the lipid 2 molecules wedged at the interface between adjacent TRPC3 monomers. D) TRPC3 monomer coloured by topological features. Colour code: orange – ankyrin repeats, dark blue – linker helical domain, pale cyan – pre-S1 elbow, red – voltage-sensing-like domain (S1-S4), green – pore forming domain (S5, S6), pale yellow – TRP box, purple – horizontal (HH) and vertical helices (VH) of the C terminus, the lipid molecules are illustrated by black spheres in this panel. E) TRPC3 full length dimer of opposite chains as depicted by the dotted rectangle in C). Lipid 1 molecules are highlighted with purple circles. F) 90° rotation of the TRPC3 dimer in E results in configuration that offers insight into the pore permeation pathway. SF – selectivity filter with the narrowest part created by G615 (Isoform 1) depicted in orange and the BC – bundle-crossing gate formed by I658 (Isoform 1) coloured in purple. G) Side view and H) intracellular entry of the pore in cartoon representation of the highly structured CD. VHs and HHs create the ‘backbone’ of the assembly and the ankyrin repeats align themselves on the outer circumference of the coiled-coil domain formed by VHs. The linker helical domain sits on the top of the HHs to create the connecting interface between the outer CD and TMDs.

3.7. Tracking the molecular elements of the TRPC3 gating machinery

The very first high-resolution model of TRPC3 detects 2 electron densities within the channel complex that were later assigned to 2 lipid molecules (76). Taking advantage of the triangular-shaped re-entrant structure of the pre-S1 elbow, Lipid 1 binding site was found wedged in the hydrophobic cavity behind it right next to the last N-terminal linker domain helix, S1 helix and the intracellular

end of S4. This positioning of the lipid is strategically localized because the cavity borders are in direct contact with the TRP helix as well as the S4-S5 linker that have been more than once implicated in modulation of the channel activity (88,89,91). Starting with the *Moonwalker* (*Mwk*) mice phenotype, a threonine to alanine gain-of-function mutation (T561A in human isoform 1) in the S4-S5 linker of TRPC3 was reported to cause cerebellar ataxia (88,91,92) in Purkinje and type II unipolar brush cells. Electrophysiological examination of *Mwk* Purkinje cells revealed increased TRPC3 basal activity resulting in increased calcium signaling and consequent cell death (92). Degeneration of Purkinje cells and evolution of cerebellar ataxia ultimately resulted in motor and coordination defects mirrored in a wider and shuffling gait of *Mwk* animals. Beck et al. described a conserved glycine in the S4-S5 liker of TRPC4 and TRPC5 whose mutation disrupts the endogenous H-bonding with the surrounding domains and results in a constitutively active channel (95). Also in the more distant TRP relative, TRPV1, a binding pocket close to the intracellular leaflet lined by parts of S3, S4 and S4-S5 linker was reported to alter the orientation of the S6 via S4-S5 linker upon resiniferatoxin binding achieving dilation of the lower BC gate of the channel (81). A similar concept was supported by a mutational study in TRPV1 that also concluded that allosteric coupling of the above mentioned binding pocket to TRP box is substantial for channel gating (96). In agreement with all the previously published results, the cryo-EM structure of TRPC3 by Tang et al. detected a cholesteryl hemisuccinate (CHS) density localized to the lipid 1 binding pocket (77). Of note, the 3.3 Å TRPC3 channel structure suggests a hydrogen coupling of the S4-S5 linker and S6 of the neighbouring subunit via serine 557 and asparagine 652 (Isoform 1).

The second lipid binding site is localized on the interface of two neighbouring subunits coming together near the actual pore. In a lateral fenestration S6 of one subunit and the P-loop of the adjacent chain maintains both, hydrophilic and hydrophobic interactions, to accommodate the lipid 2. In line with our previous work, introducing modifications to the lipid 2 binding site affects the channel's sensitivity to lipid activators (71). Similarly, a mutation of the highly conserved LFW motif of the P-loop is known to produce non-functional channels (21,81,93). Looking closely into the TRPC3 molecular model this observation is not surprising

due to many connection points, such as hydrogen bonds between the P-loop and S6 and S5 in the selectivity filter.

The authors of the latest TRPC3 cryo-EM structure (5.8 Å in resolution) introduce a rather controversial concept of TRPC channel gating being predominantly mediated through allosteric modulation of CDs (73). Valdez et al. assume, since the major architectural variation within the TRP family originates from the CDs, CD must define the subtype specific mode of activation and gating. In contrast Fan and co-authors quite extensively emphasize the differences in TMDs of various TRP members. For instance, the relative positioning of the voltage-like sensing domain (S1-S4) is different in TRPA1 and TRPM4 compared to TRPC3. Unlike TRPA1, TRPM4 and TRPV1, TRPC3 shows relatively a sharp angle between S6 and the TRP helix (90°), which is probably the reason why the turn connecting these 2 helices is unstructured and hence of high flexibility (76). As a result of that, the TRP helix is brought much closer to S4-S5 linker and the C-terminus of TRP helix reaches closer to the lipid 1 binding pocket, which is indeed relevant advantage for aforementioned hypothetical gating mechanism. Also other publications concentrate their proposition with respect to TRP channel gating rather to the TMD (98).

Modulation of TRPC3 activity via interactions with CD is so far best described for proteins, CaM and IP_3R. At higher Ca^{2+} concentrations Ca^{2+}-CaM complex binds the CIRB domain to inhibit TRPC3 activity. Once Ca^{2+} concentration decreases CaM competes for binding with IP_3R that eventually replaces it to stimulate TRPC3 function (99). The structure of this region was unfortunately not captured by any of the TRPC3 models signifying its high flexibility. Nonetheless the CIRB domain is located on the loop connecting TRP helix to the HH at the outer circumference of the channel complex just under the inner leaflet of the membrane and hence very accessible to signals coming both from cytosol and the membrane. Collectively the concept of signal recognition at the site of CD being forwarded on allosterically to the TMDs is generally accepted. An intriguing feature of this flexible loop described by Valdez et al. is that its length defines the channel activity. Based on previous report on a shorter splice variant of TRPC3 enhancing the ion flux (100), the authors designed several TRPC3 chimeras of different loop length. As predicted shorter loop variants exhibited larger channel conductances in response to GSK compared to the longer ones.

Valdez et al. further justify the importance of TRPC3 CD by describing many interactions within the CD: VH with surrounding ankyrin repeats, HH with N-terminal linker domain helices, etc. Current scientific understanding is that these interactions help to facilitate and maintain the channel assembly. Thanks to its ordered structure CD can probably tetramerize even without TMDs. The importance of this precise CD packing has been implicated in TRPC6, where mutations in ankyrin repeats close to HH resulted in FSGS (101). Unfortunately, certain level of ambiguity arises from 3 different molecular models of TRPC3. For instance, the domain swap at the connecting loop between HH and VH reported in the cryo-EM structures by Valdez et al. and Tang and co-authors is missing in the model by Fan et al. To determine which structural model is the closer to the reality additional experimental examination is required.

4. Objective

The present study takes advantage from recent insights into the basic structural features of TRPC3 channel (90) and aims to further describe and identify molecular components involved in the gating mechanism of TRPC3. With respect to the increasing interest in specific therapeutic control over TRPC3 channels for purposes of physiological investigations, the present thesis work intends to explore molecular mechanisms of TRPC3 channel manipulation via the recently introduced direct TPRC3/6 channel agonist, GSK. The effect of GSK on TRPC3 channel is be then contextualized with respect to physiological mode of gating. Regarding the unavailability of high-resolution structural information on TRPC3 channel complex at the beginning of this study, mutational analysis is employed instead to acquire information on scientific questions defined above.

5. Materials and Methods

5.1. Mutagenesis

Mutants were generated through site-directed mutagenesis using the QuickChange II Site Directed Mutagenesis Kit (Stratagene, USA). Human TRPC3 (Uniprot database ID: Q13507-3) cloned into pEYFP-C1 vector was used as template.

5.2. Tissue culture and transfection

HEK293 cells were cultured using DMEM medium (supplemented with 10% FBS, 1% penicillin/streptomycin, 2 mM L-Glutamine, 10 mM HEPES) in an incubator at 37°C and 5% CO_2. Transfection was performed with FugeneHD (Promega, USA) using vector:reagent ratio of 5:6 following the manufacturer's protocol.

5.3. Electrophysiology

5.3.1. Single-channel in cell attached configuration:

Characterization of unitary currents through TRPC3 channels was performed as published recently (71). In brief, patch pipettes were pulled from borosilicate glass (Clark Electromedical Instruments, UK). Currents were recorded at room temperature using Axopatch 200 B amplifier (Molecular devices, USA). Single channel activity was recorded in cell-attached configuration. The bath solution contained (in mM) 145 potassium gluconate, 5.3 KCl, 3 $MgCl_2$ and 15 HEPES. The pipette solution contained 137 NaCl, 5 KCl, 2 $CaCl_2$, 2 $MgCl_2$ and 10 HEPES. The pH of all solutions was adjusted to 7.4. Patch pipettes had resistances of 20-30 MΩ. Cells were stimulated with 100 µM carbachol (CCh) or 1 µM BI-2. Single channel currents were digitized at a sampling rate of 50 kHz and filtered with the Axopatch-200B internal 4-pole low-pass Bessel filter (-3 dB cut-off at 2 kHz). The holding potential ranging from -100 to 100 mV and was controlled by the holding command function of the amplifier. Data acquisition, analysis and further filtering with a low-pass Gaussian filter (-3 dB cut-off at 1.5 kHz) was done using pClamp10 software (Axon Instruments, Foster City, CA). For open- and closed-time histograms in logarithmic scale, data were compiled in bins of variable width and fitted with multi-exponential functions as described in (102) using MATLAB 2016a software (MathWorks, Natick, MA).

5.3.2. Whole-cell configuration:

Patch pipettes were pulled from thin-wall filament glass capillaries GC 150TF-7.5 (Havard Apparatus) to a resistance of 2–4 MΩ. An inverted microscope Axiovert 200 (Zeiss) was used to identify positively transfected cells by their green fluorescence when illuminated at 514 nm. Whole-cell experiments were performed at room temperature using an Axopatch 200B amplifier (Molecular Devices) and

Digidata 1440A/Digidata 1550B digitizer (Axon Instruments). Currents were filtered at 3 kHz by a 4-pole Bessel filter and digitized with 8 kHz. Application of linear voltage-ramp protocols ranging from −130 to +80 mV (holding potential 0 mV) was controlled by Clampex 10.4/11 (Axon Instruments) software. Standard pipette solution contained (in mM) 120 cesium methanesulfonate, 20 CsCl, 15 HEPES, 5 $MgCl_2$, 3 EGTA adjusted to pH 7.3 with CsOH or NMDG. Patch clamp experiments were performed using extracellular solutions containing (ECS; in mM): 140 NaCl, 10 HEPES, 10 glucose, 2 $MgCl_2$, 2 $CaCl_2$ pH adjusted to 7.4 with NMDG.

5.4. Ca^{2+} imaging

Changes in $[Ca^{2+}]_i$ were monitored using the Fura-2 technique as previously described [13, 14]. Briefly, cells on cover slips were loaded with 2 μM Fura-2 AM for 30 min in loading buffer (LB, containing in mM: 137 NaCl, 5.4 KCl, 10 HEPES, 10 glucose, 1 $MgCl_2$, 2 $CaCl_2$) at 37°C in the dark. After the incubation period, cells were washed twice with LB, and left to equilibrate for at least 15 min in LB. The coverslip was then mounted in a perfusion chamber on an inverted microscope (Olympus IX71) and perfused with empty/ TRPC3 agonist containing LB buffer at room temperature. During the recordings using Live Acquisition 2.5 software (FEI, Germany), cells were excited alternately at 340 and 380 nm every second using an Oligochrome excitation system (FEI, Germany) and fluorescent images were captured at 510 nm with an ORCA-03G digital CCD camera (Hamamatsu, Germany). The $[Ca^{2+}]_i$ imaging figures display the quantity: (Ratio F_{340}/F_{380}) = (F_{340} (cell) − F_{340} (background)) / (F_{380} (cell) − F_{380} (background)), where the “background” means fluorescence values were calculated from a region-of-interest (ROI) in each channel image (340 and 380 nm) drawn in an area without any cells.

5.5. Total internal reflection fluorescent (TIRF) microscopy

HEK293 cells transfected with pE-YFP-hTRPC3 were grown on 30 mm glass slips. At day 2 after transfection fluorescence was monitored every 3 s before and after stimulation with CCh (100 μM)/ GSK (1 μM). A Hamamatsu Orca-D2 split view camera was used and attached to an Observer D1 Microscope (Zeiss, Germany) in conjunction with a 488 nm Laser System (Visitron Systems Gmbh., Germany). 542 yellow emission filter set was utilized for the experiments (Hamamatsu).

VisiVIEW imaging software (Visitron Systems) was employed to acquire images. Images were analysed using ImageJ (Rasband, W.S., U. S. National Institutes of Health, Bethesda, Maryland, USA, http://imagej.nih. Gov/ij/, 1997-2014). For analysis the raw images were first background subtracted (BG) using the sliding paraboloid tool. Unstimulated part of the measurement was used to fit the BG data to a bleaching curve. The bleaching curve was then subtracted from the BG signal that was finally normalized to the average intensity after BG and bleach-corrected signal.

5.6. Statistical analysis

Whenever stated two groups comparisons were carried out using student‘s t-test whenever normal distribution and equal variance of data set was observed otherwise the significance was evaluated using Mann-Whitney rank sum test. Comparison of multiple groups was performed using One way ANOVA.

6. Results

6.1. A conserved glycine within S6 impacts physiological TRPC3/6 channel activation

Before the high-resolution structural information on TRPC channels was available, prediction to localize the potential TRPC3 gating regions within the molecular architecture were predominantly based on the structural knowledge of K^+ and Na^+ voltage-gated channels. Their gating machinery has been described to involve a flexible hinge point represented by a glycine residue within the pore lining S6 helix that undergoes a rearrangement upon channel opening [94, 102]. In analogy, we looked for conserved glycine residues in the gating relevant regions using online multiple sequence alignment tool (Figure 5). We identified a few promising candidates in the S6 that were subjected to site-directed mutagenesis and the functionality of the mutation-carrying TRPC3 channels was analysed in whole-cell patch clamp experiments (data not shown). During this small-scale screening glycine 652 was identified (Isoform 3) as the amino acid critical for channel gating.

Figure 5: Sequence alignment of the pore domain of canonical TRP channels, TRPV1 and voltage-gated K^+/Na^+ channels

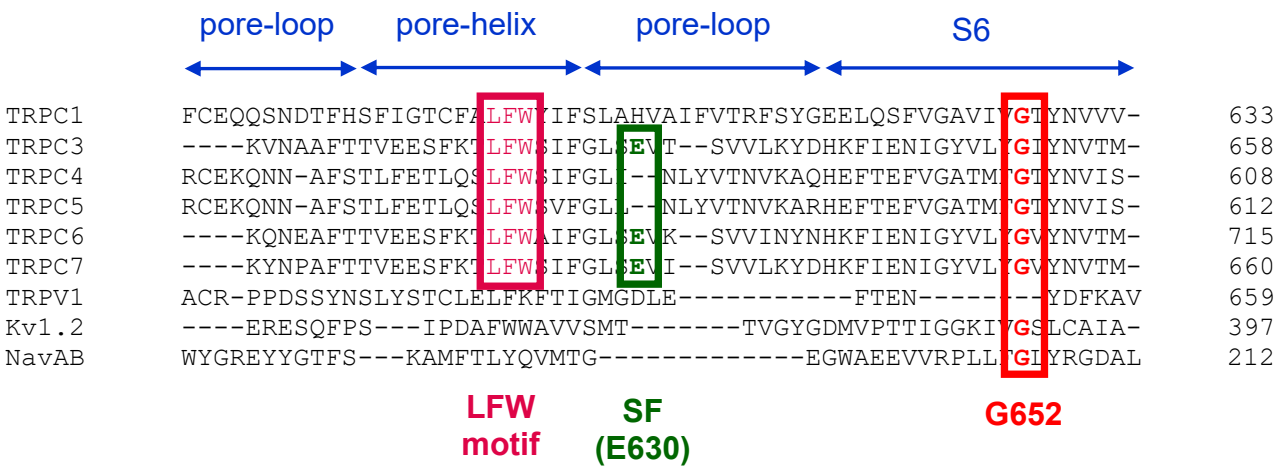

Multiple sequence alignment of TRPC1 (Uniprot ID: P48995), TRPC3 (Uniprot ID: Q13507-3), TRPC4 (Uniprot ID: Q9UBN4), TRPC5 (Uniprot ID: Q9UL62), TRPC6 (Uniprot ID: Q9Y210), TRPC7 (Uniprot ID: Q9HCX4), TRPV1 (Uniprot ID: Q8NER1), $K_v1.2$ (Uniprot ID: P16389), Na_vAB (Uniprot ID: A0A0M0JVU2) generated using online sequence alignment tool Clustal Omega (1.2.4). All sequences are of human origin except for the Na_vAB ion channel sequence from *Chrysochromulina* species. Conserved glycines corresponding to G652 in TRPC3 sequence (human isoform 3) are highlighted in red. For better orientation LFW motif and the selectivity filter (SF) characteristic for TRPC channels are denoted. For full length sequence alignment see the Appendix (Figure 1).

As described earlier, the G652A mutation rendered the TRPC3 channel insensitive to endogenous lipid activation via stimulation of the PLC pathway with muscarinic receptor agonist, carbachol (CCh) (71) (Figure 6). Neither did exogenous administration of DAG analogue, 1-stearoyl-2-arachidonoyl glycerol (SAG), elicit a TRPC3 current.

Figure 6: Super-sensitivity of $TRPC3_{G652A}$ channels to benzimidazole activators in comparison with WT and their physiological activation

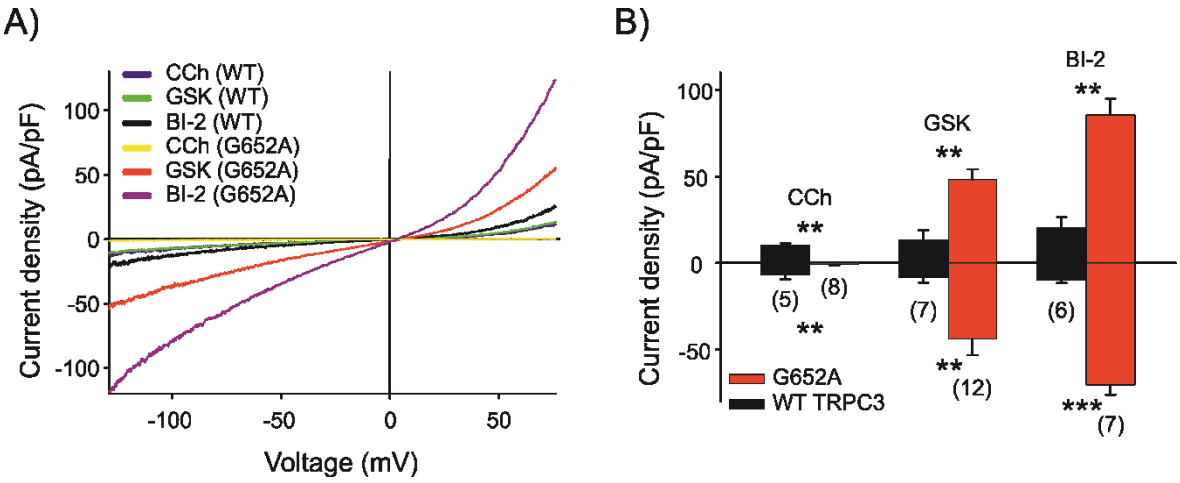

A) Representative I-V curves obtained in whole-cell recordings of HEK293 cells overexpressing WT/G652A TRPC3 channels activated with 100 µM CCh / 1 µM GSK / 1 µM BI-2. B) Statistical evaluation of maximum current densities generated in the experimental setting of panel A) at -90/70 mV; mean ± SEM are shown; number of cells measured is indicated in parentheses; two tailed t-test (normally distributed values) or Mann–Whitney tests (non-normally distributed data sets) were applied, (**p < 0.01, ***p < 0.001). This figure has been previously published in (72).

Knowing that TRPC3 shares 73% sequence identity with its close relative, TRPC6, we tried to reproduce $TRPC3_{G652A}$ phenotype in TRPC6. Indeed, mutating the conserved glycine G709 to alanine in TRPC6 drastically reduced the CCh response as observed in electrophysiology measurements of WT or G709A TRPC6 overexpressing HEK293 cells (Figure 7). Intact functionality of $TRPC6_{G907A}$ channels was additionally probed with GSK agonist but the benzimidazole

modulation of mutant TRPC3/6 channels will be discussed in more details in the following section.

Figure 7: Endogenous lipid-insensitive $TRPC6_{G709}$ mutant channel mimics $TRPC3_{G652A}$ phenotype

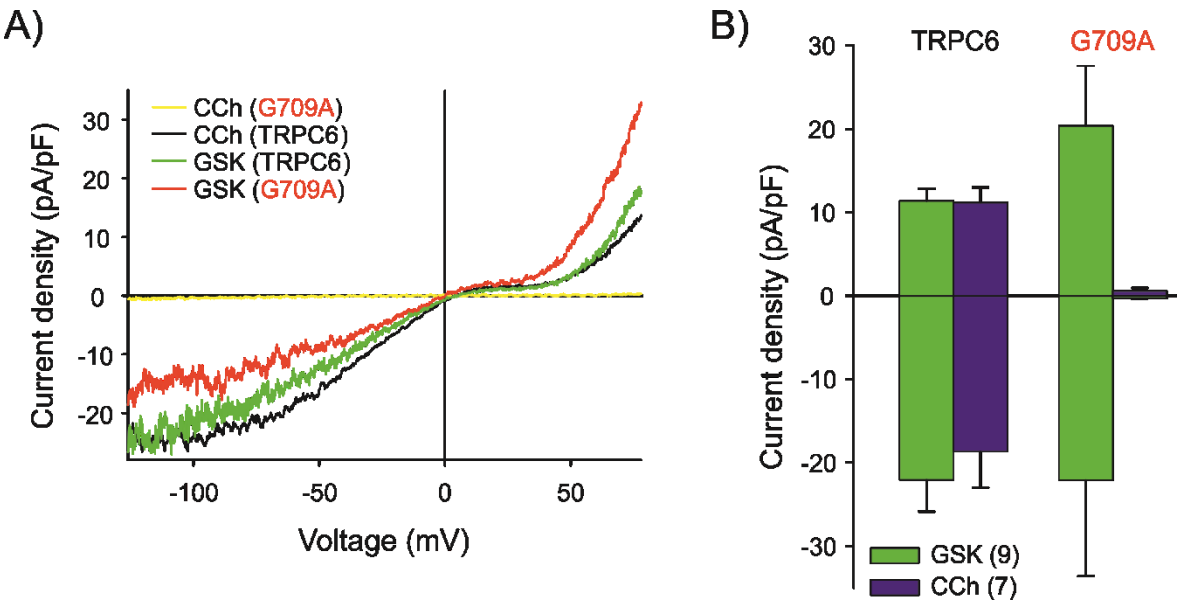

A) Representative I-V curves obtained in whole-cell recordings of HEK293 cells overexpressing WT/G709A TRPC6 channels activated with 100 µM CCh / 1 µM GSK. B) Statistical evaluation of maximum current densities generated in the experimental setting of panel A) at -90/70 mV; mean ± SEM are shown; number of cells measured is indicated in parentheses.

6.2. Mutant $TRPC3_{G652A}$ and $TRPC6_{G709A}$ channels retain their sensitivity to synthetic benzimidazole-based channel agonists

Taking advantage from the direct pharmacological modulator, GSK, we could verify that despite lack of response to endogenous stimuli $TRPC3_{G652A}$ channel remains functional. Administration of 1 µM GSK showed clear channel activation (Figure 6A, B) in electrophysiology measurements. Likewise, the endogenous lipid-insensitive TRPC6 mutant G907A responded to 1 µM GSK application (Figure 6). Both channels preserved general benzimidazole sensitivity.

TRPC3 and its conjugate mutant channel were probed for reactivity to other benzimidazole-based compounds to see if there is a correlation between the individual benzimidazole functional groups and the apparent potency on the channel (Figure 8). Interestingly, some GSK analogues induced distinct activation patterns in WT compared to G652A channels in whole cell patch clamp experiments in HEK293 cells. While the majority of GSK analogues generated larger response in the mutant channel (GSK, 1b, 1d, BI-2), a smaller subset of them showed reduced agonist activity in the mutant channel (1e, 1f; Figure 8). This observation is in accordance with a modified lipid-sensitivity profile that was reported for G652A in comparison with the WT channel by Lichtenegger et al. (71). The activator potency series, starting with the most effective lipid agonist, was 1-oleoyl-2-acetyl-sn-glycerol (OAG) > SAG > 1,2-dioctanoyl-sn-glycerol (DiC8) in WT TRPC3 channels compared to DiC8 > OAG > SAG in $TRPC3_{G652A}$ channels. The distinct benzimidazole activity in mutant vs. WT channels is probably due to modified geometry of the benzimidazole binding pocket as a result of the G652A mutation. The agonist molecule has to rearrange itself in the altered binding cavity not being able to induce the same conformational rearrangements as in the WT TRPC3 channels. The different apparent potency of various GSK analogues in both, WT and G652A channels most probably signifies that GSK molecular geometry matters as well. Hence some benzimidazole functional groups are more vital for agonist activity than others similarly as previously reported for distinct lipid activating moieties in TRPV1 (106).

Figure 8: Chemical formulas and activation potency of GSK analogues in WT and G652A TRPC3 channels

A)

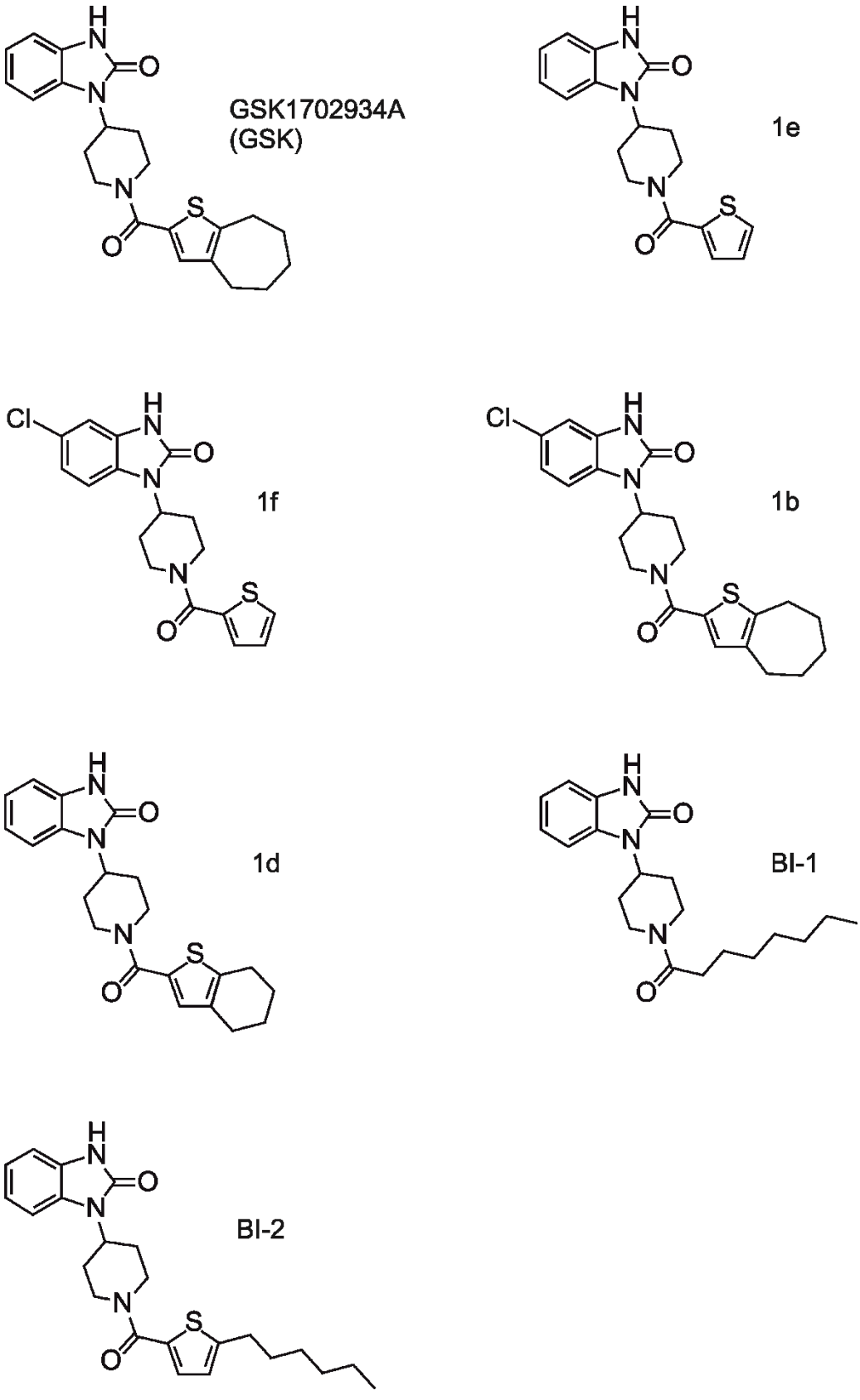

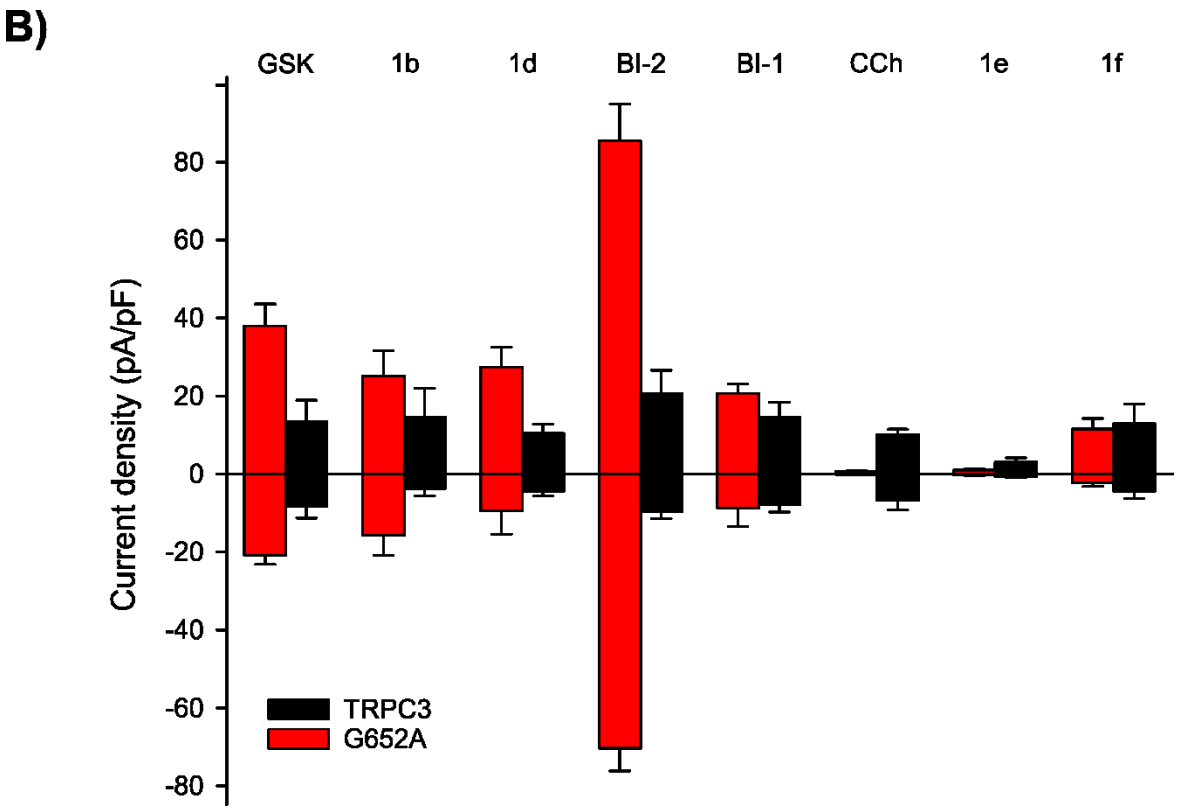

A) Molecular structures of the TRPC3 agonists, GSK, BI-2 and other benzimidazole compounds. This figure has been previously published with slight modifications in (72). B) Bar graph representation of maximum current densities induced by 1 µM benzimidazole compounds and 100 µM CCh in whole cell patch clamp recordings of HEK293 cells overexpressing WT or G652A TRPC3 channels. Mean ± SEM at -90/70 mV are shown. Parts of these data were previously published in (74).

6.3. GSK does not affect TRPC3 activity by inducing ion flux through a secondary pore

Due to lack of molecular and functional information as to how benzimidazole compounds activate TRPC3/6 channels we could not exclude the hypothesis that GSK interacts with the channel complex to induce formation of an ion permeation path outside the central pore domain. For instance, formation of a secondary pore could result in atypical current flow. The rationale behind formation of such pore

has been described for Cl^-/H^+ exchangers (107). To test this hypothesis we used a confirmed pore impermeable $TRPC3_{E630K}$ (isoform 3) mutant channel (108) and probed it in functional electrophysiology assay. HEK293 cells expressing $TRPC3_{E630K}$ did not show generation of any current upon application of 1 µM GSK (Figure 9). Hence, we conclude GSK-induced currents pass exclusively through the conventional pore of TRPC3.

Figure 9: GSK fails to induce TRPC3 current in the pore-impermeable E630K mutant channel

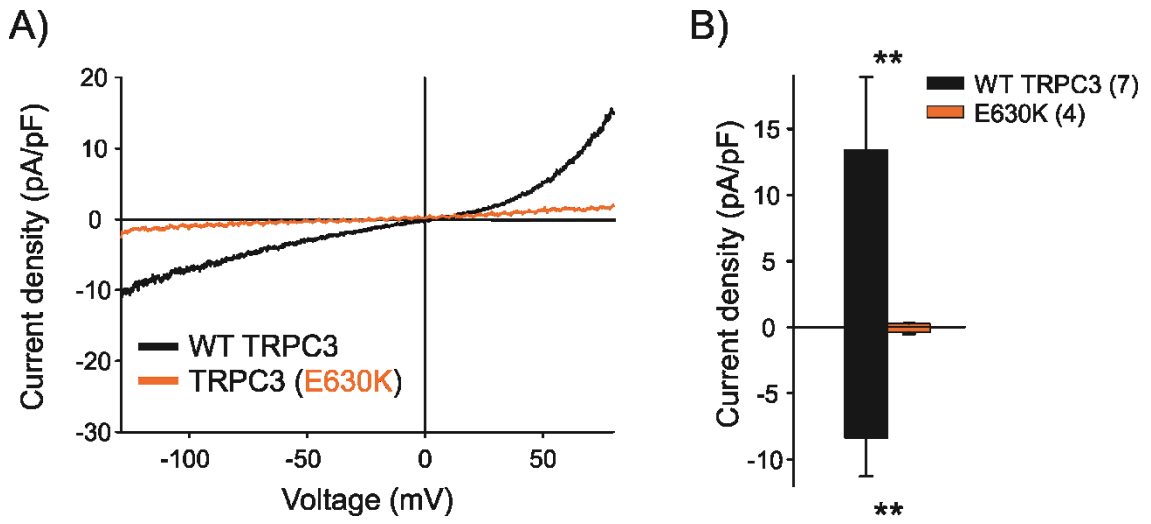

A) Representative I-V curves obtained in whole-cell recordings of HEK293 cells overexpressing WT TRPC3/$TRPC3_{E630K}$ channels stimulated with 1 µM GSK. B) Statistical evaluation of maximum current densities generated in the experimental setting of panel A) at -90/70 mV; mean ± SEM are shown. Number of cells measured is indicated in parentheses; Mann–Whitney test (non-normally distributed data set) was applied to compare experimental groups (**p < 0.01).

6.4. $TRPC3_{G652A}$ channels exhibit enhanced responsiveness to benzimidazole activators

By comparing the electrophysiology data from benzimidazole-stimulated WT or mutant TRPC3/6 channels we noticed that benzimidazole-derived response was

significantly enhanced in the $TRPC3_{G652A}$ mutant channel expressing cells. While the peak current densities (Figure 8B, 6B) induced by benzimidazole compounds (GSK, 1f, 1b, 1d, BI-2, BI-1) in the WT TRPC3 channels appeared to be similar in magnitude, $TRPC3_{G652A}$ channels showed at least 3-fold larger peak current amplitudes in the corresponding condition (Figure 6). This behaviour was then mirrored in the current-voltage (I-V) characteristic (Figure 6A).

While endogenous activation of WT TRPC3 channels via CCh generates TRPC3 currents of similar magnitude as stimulation with benzimidazole compounds (Figure 6), in the mutant channels the endogenous lipids, unlike most of the benzimidazoles, fail to induce TRPC3 current. As the inspection of the structure-activity profile of benzimidazole compounds in TRPC3 channels discussed in the previous section suggests the compound's geometry impacts the agonist potency. Certain GSK analogues (1e, 1f) follow the activity profile of endogenous lipids (Figure 8). We can only speculate that this structurally related group of GSK analogues probably occupies the identical binding pocket as the lipid molecules and hence its activity profile is affected in similar manner.

6.5. Facilitation of benzimidazole-mediated $TRPC3_{G652A}$ current is not a consequence of increased agonist potency

Provided the clear impact of G652A mutation in TRPC3 channel gating, we first examined the hypothesis of the increased current densities induced by benzimidazoles in the mutant channels being a result of a gain in agonist potency or affinity. For this purpose, we constructed concentration-response curve for BI-2 activation of WT and mutant TRPC3 channels in whole-cell patch clamp recordings. As depicted in the Figure 10 the EC_{50} parameters derived from BI-2 induced inward currents were comparable both, in WT and G652A TRPC3 channels (203 and 282 nM respectively). Collectively, these results suggest that the enhanced current densities observed are not due to augmented BI-2 potency. Consequently, we can assume that also the BI-2 affinity to the channel complex remained unchanged by the G652A mutation. On the other hand, since BI-2 generated increased current densities at all tested concentrations we propose profound rise in the efficacy of benzimidazole compounds. Of note, similar trend of

benzimidazoles super-sensitizing the mutant channels only can be observed also in TRPC6$_{G709A}$ (Figure 6). Nonetheless, to confirm this trend in the TRPC6 as well would require further experiments.

Figure 10: Facilitation of benzimidazole-induced currents in TRPC3$_{G652A}$ mutant channels is not caused by a gain in agonist potency

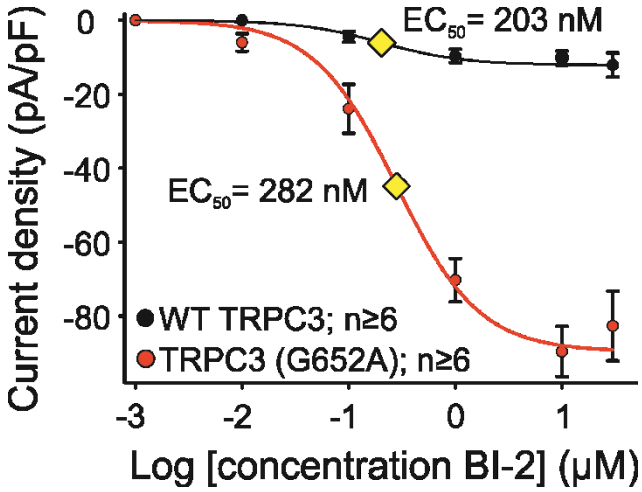

Concentration-response curve of BI-2 obtained from whole cell patch clamp recordings of HEK293 cells overexpressing either WT/G652A TRPC3 channels. EC_{50} reflecting BI-2's affinity to the channel is highlighted with yellow diamonds: 203 (WT) vs. 282 (G652A) nM respectively. This figure has been previously published in (72).

6.6. Enhanced responsiveness of TRPC3$_{G652A}$ channels to benzimidazole agonist is not a result of pore dilation

TRP channels are unique for their plasticity of the pore domain. It has been demonstrated earlier that structural rearrangements in the pore domain can be a part of gating mechanism in certain TRP channels [106–108]. Moreover the pore architecture is obviously tightly controlled via tight coupling between SF and BC (90). To determine the influence of the G652A mutation localized in close proximity of the SF on the plasticity of the pore, we examined the unitary currents and the gating behaviour of WT and mutant TRPC3 channels upon activation with BI-2 compared to CCh in single channel recordings.

Although high-resistance patch pipettes (20-30 MΩ) were utilized in these experiments to achieve very small pipette openings (< 1μM), multiple channels per patch could not be completely avoided (not illustrated). For this reason, we utilized for gating analysis only the recordings with a minimum number of overlapping channel openings in the initial transient peak of activation. Typically, we observed more transiently activated channels in the patches of the $TRPC3_{G652A}$ mutant (N denotes the number of activated channels in the patch, N = 6) in contrast to patches of the WT channels (N = 2). The transient activation of available channels in the patches ceased rapidly (no channel activity was observed after at latest 2 min) in experiments of both WT and mutant channels. Nevertheless, the late activation phase was characterized by a period where a single conductance level could be observed while modified gating was still obvious. Inspection of the time-dependent events in our recordings forced us to use relatively high agonist concentrations in the measurements in order to achieve time window long enough where sufficient open probability and gating transitions were observed to allow for subsequent analysis. For determination of the gating behaviour only the recordings of consistent activity (as described above lasting for at least one minute) and lacking multiple conductance levels were collected.

Figure 11A summarizes the unitary current-voltage relationship constructed based on the cell-attached recordings of HEK293 cells overexpressing WT or G652A TRPC3 channels stimulated with BI-2 or CCh. No deviations in unitary current properties were detected at any of the recorded potentials neither for WT nor for mutant channels activated by BI-2 or CCh. These results suggest that the pore architecture remains the same in all 4 conditions described above. This finding is consistent with the results obtained in whole-cell experiments illustrating that $TRPC3_{G652A}$ channels activated with benzimidazoles remain sensitive to the typical pore blocker (eliminating exclusively the inward current of TRPC channels), ruthenium red, as depicted in Figure 11B. In conclusion, the enhanced current densities observed in whole-cell patch clamp recordings of mutant channels activated with BI-2 are not a result of altered ion permeation or increased unitary conductance.

Figure 11: Unaltered ion permeation via $TRPC3_{G652A}$ mutant pore verified by consistent unitary conductance and effectivity of ruthenium red, TRPC3 pore blocker

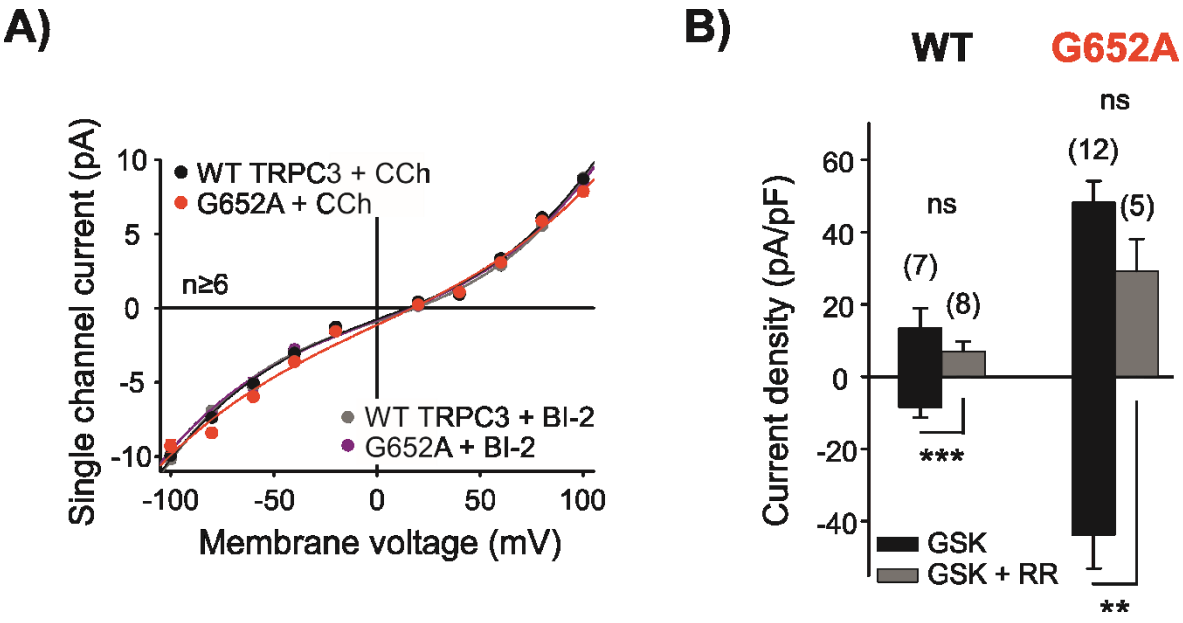

A) Unitary current to voltage (I-V) relationships of WT and G652A TRPC3 channels activated by 100 µM CCh or 1 µM BI-2. Data points represent the mean ± SEM*, number n of cells/patches measured at each voltage as indicated, *note that symbol size exceeds error bars at most voltages. Curves represent the least-squares fit to the third-order polynomial relationship. Data were not corrected for liquid junction potentials. B) Maximum net current responses at -90/70 mV acquired in whole cell recordings of HEK293 cells overexpressing WT/G652A TRPC3 channels activated with 1 µM GSK in presence and absence of 3 µM ruthenium red (RR). Mean ± SEM are shown (ns = not significant, **p < 0.01, ***p < 0.001).

6.7. Enhanced responsiveness of $TRPC3_{G652A}$ channels to benzimidazole activators is caused by prolonged open channel lifetimes

As rationalized earlier, due to transient nature of BI-2 and CCh responses our evaluation of the gating behaviour was restricted to the stable phase of the single channel recordings typically following an initial rise in channel activity due to

agonist administration. This quasi-steady state of the activated channels was stable for about 1 min. During this period an increase in the open probability due to agonist application was clearly evident. The open probability increase in BI-2 response was more profound in $TRPC3_{G652A}$ channels compared to WT (91% vs 24% respectively, Figure 12).

Figure 12: Open probability of benzimidazole- and CCh-stimulated WT and G652A TRPC3 channels

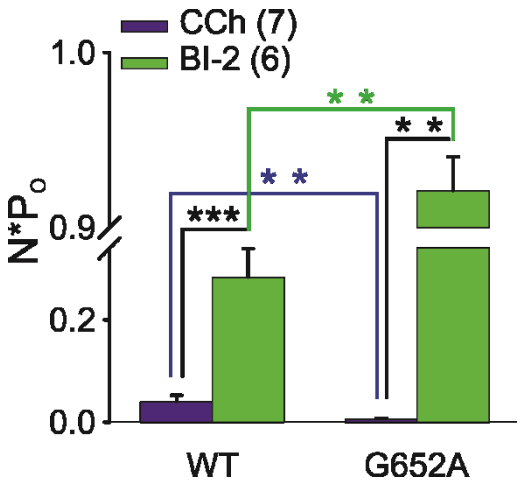

Mean values ± SEM of the open probability of WT vs. G652A TRPC3 channels under CCh/BI-2 stimulated conditions. Values were derived from the single channel traces at a temporary steady state where only one channel was active. Number of cells is indicated in parenthesis. Two tailed t-test or Mann-Whitney test were applied to assess the statistical significances between data sets, **p < 0.01, ***p < 0.001). This figure has been previously published in (72).

Examination of the single channel traces at different membrane voltages showed remarkable distinction in gating pattern of WT and mutant TRPC3 channels upon stimulation with BI-2 (Figure 13A). Unlike the WT channels, $TRPC3_{G652A}$ channels resided predominantly in long-lived open states. This phenomenon is more comprehensively illustrated in the probability density function histograms reflecting the dwell time constants of representative recordings in Figure 13B. While the closed time constants do not show a dramatic difference

between WT and mutant channels, open lifetime constants are significantly prolonged and more populated in $TRPC3_{G652A}$ BI-2 modulated channels.

Figure 13: Representative single channel traces and probability density function histograms of BI-2 activated channels

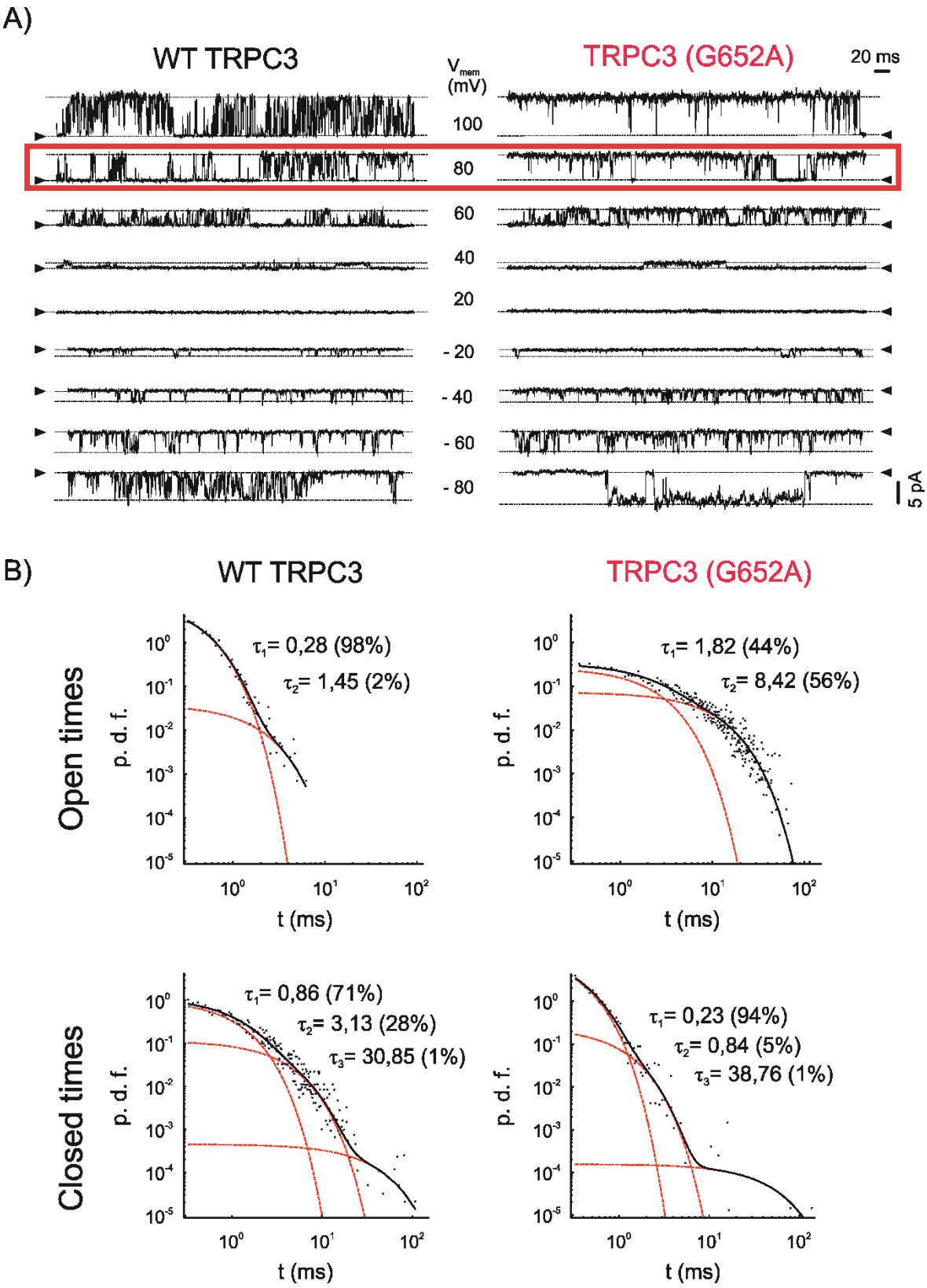

A) Representative unitary current traces at various voltages (from -80 to 100 mV) recorded in HEK293 cells expressing either WT or G652A TRPC3 channels activated with 1 µM BI-2. Arrowhead indicates the closed state. All traces displayed are filtered as described in the Method section. Red box indicates the membrane potential of +80 mV at which further statistical analysis of open/closed dwell time constants and open probability was carried out. B) Representative probability density histograms (probability density function - p.d.f.) of open and closed time constants of BI-2 stimulated (1 µM) WT and G652A TRPC3 channels expressed in HEK293 cells. Data are derived from single-cell-attached patches at the membrane potential of + 80 mV. The sum of multiple exponential equations (black) and the individual components (red line) with time constants (τ_1– τ_2) are indicated. The data set size of the open/closed events is as follows: For WT channels 2044 / 1155 open events and 2405 / 1910 closures (detected / fulfilling the 0,3 ms delimiter criterion for further exponential function fitting) were collected. In $TRPC3_{G652A}$ channels 2657 / 2496 open events and 2665 / 1188 closures were collected. This figure has been previously published in (72)

The statistical comparison of open time constants obtained for WT and $TRPC3_{G652A}$ channels at basal condition or activated with CCh / BI-2 at a membrane potential of + 80 mV is summarized in Figure 14. Upon activation with BI-2, considerable proportion of mutant channels (approximately 58% in average) occupy the exceptionally long-lived openings (>12 ms in average). In turn short-lived openings are significantly less populated in the $TRPC3_{G652A}$ channels (Figure 13B, Figure 14). Since the long-lived open state was exclusively observed in BI-2 activated $TRPC3_{G652A}$ channel and was absent in CCh-activated mutant and WT channels, we consider it strictly G652A-specific phenomenon.

Figure 14: BI-2 activated TRPC3$_{G652A}$ channels are characteristic by prolonged open channel lifetimes

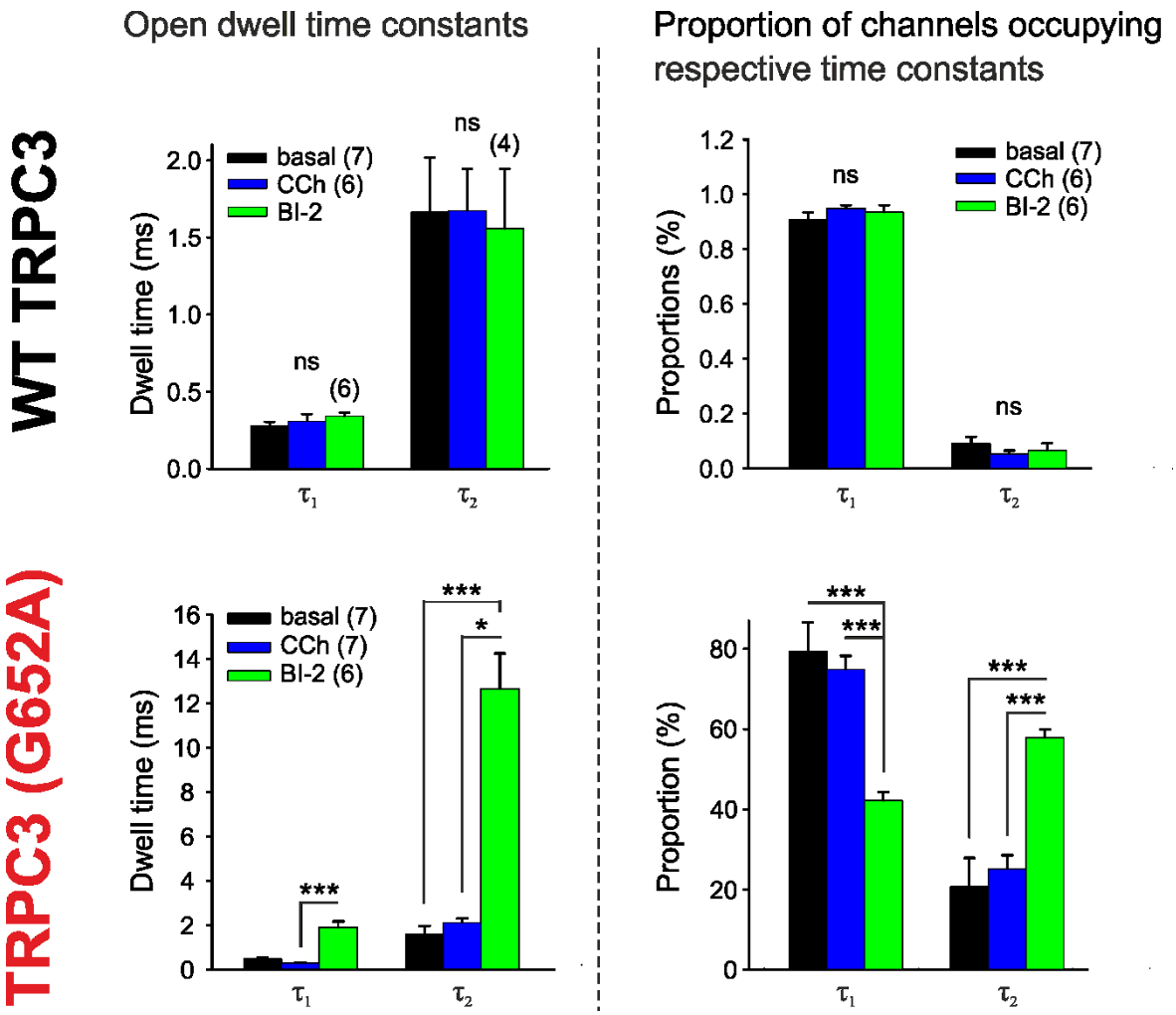

Comparison of open dwell time constants and their occupancies derived from single channel recordings in cell-attached patches of WT (upper panel)/G652A (lower panel) TRPC3 channels activated with 1 µM BI-2, 100 µM CCh or at basal conditions at V_{mem} = + 80 mV. Mean ± SEM, number of cells measured is indicated in parentheses. One way ANOVA was employed to compare the triplets of data and two tailed t-test or Mann-Whitney test were used to evaluate the differences between two experimental groups (*p < 0.05, ***p < 0.001, ns = not significant). This figure has been previously published in (72)

Statistical analysis revealed only minor differences in the closed time constants between WT and TRPC3$_{G652A}$ channels, their comparison is shown in Figure 15. In

general BI-2 application caused channel closures to become shorter in both WT and mutant channels. In addition, the BI-2 causes the channels to preferably reside in the shortest time closures resulting in general destabilization of closed state in both, WT and mutant channels (Figure 15).

Figure 15: Statistical comparison of closed dwell time constants

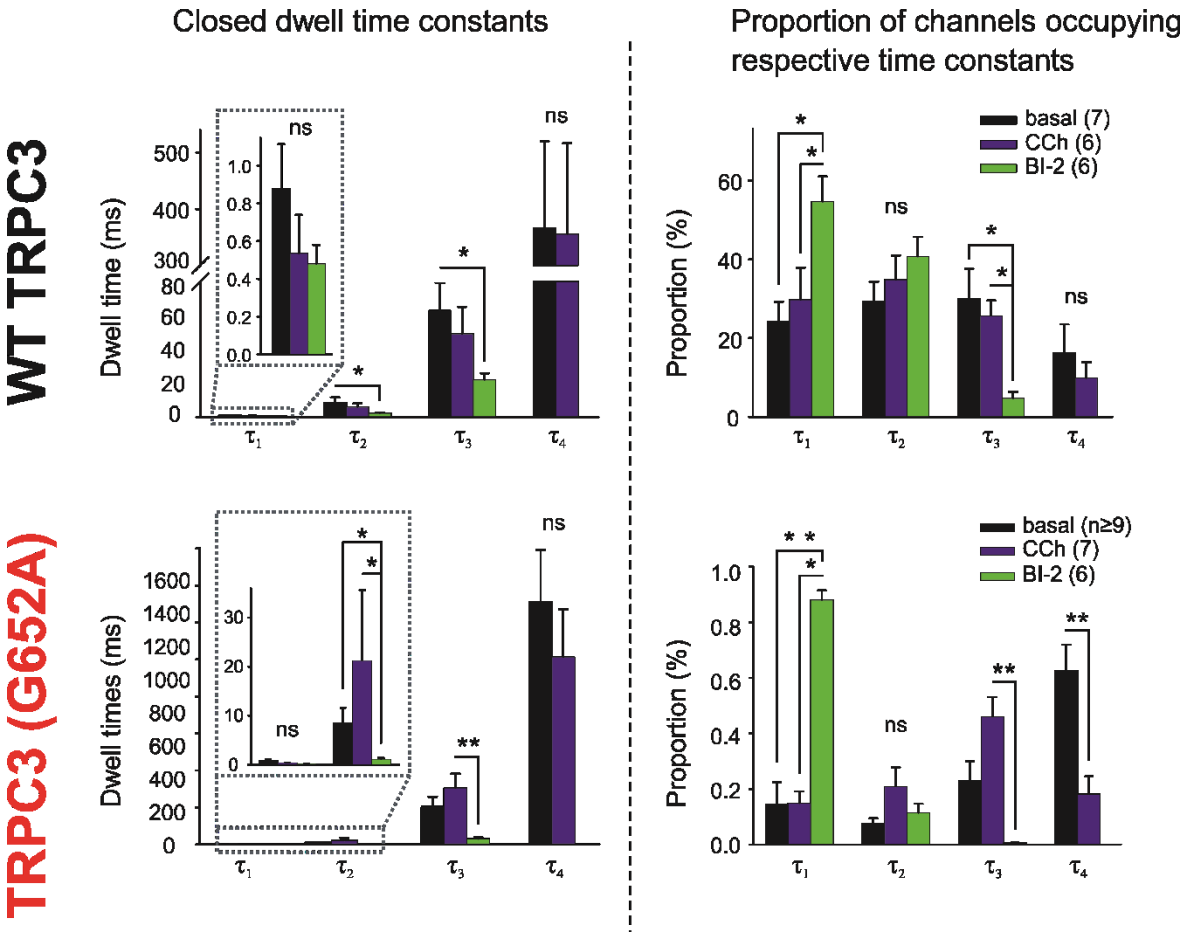

Comparison of closed dwell time constants and their occupancies derived from single channel recordings in cell-attached patches of WT (upper panel) / G652A TRPC3 channels (lower panel) activated with 1 µM BI-2, 100 µM CCh or at basal conditions at V_{mem} = + 80 mV. Mean ± SEM, number of cells measured is indicated in parentheses. One way ANOVA was employed to evaluate the multiple data sets, two tailed t-test or Mann-Whitney test were used to compare 2 experimental groups (*p < 0.05, **p < 0.01, ns = not significant). This figure has been previously published in (72).

6.8. Benzimidazole modulation of TRPC3 channels is probably associated with channel internalization

The observation of multiple active channels upon agonist stimulation that disappeared during recording of the single channel current (Figure 16C) made us speculate if there are other processes involved apart from classical channel inactivation. An alternative explanation for the disappearing channels is channel trafficking and their retrieval from the plasma membrane. To address this hypothesis, we monitored the fluorescent signal of YPF-tagged WT TRPC3 channels in TIRF microscopy upon activation with GSK and CCh. To our surprise, while endogenous signaling did not result in considerable fluorescent signal deviations, we observed a late drop in the fluorescent signal upon GSK administration (Figure 16A).

Figure 16: TIRF microscopy and single channel recordings suggest that benzimidazole action is associated with TRPC3 channel internalization

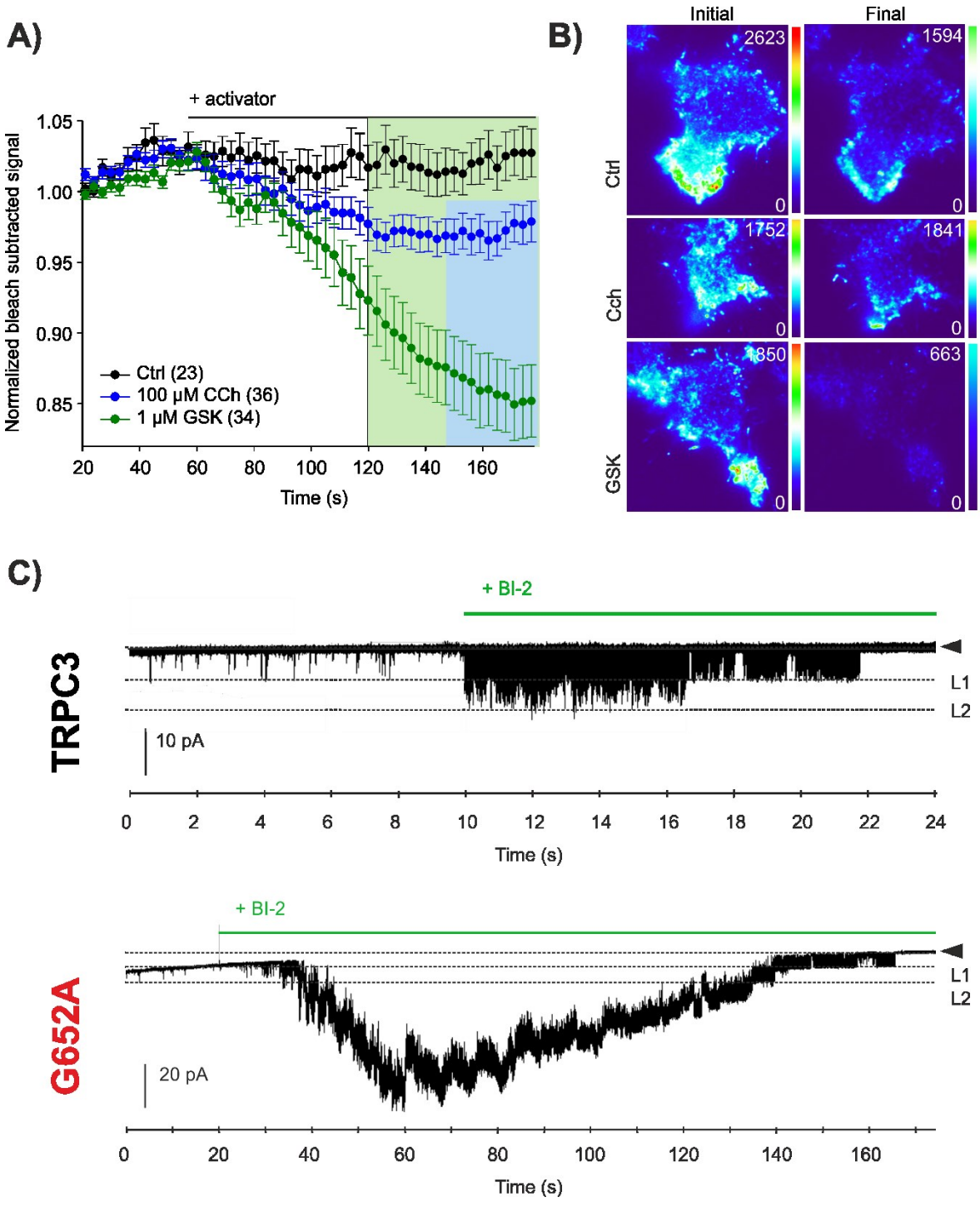

A) Time traces of normalized fluorescent signal derived from TIRF microscopy of HEK293 cell overexpressing YFP-labelled WT TRPC3 channels stimulated with CCh (100 µM), GSK (1 µM) vs. ctrl. (= agonist free buffer). Green background of the graph signifies GSK data set with significant difference from control, blue

background stands for CCh data set with significant difference from GSK data set (**p < 0.05). Two tailed t-test or Mann-Whitney test were applied. B) Representative TIRF images for each of the conditions mention in A) with a colour coded-signal intensity bar. For statistical analysis the raw figures were first background subtracted using rolling paraboloid method, followed by bleach subtraction and normalization to the average signal before stimulation. C) Representative time courses of single channel recordings of HEK293 cells overexpressing either WT (upper panel) or G652A (lower panel) TRPC3 channels at the membrane potential of +80 mV activated with BI-2 (1 μM) suggesting gradual retrieval of the channels over time. Closed state is indicated with an arrowhead.

6.9. G652A uncouples cross-desensitization between endogenous and pharmacological activation stimuli in WT TRPC3 channels

Assuming benzimidazole compounds activate TRPC3 channels in a direct manner bypassing the PLC pathway and provided this mechanism of activation is facilitated in $TRPC3_{G652A}$ mutant channels, we expected the physiological and benzimidazole activation to be additive. To examine the additive nature of the two activation modes we applied corresponding agonists consecutively in whole cell patch clamp recordings of HEK293 cells overexpressing WT TRPC3 channels. In the experiments where CCh stimulus was applied first followed by activation with GSK, no additive effect was observed (Figure 17). Taking the transient nature of both physiological and pharmacological responses of the channel into account and to prevent any desensitization or inactivation processes, in the next set of experiments we administered GSK at the point of maximum CCh response. Using this modified protocol, we were not able to induce TRPC3 currents by GSK administration after PLC pathway pre-activation (Figure 17).

Figure 17: The G652A mutation blunts cross-desensitization between physiological and benzimidazole-induced TRPC3 activation

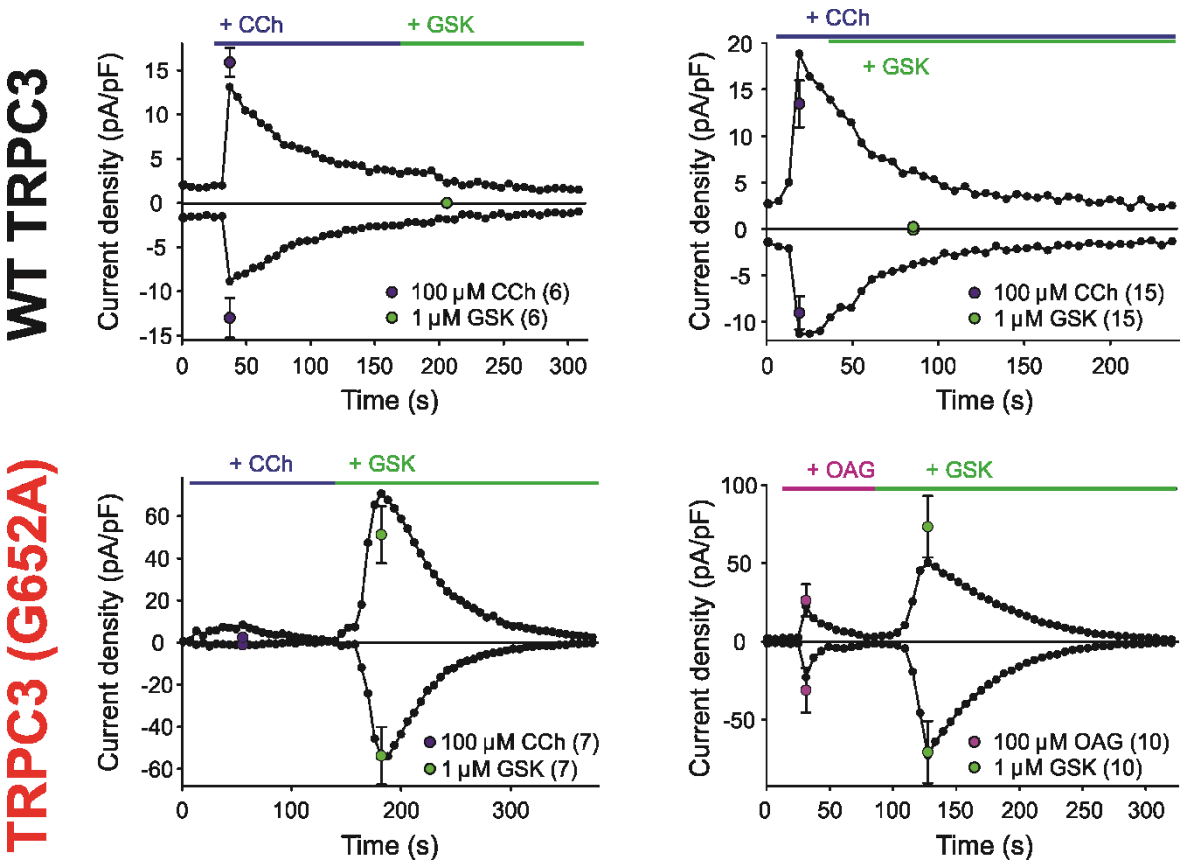

Representative time courses of current activation by 100 µM CCh followed by application of 1 µM GSK in WT (upper panel) and G652A (lower panel) TRPC3 channels derived from whole cell patch clamp recordings. In case of G652A mutant the current trace is also shown for modulation with 100 µM OAG followed by application of 1 µM GSK to compensate for lack of CCh response. Mean peak current densities ± SEM of the maximum responses due to activator addition are displayed as dots with error bars; number of cells measured is indicated in parentheses. This figure has been previously published in (72).

Likewise, switching the order of agonist application did not manifested expected additive effect (Figure 18A). While the GSK concentration used in these experiments is in its submaximum, CCh agonist was applied in saturating condition (100 µM) as is commonly done to ensure maximum stimulation of the PLC signaling. To test the hypothesis that the absence of GSK response is caused

by the close to maximum pre-stimulation via the PLC pathway, we examined GSK response of WT TRPC3 channels after minimum stimulating CCh concentration. Indeed, current generated due to GSK administration was observed in that experimental settings but its amplitude was drastically reduced in comparison to the absence of lipid-mediated pre-activation of the WT TRPC3 channels (Figure 18B). These results demonstrate that physiological and benzimidazole-mediated activation share certain features of the gating machinery for which they compete and that maximum PLC-induced activation desensitizes WT channels for benzimidazole stimulation.

Figure 18: Benzimidazole-induced and physiological TRPC3 activation mechanisms share a part of the gating machinery

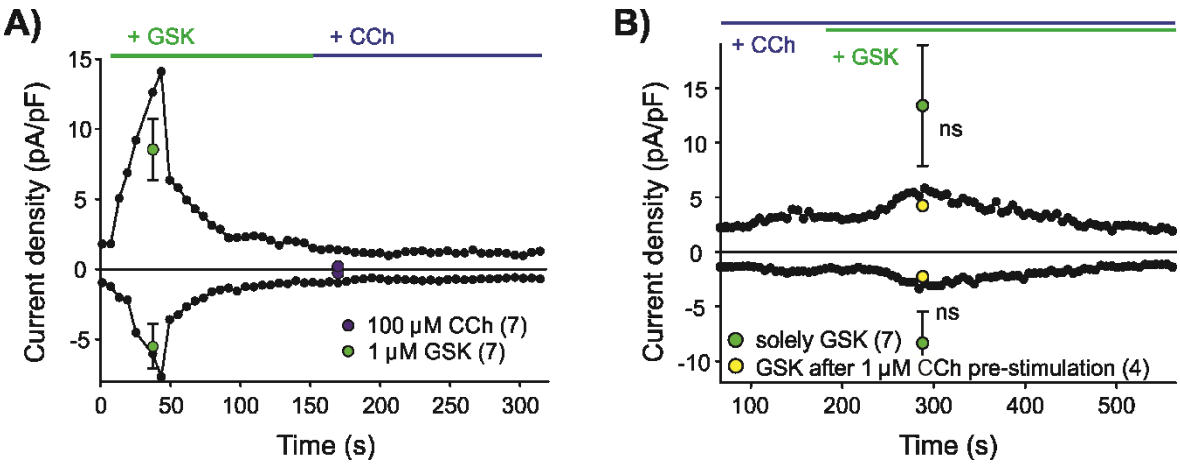

Representative time course of current activation by A) 1 µM GSK followed by application of 100 µM CCh or B) 1 µM CCh followed by administration of 1 µM GSK derived from whole cell patch clamp recordings of HEK293 cells overexpressing WT TRPC3 channels. Mean peak current densities ± SEM of the maximum responses due agonist addition are displayed as circles with error bars. Number of cells measured is indicated in parentheses. This figure has been previously published in (72).

Next, we examined if similar interference of the two activation pathways exists in the $TRPC3_{G652A}$ mutant channels. To avoid their general insensitivity to respond to endogenous stimulation via CCh, we employed in addition a DAG lipid

analogue, OAG, in the electrophysiology measurements. OAG belongs to the lipid mediators with preserved ability to induce currents also in the mutant $TRPC3_{G652A}$ channels. Unlike in WT channels, GSK was effective in current stimulation of mutant channels following a desensitizing stimulus both, by CCh or OAG (Figure 17). On the other hand, when the order of the two agonists was reversed, we failed to observe currents in response to the secondary lipid stimulus (Figure 19). This observation suggests that GSK might employ the identical elements of the gating machinery as the lipid agonists. In addition, GSK might be binding $TRPC3_{G652A}$ channels with higher affinity than the lipid preventing it from interaction with the channel resulting in lack of subsequent $TRPC3_{G652A}$ response. Alternatively, the rather large Ca^{2+} signal entering via the mutant channel upon GSK activation is large enough to induce Ca^{2+}-dependent inactivation processes which are absent or down-tuned in the WT channel. Unfortunately to confirm one or the other case more experiments would be necessary.

Collectively, the G652A mutation does not only sensitize the TRPC3 channel towards benzimidazole compounds but also circumvents the desensitization of the channel to benzimidazoles due to preceding lipid-mediated activation.

Figure 19: Benzimidazole compound desensitize $TRPC3_{G652A}$ channels for lipid-mediated activation

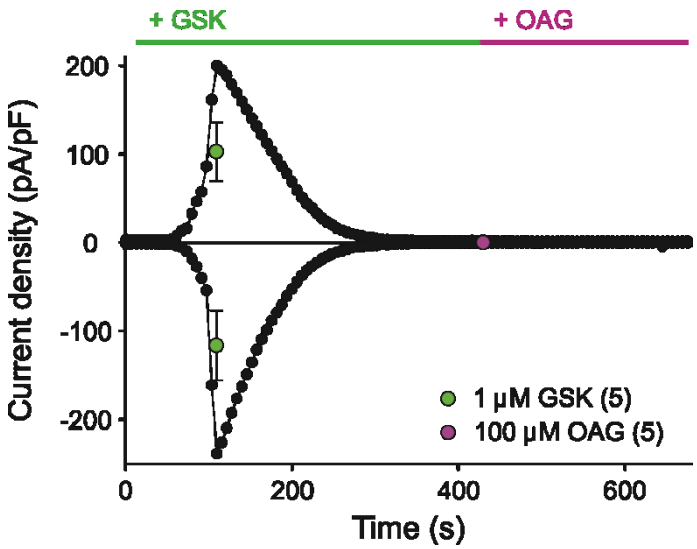

Representative time course of current generation by 1 µM GSK followed by stimulation with 100 µM OAG in $TRPC3_{G652A}$ channel derived from whole cell patch clamp recordings. Mean peak current densities ± SEM of the maximum responses due to activator addition are displayed as dots with error bars (net current); number of cells measured is indicated in parentheses.

To support our electrophysiological results, we tested the phenomenon of inhibited cross-desensitization of the mutant channel towards benzimidazoles at the level of cellular Ca^{2+} signaling. Indeed, Ca^{2+} imaging confirmed our previous findings. HEK293 cells expressing WT TRPC3 channels did not show any intracellular Ca^{2+} rise in response to GSK or BI-2 if applied after physiological stimulation with CCh (Figure 20). On the contrary, when mutant $TRPC3_{G652A}$ channels were stimulated with benzimidazoles following lipid-mediated activation, high intracellular elevations of Ca^{2+} were observed. This effect was specific to WT/G652A TRPC3 expressing cells and was absent in control WT HEK293 cells (Figure 20D). Statistical evaluation of the maximum Ca^{2+} peak amplitudes in response to benzimidazoles in the absence or presence of CCh pre-activation is depicted in Figure 20D.

Figure 20: Ca^{2+} imaging confirms $TRPC3_{G652A}$ channels do not cross-desensitize to benzimidazole stimulation after physiological stimuli

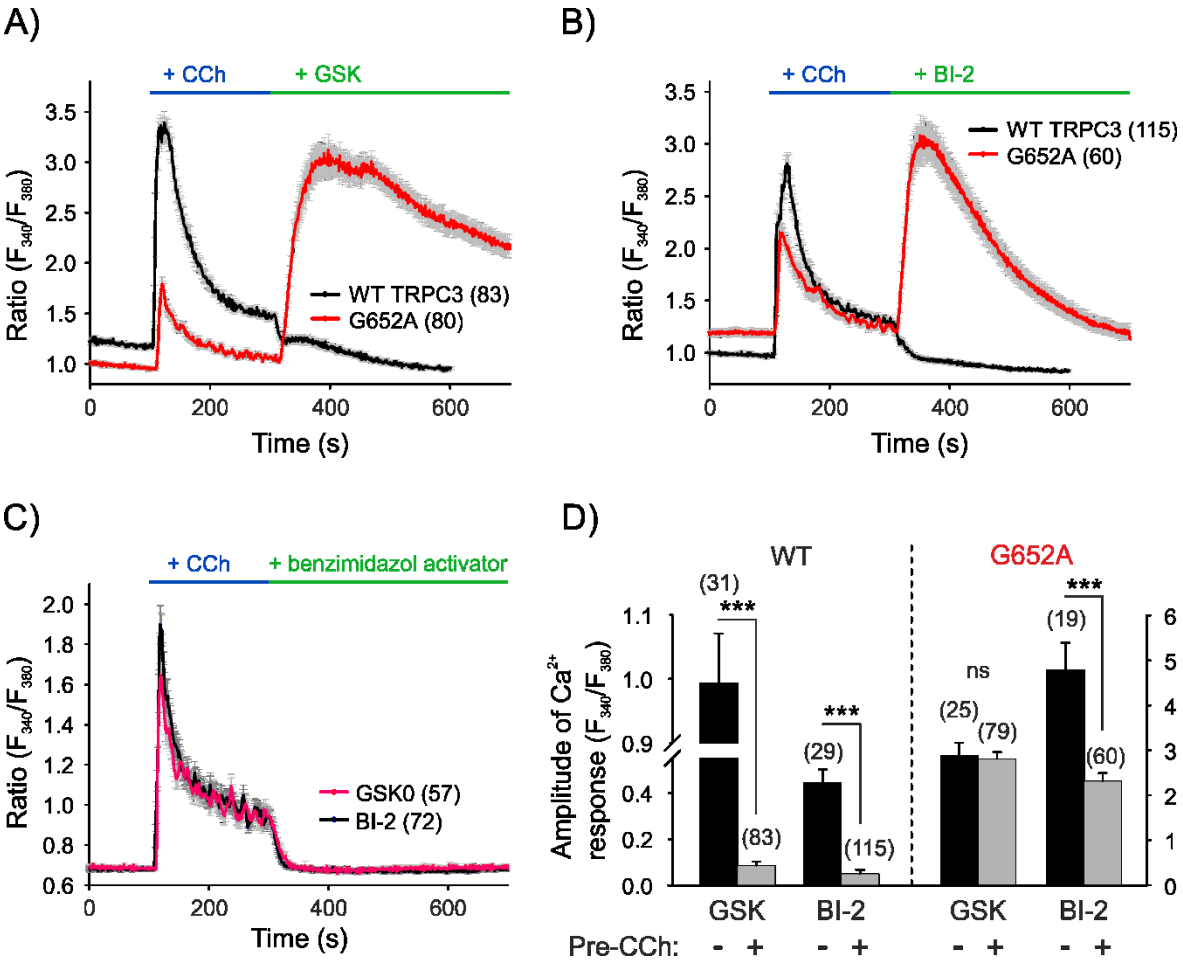

Time courses of single cell cytosolic Ca^{2+} $[Ca^{2+}]_i$ imaging experiments using FURA-2 dye in HEK293 cells overexpressing either WT or G652A TRPC3 channels stimulated with 100 µM CCh first and with A) 1 µM GSK/ B) 1 µM BI-2 second. Mean ± SEM are shown, number of cells measured is indicated in parentheses. C) Negative control $[Ca^{2+}]_i$ imaging experiments using FURA-2 dye complement to panel A) and B) performed in WT HEK293 cells stimulated with 100 µM CCh followed by 1 µM GSK/ 1 µM BI-2. D) Bar chart summarizing the amplitudes (maximum response – initial Ca^{2+} loading) of $[Ca^{2+}]_i$ increase due to benzimidazole (GSK/BI-2) administration in HEK293 cells overexpressing either WT or G652A TRPC3 channels with or without previous stimulation using 100 µM CCh. Mean ± SEM are displayed, number of cells measured is indicated in parentheses. Two tailed t-test or Mann-Whitney test were applied to evaluate the

differences between the individual groups (ns = not significant, ***p < 0.001). This figure has been previously published in (72).

7. Discussion

7.1. Structural evolution of the molecular information of TRPC3

Before the high-resolution structural information was available on any of the members of the canonical TRP subfamily, secondary structure prediction tools and homology modelling were utilized extensively to obtain a realistic idea of the molecular architecture of a protein. Our TRPC3 homology model was kindly constructed by Thomas Stockner as described in (71). The cryo-EM structure of the closest TRP relative available at that time was chosen as a template, TRPV1 in a non-conducting state (PDB ID: 3J9J). Since TRP proteins exhibit a high sequence identity only within the TMDs, our TRPC3 homology model comprises only TM helices and the pre-S1 motif, CD as well as the pseudo ECD were omitted.

For evaluation of our homology model we compared it to the cryo-EM model by Fan et al. as it displays the channel architecture in the highest resolution. Figure 21 illustrates that our model was good enough to predict the orientation and packing of the displayed TM helices. There are slight differences in folding of the adjacent subunits, the S6-TRP box turn and the last helix of the pre-S1 elbow. On the contrary the conserved glycine in S6 (G652, isoform 3) is localized right at the lipid 2 binding cavity as reported by Fan et al. (76) consistent with the prediction of a lipid recognition site by our homology model-guided mutagenesis study. The pre-S1 elbow helix in our model is turned towards the cytosolic space and tilted towards the pore axis in contrast to both cryo-EM models probably due to lack of the constrains coming from the CD that is missing in our model.

A π-turn (helical secondary structure of an amino acid chain exhibiting atypical hydrogen bonding in comparison to conventional α-helix) approximately in the middle of S6 present in our model is most probably an artefact transferred from the TRPV1 template. This π-turn was a subject of discussion amongst the structural biologists, as it was not clear whether it is a valid feature of S6 helix or an artefact resulting from computational methodology deriving models out of cryo-EM density maps (98). As a result of the boom of cryo-EM structures the current opinion in the

field of structural biology is that ways of refinement and 3D model validation are necessary in order to assess the correctness of the models as has been performed for TRPV1 (109, 110).

As a result of the π-turn in S6, the typical α-helical hydrogen bonding is disrupted, shifting the strain of the π-turn more downstream towards the TRP box. Consequently, the S6-TRP box connection observed in our homology model is different compared to the cryo-EM derived structure. While our model retains a highly ordered α-helix representation of S6-TRP box connecting loop, in the cryo-EM based model of TRPC3 this connection stays unstructured suggesting its high flexibility. The angles between the TRP box and S6 also seems to be slightly different. This property is of decisive impact since the connection between the TRP box and the HH in the CD was reported to influence TRPC3 channel activity (73). The parallel orientation of the TRP box and the HH exerts less constrains on the connecting loop between them and hence will keep the channel less active. Despite the overall fit of our homology model with the reported high-resolution cryo-EM structure, one needs to take care when working with the side chain rotamer orientations in our model, the positioning of the side chains is only estimated and hence might not reflect the reality. Consequently, the interactions within the channel assembly such as hydrogen bonding, salt bridges or hydrophobic contacts have to be considered with caution.

Of note, the conserved glycine at position 709 in TRPC6 also localizes to a lateral lipid fenestration within the cryo-EM structure of TRPC6, which is in agreement with our electrophysiological data, showing that $TRPC6_{G709A}$ channel response to physiological lipid stimuli is dramatically reduced (See Appendix, Figure 2).

Figure 21: Comparison of our TRPC3 homology model to the high-resolution cryo-EM TRPC3 structure

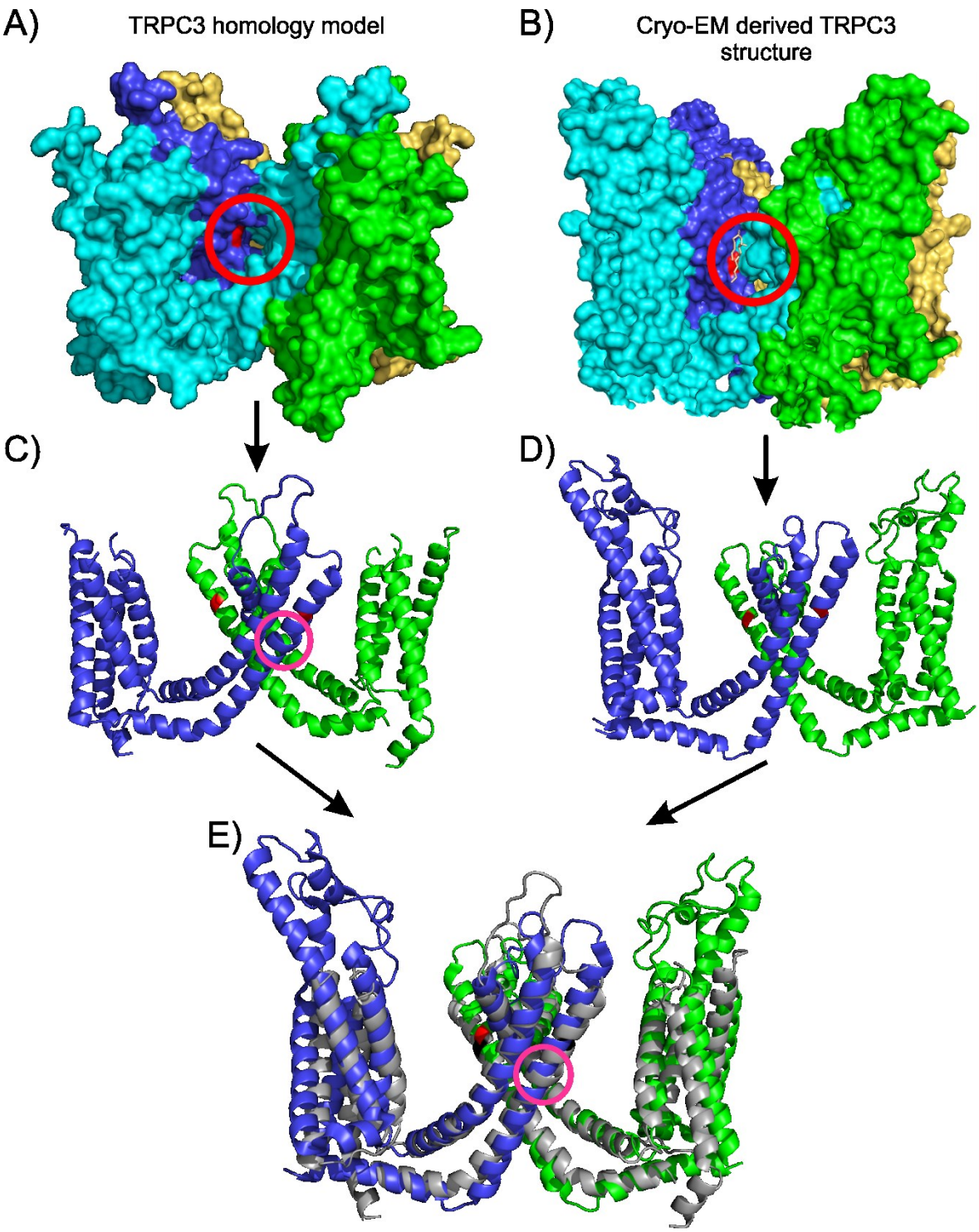

Surface representation of the TRPC3 ion channel complex A) based on TRPV1 homology model (kindly provided by Thomas Stockner as described in (71) or B) reproduced from cryo-EM imaging (PDB ID: 6CUD, (76)). The chain colour-coding

is the same as in Figure 4. G652/G640 (Isoform 3 / isoform 1) is highlighted in red (circle) lining the lipid 2 binding pocket. In B) the lipid 2 molecule is visualized in stick representation of sand colour. For more comprehensive comparison, the parts of TRPC3 tetramer missing in the homology model are also omitted in the cryo-EM structure. C) and D) show the corresponding cartoon representation of the TRPC3 dimers of the individual models. The pink circle emphasizes the π-turn in the S6 present in the homology model. E) Overlay of the TRPC3 dimer originating from the homology model (in grey) and the cryo-EM structure (coloured as in D) for better comparison.

7.2. Intramolecular TRPC3 cavities as potential agonist binding pockets

To localize and assess the suitability of channel cavities as potential modulatory sites, TRPC3 cryo-EM based molecular model published by Fan et al. (76) will be considered (PDB ID: 6CUD), provided it is the only template achieving a resolution high enough (3,3 Å respectively) to determine the precise orientation of the amino acid side chains whose configuration in 3D space plays a crucial role when discussing unoccupied chambers.

Previous results show that many TRP channel modulators tend to occupy the area around the S4-S5 linker (e.g. capsaicin in TRPV1). Similarly Tang et al. (77) reported a binding pocket for a small TRPC6 blocker, 2-(benzo[d][1,3]dioxol-5-ylamino) thiazol- 4-yl)((3 S,5 R)-3,5-dimethylpiperidin-1-yl) methanone (abbreviated BTDM), behind the lipid 1 binding cavity right at the interface of S3, S4 and S4-S5 of one subunit and S5 and S6 of the neighbouring one. The authors hypothesized that other direct lipid agonists (OAG) could access the cavity. However, their TRPC3 model proved otherwise, no density was observed in that area. This finding appears to be logical considering the TRPC3 model by Fan and co-authors shows only 2 small openings that will very unlikely accommodate any modulators (Figure 22E). The surface potential (mostly neutral or slightly positive) of that cavity also does not resemble either of the lipid1/2 binding pockets and hence does not appear suitable for accommodating lipid molecules.

A considerably larger fenestration that the one discussed above can be found just below the conserved glycine involved in TRPC3 gating, G640 (Isoform 1). On

the interface between two neighbouring subunits, S6 on one side and the pore helix and S5 on the other, there are two openings protruding directly to the core of the permeation pathway (Figure 22E, H). It has been reported for some channels that such lateral fenestration leading to the pore works as a point of entry for physical occlusion of the permeation pathway by lipids. Such mechanism of gating was previously reported for mechanosensitive TRAAK channel (114). Nevertheless, the orientation of the lipid 2 recorded in the TRPC3 structure by Fan et al. disproves it. In addition, there is a strong electrostatic barrier coming from the large negative charge on the pore-facing side of this opening, therefore a lipid molecule penetrating into that opening would have to face strong repulsive forces.

A remarkable channel cavity is localized in the pseudo ECD (Figure 22A, D). Unlike the other cavities or fenestrations discussed before, it is easily accessible from the extracellular pool. Therefore, even polar compounds encountering hydrophobicity barrier upon crossing the lipid bilayer can reach it comfortably. The cavity spreads from under the extracellular extension of S3 of one subunit receding quite deep in the direction of cytosolic side of the membrane along the S4 and S1 of one subunit and S5 and the pore loop of the adjacent subunit. Since there is a direct connection of that cavity to the pore and SF (via hydrogen bridging of Y589 (isoform 1)), modulation of the channel activity from that site is highly probable. Of note, DkTx – spider toxin binds to TRPV1 in similar location (81).

Where could the benzimidazole compounds bind within the TRPC3 channel architecture? The benzimidazole analogues do not carry charges and are not highly polar despite having some polar moieties that could allow them to orient themselves slightly in a polar/charged environment. Although the ECD cavity would be the easiest to reach it exhibits quite charged surface that would exert electrostatic hindrance on benzimidazoles accessing it. Moreover, the overall hydrophobic nature of benzimidazole compounds allows them to penetrate deeper into the lipid bilayer and hence access more hydrophobic patches in TPRC3 architecture.

Figure 22: Structural analysis of electrostatic surface potential of TRPC3 channel complex

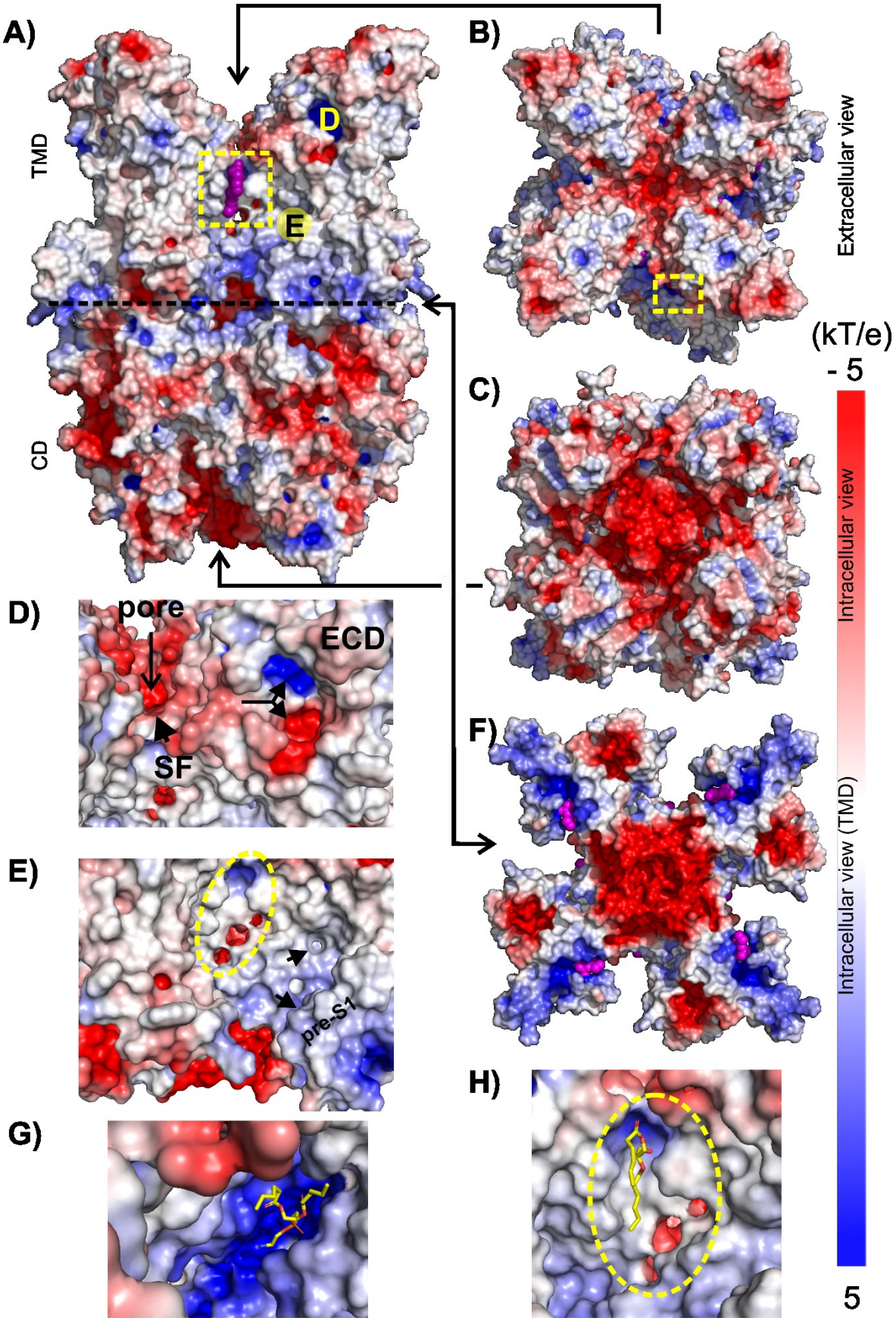

A) Side view of the total TRPC3 ion channel assembly in surface potential representation based on the cryo-EM structure published by Fan et al. (76). Yellow dashed square denotes the lipid 2 (sphere representation) in its binding pocket close to the lateral fenestration penetrating directly into the pore. Letters localize the magnified areas in the following panels. B) Extracellular view of the TRPC3 tetramer, notice the negatively charged pore mouth equipped for attraction of cations. The yellow dashed rectangle illustrates where the lipid 1 is wedged into the cavity behind the pre-S1 elbow visible only partially from the extracellular perspective. C) Intracellular view of the pore opening; notice the central CC domain formed by VHs that carries a strong negative charge. D) Bi-polar extracellular cavity accomodated by the elongated S3 helix adjacent and connected to the SF potentially allowing for modulation of TRPC3 function. E) Magnified view of the lipid window (lipid 2 binding pocket, denoted with yellow dashed shape), lateral fenestration into the pore, BTDM ‘opening‘ marked with an arrowhead. The adjacent lipid 1 binding pocket covered by the pre-S1 elbow is labelled with an arrowhead too. F) Intracellular view of the pore just at the lipid bilayer/cytosol interface as denoted by the black dashed line in panel A). Notice the strong negative charge of the pore lining. Lipid 1 molecules depicted in magenta spheres can be observed on the outer circumference in positively charged patches. Orientation of the lipid 1 molecule within its highly positive binding pocket is shown in panel G). Note the beneficial orientation of the lipid molecule within the binding pocket to minimize the repulsive electrostatic forces. H) Magnification of the lipid 2 binding pocket. Despite overal neutral surface the lipid 2 molecule orients itself with the polar head towards the positive patch and the hydrophobic tale towards the neutral surface of the binding site. The yellow dashed oval shape marks the identical area as in panel E). The scale bar on the right shows the surface potential range.

Regarding the importance of the functional groups of benzimidazole analogues for a potent stimulation of the channel, according to our electrophysiology data, Cl attached to the benzimidazole core is not vital for activity. Probably due to the hydrophobic barrier it might encounter upon accession of the deeper buried cavities. On the other hand, the thiophen ring and the hydrophobic tail at the opposite pole of the benzimidazole molecule seems to have a positive impact on

the agonist potency. These 2 poles of the benzimidazole molecule distantly resemble the polar head and a hydrophobic tail of a lipid molecule, only of lesser polarity. Consequently, the expectation is that benzimidazole compounds will bind to overall hydrophobic pockets resembling the lipid 2 binding site.

7.3. Glycine 652 is a pivotal determinant of both lipid and benzimidazole TRPC3 modulation

We aimed to characterize the modulation behaviour of a functionally unique TRPC3 mutant channel. Investigating the hypothesis of G652 being the flexible point or hinge point vital for gating rearrangements as previously reported for K^+- and Na^+-voltage gated channels [89, 96], we can sum up the following observations:

The G652A mutant is largely insensitive to physiological stimulation via CCh. On the other hand our functional electrophysiological data demonstrate that certain exogenous TRPC3 lipid agonists can activate the mutant channel to a higher extent than the WT channel (e.g. DiC8 (71)). The modified lipid activation profile of the $TRPC3_{G652A}$ channels indicates that G652 is direct part of the lipid-binding pocket as suggested by our TRPC3 homology model and confirmed by high resolution structure by cryo-EM microscopy later. Consistent with our results, Fan et al. report direct hydrophobic interaction of the glycine side chain with the hydrocarbon tail of lipid 2 (76).

Interestingly, while we observed similarly distinct activation profiles in WT and G652A TRPC3 channels in response to benzimidazole compounds, our concentration-response curve of BI-2 modulation suggests that glycine 652 does not directly participate in benzimidazole recognition. It is more likely that G652's effect in benzimidazole gating is solely driven by the shape of the binding pocket. In agreement with this hypothesis, introduction of bulkier and more rigid side chains at position 652 (G652L (71)) reduces the channel's response to GSK. Nevertheless, even if G652 does not coordinate the benzimidazole binding in the 'lipid window' directly, as discussed in section 7.2. there remain multiple potential binding cavities within the TRPC3 channel assembly accessible to small modulatory compounds.

While benzimidazole and physiological modulation of $TRPC3_{G652A}$ channels contrast each other in many aspects, our additivity experiments demonstrate certain overlap of the two activation mechanisms in WT TRPC3 channels. Presence of the first stimulus, irrespective whether it is direct stimulation via benzimidazole compounds or physiological activation via the PLC pathway, prevented further increase in current as a consequence of the application of the second agonist in WT TRPC3 channels. CCh pre-sensitized WT channels cross-desensitized for subsequent benzimidazole activation even at early stage of inactivation/desensitization processes. Only upon minimizing the PLC-derived activating stimulus to minimum GSK response of WT channels was detectable but never reaching its full maximum (Figure 18B). On the contrary, $TRPC3_{G652A}$ channels exhibited full benzimidazole activation after saturating initial lipid-stimulus. Interestingly, when the order of the stimulating agonists was swapped, $TRPC3_{G652A}$ channels responded like WT channels (Figure 19). Of note, the Ca^{2+} signal due to GSK stimulation of $TRPC3_{G652A}$ channels is substantially higher than the one due to OAG administration, therefore Ca^{2+}-dependent inactivation/desensitization processes might be triggered earlier during that particular experimental settings and cause the lack of subsequent OAG-derived current. Hence, we conclude that both kinds of activating stimuli share parts of the TRPC3 gating machinery and that crosstalk within the TRPC3 architecture exists probably preventing overactivity of the channel caused by integration of multiple activating stimuli. Collectively, G652 and the flexibility it provides to the S6 helix serves as a critical gating element of physiological and pharmacological modulation of TRPC3 channels.

7.4. $TRPC3_{G652A}$ mutant channels as a tool for chemogenetic control in complex tissues

In the present work we characterized pharmacological features of the $TRPC3_{G652A}$ mutant channel. Our findings suggest that the mutant channel exhibits diminished sensitivity to physiological stimuli conveyed via PLC pathway as well as altered sensitivity profile to other directly-administered lipid agonists. At the same time the mutant channel retains sensitivity to benzimidazole compounds employing different gating pattern. Likewise, $TRPC3_{G652A}$ current can be ‘tuned’ to

desired amplitude with various benzimidazole structural analogues generating a distinct response than in WT TRPC3 channels. These unique characteristics of $TRPC3_{G652A}$ channel make it a suitable tool for selectively addressing the function of TRPC channels in various tissue. Combining gene therapy with pharmacological control of recombinant channels might prove effective in dissecting TRPC contributions in cellular processes. The chemogenetic control will allow for selective tracking of recombinant mutant channels separating them from endogenous TRPC-dependent functions. Mutations as a tool for chemogenetic targeting strategies, could be applied in studies deciphering the selective role of TRPC channels in that particular tissue. Hence, we provide the basis for direct intervention to precisely manipulate TRPC3 signaling in complex native tissues such as the brain, heart or tumors.

8. Conclusion

The goal of this study was the identification and description of the TRPC3 gating machinery in the context of physiological and pharmacological activation. A number of non-conventional techniques have been used in order to accomplish the task: site-directed mutagenesis, functional electrophysiological techniques, live intracellular Ca^{+2} imaging and TIRF microscopy.

Although not all research questions were provided with a conclusive answer, the results collected are valuable as pointers and boundaries to guide future investigations. We brought the scientific knowledge of the TRPC3 channel gating machinery forward by characterizing a gating relevant G652A (Isoform 3) mutation in the context of physiological and pharmacological activation. Undoubtedly, obtaining the high-resolution molecular model of TRPC3 by cryo-EM imaging was an important milestone in the structural TRPC channel field, providing a solid foundation not only for basic research but also for physiological studies.

As has been done already for other channel complexes such as Orai (115) and IP3R (116), the next step in describing the molecular components of the TRPC3 gating mechanism is acquiring the near atomic resolution structure in its conducting state. This will allow for definitive precise mapping of the regions undergoing structural rearrangements upon gating.

Along with the high resolution TRPC3 model, computational and bioinformatic tools may be employed to carry out educated and systematic design of therapeutic compounds targeting TRPC3. This strategy will ensure high standards while optimizing for high selectivity and efficacy of pharmacological tools applicable in TRPC-related physiological research. Additionally, it provides the advantage of minimizing adverse effects of potential TRPC3 therapeutic agents, by providing a highly efficient straight forward approach to drug design.

9. Bibliography

1. Montell C. The TRP superfamily of cation channels. Sci STKE. 2005 Feb 22;2005(272):re3.
2. Clapham DE. TRP channels as cellular sensors. Nature. 2003 Dec;426(6966):517–24.
3. Huang K, Diener DR, Mitchell A, Pazour GJ, Witman GB, Rosenbaum JL. Function and dynamics of PKD2 in Chlamydomonas reinhardtii flagella. J Cell Biol. 2007 Nov 5;179(3):501–14.
4. Calupca MA, Locknar SA, Parsons RL. TRPC6 immunoreactivity is colocalized with neuronal nitric oxide synthase in extrinsic fibers innervating guinea pig intrinsic cardiac ganglia. J Comp Neurol. 2002 Aug 26;450(3):283–91.
5. Elsaesser R, Montani G, Tirindelli R, Paysan J. Phosphatidyl-inositide signalling proteins in a novel class of sensory cells in the mammalian olfactory epithelium. Eur J Neurosci. 2005 May 1;21(10):2692–700.
6. Warren EJ, Allen CN, Brown RL, Robinson DW. The light-activated signaling pathway in SCN-projecting rat retinal ganglion cells. Eur J Neurosci. 2006 May;23(9):2477–87.
7. Okada T, Inoue R, Yamazaki K, Maeda A, Kurosaki T, Yamakuni T, et al. Molecular and functional characterization of a novel mouse transient receptor potential protein homologue TRP7. Ca(2+)-permeable cation channel that is constitutively activated and enhanced by stimulation of G protein-coupled receptor. J Biol Chem. 1999 Sep 24;274(39):27359–70.
8. Yang L-L, Liu B-C, Lu X-Y, Yan Y, Zhai Y-J, Bao Q, et al. Inhibition of TRPC6 reduces non-small cell lung cancer cell proliferation and invasion.

Oncotarget. 2017 Jan 17;8(3):5123–34.

9. Tiruppathi C, Freichel M, Vogel SM, Paria BC, Mehta D, Flockerzi V, et al. Impairment of store-operated Ca2+ entry in TRPC4(-/-) mice interferes with increase in lung microvascular permeability. Circ Res. 2002 Jul 12;91(1):70–6.
10. Yu Y, Sweeney M, Zhang S, Platoshyn O, Landsberg J, Rothman A, et al. PDGF stimulates pulmonary vascular smooth muscle cell proliferation by upregulating TRPC6 expression. Am J Physiol Physiol. 2003 Feb;284(2):C316–30.
11. Freichel M, Vennekens R, Olausson J, Stolz S, Philipp SE, Weissgerber P, et al. Functional role of TRPC proteins in native systems: implications from knockout and knock-down studies. J Physiol. 2005 Aug 15;567(Pt 1):59–66.
12. Dietrich A, Gudermann T. TRPC6: Physiological Function and Pathophysiological Relevance. In: Handbook of experimental pharmacology. 2014. p. 157–88.
13. Dryer SE, Roshanravan H, Kim EY. TRPC channels: Regulation, dysregulation and contributions to chronic kidney disease. Biochim Biophys Acta - Mol Basis Dis. 2019 Jun 1;1865(6):1041–66.
14. Beech DJ. Emerging functions of 10 types of TRP cationic channel in vascular smooth muscle. Clin Exp Pharmacol Physiol. 2005 Aug;32(8):597–603.
15. Tiruppathi C, Ahmmed GU, Vogel SM, Malik AB. Ca 2+ Signaling, TRP Channels, and Endothelial Permeability. Microcirculation. 2006 Jan 1;13(8):693–708.
16. Kim BJ, So I, Kim KW. The relationship of TRP channels to the pacemaker activity of interstitial cells of Cajal in the gastrointestinal tract. J Smooth Muscle Res. 2006 Feb;42(1):1–7.
17. Strübing C, Krapivinsky G, Krapivinsky L, Clapham DE. TRPC1 and TRPC5 Form a Novel Cation Channel in Mammalian Brain. Neuron. 2001 Mar 1;29(3):645–55.
18. Strübing C, Krapivinsky G, Krapivinsky L, Clapham DE. Formation of novel TRPC channels by complex subunit interactions in embryonic brain. J Biol Chem. 2003 Oct 3;278(40):39014–9.
19. Gomis A, Soriano S, Belmonte C, Viana F. Hypoosmotic- and pressure-

induced membrane stretch activate TRPC5 channels. J Physiol. 2008 Dec 1;586(Pt 23):5633–49.

20. Maroto R, Raso A, Wood TG, Kurosky A, Martinac B, Hamill OP. TRPC1 forms the stretch-activated cation channel in vertebrate cells. Nat Cell Biol. 2005 Feb;7(2):179–85.
21. Spassova MA, Hewavitharana T, Xu W, Soboloff J, Gill DL. A common mechanism underlies stretch activation and receptor activation of TRPC6 channels. Proc Natl Acad Sci. 2006 Oct 31;103(44):16586–91.
22. Obukhov AG, Nowycky MC. TRPC4 can be activated by G-protein-coupled receptors and provides sufficient Ca2+ to trigger exocytosis in neuroendocrine cells. J Biol Chem. 2002 May 3;277(18):16172–8.
23. Riccio A, Li Y, Moon J, Kim K-S, Smith KS, Rudolph U, et al. Essential role for TRPC5 in amygdala function and fear-related behavior. Cell. 2009 May 15;137(4):761–72.
24. Zhang Z, Reboreda A, Alonso A, Barker PA, Séguéla P. TRPC channels underlie cholinergic plateau potentials and persistent activity in entorhinal cortex. Hippocampus. 2011 Apr 1;21(4):386–97.
25. Zhou J, Du W, Zhou K, Tai Y, Yao H, Jia Y, et al. Critical role of TRPC6 channels in the formation of excitatory synapses. Nat Neurosci. 2008 Jul 30;11(7):741–3.
26. Storch U, Forst A-L, Philipp M, Gudermann T, Mederos y Schnitzler M. Transient receptor potential channel 1 (TRPC1) reduces calcium permeability in heteromeric channel complexes. J Biol Chem. 2012 Jan 27;287(5):3530–40.
27. Jia Y, Zhou J, Tai Y, Wang Y. TRPC channels promote cerebellar granule neuron survival. Nat Neurosci. 2007 May 1;10(5):559–67.
28. Westlund KN, Zhang LP, Ma F, Nesemeier R, Ruiz JC, Ostertag EM, et al. A rat knockout model implicates TRPC4 in visceral pain sensation. Neuroscience. 2014 Mar 14;262:165–75.
29. Wei H, Sagalajev B, Yüzer MA, Koivisto A, Pertovaara A. Regulation of neuropathic pain behavior by amygdaloid TRPC4/C5 channels. Neurosci Lett. 2015 Nov 3;608:12–7.
30. Ikeda K, Nakajima T, Yamamoto Y, Takano N, Tanaka T, Kikuchi H, et al. Roles of transient receptor potential canonical (TRPC) channels and

reverse-mode Na+/Ca2+ exchanger on cell proliferation in human cardiac fibroblasts: Effects of transforming growth factor β1. Cell Calcium. 2013 Sep 1;54(3):213–25.

31. Seth M, Zhang Z-S, Mao L, Graham V, Burch J, Stiber J, et al. TRPC1 channels are critical for hypertrophic signaling in the heart. Circ Res. 2009 Nov 6;105(10):1023–30.
32. Camacho Londoño JE, Tian Q, Hammer K, Schröder L, Camacho Londoño J, Reil JC, et al. A background Ca2+ entry pathway mediated by TRPC1/TRPC4 is critical for development of pathological cardiac remodelling. Eur Heart J. 2015 Sep 1;36(33):2257–66.
33. Yue Z, Xie J, Yu AS, Stock J, Du J, Yue L. Role of TRP channels in the cardiovascular system. Am J Physiol Heart Circ Physiol. 2015 Feb 1;308(3):H157-82.
34. Seo K, Rainer PP, Lee D-I, Hao S, Bedja D, Birnbaumer L, et al. Hyperactive adverse mechanical stress responses in dystrophic heart are coupled to transient receptor potential canonical 6 and blocked by cGMP-protein kinase G modulation. Circ Res. 2014 Feb 28;114(5):823–32.
35. Harada M, Luo X, Qi XY, Tadevosyan A, Maguy A, Ordog B, et al. Transient receptor potential canonical-3 channel-dependent fibroblast regulation in atrial fibrillation. Circulation. 2012 Oct 23;126(17):2051–64.
36. Makarewich CA, Zhang H, Davis J, Correll RN, Trappanese DM, Hoffman NE, et al. Transient receptor potential channels contribute to pathological structural and functional remodeling after myocardial infarction. Circ Res. 2014 Aug 29;115(6):567–80.
37. Freichel M, Berlin M, Schürger A, Mathar I, Bacmeister L, Medert R, et al. TRP Channels in the Heart. Neurobiology of TRP Channels. CRC Press/Taylor & Francis; 2017.
38. Kuwahara K, Wang Y, McAnally J, Richardson JA, Bassel-Duby R, Hill JA, et al. TRPC6 fulfills a calcineurin signaling circuit during pathologic cardiac remodeling. J Clin Invest. 2006 Dec;116(12):3114–26.
39. Ahmad AA, Streiff M, Hunter C, Hu Q, Sachse FB. Physiological and pathophysiological role of transient receptor potential canonical channels in cardiac myocytes. Prog Biophys Mol Biol. 2017;130:254–63.
40. Riccio A, Li Y, Tsvetkov E, Gapon S, Yao GL, Smith KS, et al. Decreased

anxiety-like behavior and Gαq/11-dependent responses in the amygdala of mice lacking TRPC4 channels. J Neurosci. 2014 Mar 5;34(10):3653–67.

41. Tai C, Hines DJ, Choi HB, MacVicar BA. Plasma membrane insertion of TRPC5 channels contributes to the cholinergic plateau potential in hippocampal CA1 pyramidal neurons. Hippocampus. 2011 Sep 1;21(9).
42. Wescott SA, Rauthan M, Xu XZS. When a TRP goes bad: transient receptor potential channels in addiction. Life Sci. 2013 Mar 19;92(8–9):410–4.
43. Hong C, Seo H, Kwak M, Jeon J, Jang J, Jeong EM, et al. Increased TRPC5 glutathionylation contributes to striatal neuron loss in Huntington's disease. Brain. 2015 Oct;138(Pt 10):3030–47.
44. Mizoguchi Y, Monji A. TRPC Channels and Brain Inflammation. In: Adv Exp Med Biol. 2017. p. 111–21.
45. Liu Z, Ma C, Zhao W, Zhang Q, Xu R, Zhang H, et al. High Glucose Enhances Isoflurane-Induced Neurotoxicity by Regulating TRPC-Dependent Calcium Influx. Neurochem Res. 2017 Apr 6;42(4):1165–78.
46. Yang Z, Wu F, Zhang S-L. Effects of ganoderic acids on epileptiform discharge hippocampal neurons: insights from alterations of BDNF,TRPC3 and apoptosis. Pharmazie. 2016 Jun;71(6):340–4.
47. Min S-J, Kang T-C. Positive feedback role of TRPC3 in TNF-α-mediated vasogenic edema formation induced by status epilepticus independent of ETB receptor activation. Neuroscience. 2016 Nov 19;337:37–47.
48. Winn MP, Conlon PJ, Lynn KL, Farrington MK, Creazzo T, Hawkins AF, et al. A mutation in the TRPC6 cation channel causes familial focal segmental glomerulosclerosis. Science. 2005 Jun 17;308(5729):1801–4.
49. Heeringa SF, Möller CC, Du J, Yue L, Hinkes B, Chernin G, et al. A novel TRPC6 mutation that causes childhood FSGS. PLoS One. 2009 Nov 10;4(11):e7771.
50. Du W, Huang J, Yao H, Zhou K, Duan B, Wang Y. Inhibition of TRPC6 degradation suppresses ischemic brain damage in rats. J Clin Invest. 2010 Oct;120(10):3480.
51. Li H, Huang J, Du W, Jia C, Yao H, Wang Y. TRPC6 inhibited NMDA receptor activities and protected neurons from ischemic excitotoxicity. J Neurochem. 2012 Dec 1;123(6):1010–8.
52. Wang J, Lu R, Yang J, Li H, He Z, Jing N, et al. TRPC6 specifically interacts

with APP to inhibit its cleavage by γ-secretase and reduce Aβ production. Nat Commun. 2015 Nov 19;6:8876.

53. Li S, Wang J, Wei Y, Liu Y, Ding X, Dong B, et al. Crucial role of TRPC6 in maintaining the stability of HIF-1α in glioma cells under hypoxia. J Cell Sci. 2015 Sep 1;128(17):3317–29.
54. Ding X, He Z, Zhou K, Cheng J, Yao H, Lu D, et al. Essential Role of TRPC6 Channels in G2/M Phase Transition and Development of Human Glioma. JNCI J Natl Cancer Inst. 2010 Jul 21;102(14):1052–68.
55. Satoh S, Tanaka H, Ueda Y, Oyama J, Sugano M, Sumimoto H, et al. Transient receptor potential (TRP) protein 7 acts as a G protein-activated Ca2+ channel mediating angiotensin II-induced myocardial apoptosis. Mol Cell Biochem. 2007 Jan 19;294(1–2):205–15.
56. Alvarez J, Coulombe A, Cazorla O, Ugur M, Rauzier J-M, Magyar J, et al. ATP/UTP activate cation-permeable channels with TRPC3/7 properties in rat cardiomyocytes. Am J Physiol Circ Physiol. 2008 Jul;295(1):H21–8.
57. Hofmann T, Obukhov AG, Schaefer M, Harteneck C, Gudermann T, Schultz G. Direct activation of human TRPC6 and TRPC3 channels by diacylglycerol. Nature. 1999 Jan 21;397(6716):259–63.
58. Albert AP, Pucovsky V, Prestwich SA, Large WA. TRPC3 properties of a native constitutively active Ca2+-permeable cation channel in rabbit ear artery myocytes. J Physiol. 2006 Mar 1;571(Pt 2):361–9.
59. Dietrich A, Mederos y Schnitzler M, Emmel J, Kalwa H, Hofmann T, Gudermann T. N-linked protein glycosylation is a major determinant for basal TRPC3 and TRPC6 channel activity. J Biol Chem. 2003 Nov 28;278(48):47842–52.
60. Ong HL, Souza LB De, Ambudkar IS. Calcium Entry Pathways in Non-excitable Cells. 2016;898:87–109.
61. Worley PF, Zeng W, Huang GN, Yuan JP, Kim JY, Lee MG, et al. TRPC channels as STIM1-regulated store-operated channels. Cell Calcium. 2007 Aug;42(2):205–11.
62. Kim MS, Hong JH, Li Q, Shin DM, Abramowitz J, Birnbaumer L, et al. Deletion of TRPC3 in mice reduces store-operated Ca2+ influx and the severity of acute pancreatitis. Gastroenterology. 2009 Oct;137(4):1509–17.
63. Choi S, Maleth J, Jha A, Lee KP, Kim MS, So I, et al. The TRPCs–STIM1–

Orai Interaction. In: Handb Exp Pharmacol. 2014. p. 1035–54.

64. Lee KP, Yuan JP, So I, Worley PF, Muallem S. STIM1-dependent and STIM1-independent function of transient receptor potential canonical (TRPC) channels tunes their store-operated mode. J Biol Chem. 2010 Dec 3;285(49):38666–73.

65. Smyth JT, Lemonnier L, Vazquez G, Bird GS, Putney JW. Dissociation of Regulated Trafficking of TRPC3 Channels to the Plasma Membrane from Their Activation by Phospholipase C. J Biol Chem. 2006 Apr 28;281(17):11712–20.

66. Svobodova B, Groschner K. Mechanisms of lipid regulation and lipid gating in TRPC channels. Cell Calcium. 2016;59(6):271–9.

67. Qu C, Ding M, Zhu Y, Lu Y, Du J, Miller M, et al. Pyrazolopyrimidines as Potent Stimulators for Transient Receptor Potential Canonical 3/6/7 Channels. J Med Chem. 2017;60(11):4680–92.

68. Leuner K, Heiser JH, Derksen S, Mladenov MI, Fehske CJ, Schubert R, et al. Simple 2,4-Diacylphloroglucinols as Classic Transient Receptor Potential-6 Activators--Identification of a Novel Pharmacophore. Mol Pharmacol. 2010 Mar 1;77(3):368–77.

69. Xu X, Lozinskaya I, Costell M, Lin Z, Ball JA, Bernard R, et al. Characterization of Small Molecule TRPC3 and TRPC6 agonist and Antagonists. Biophys J. 2013;104(2):454a.

70. Doleschal B, Primessnig U, Wö Lkart G, Wolf S, Schernthaner M, Lichtenegger M, et al. TRPC3 contributes to regulation of cardiac contractility and arrhythmogenesis by dynamic interaction with NCX1. Cardiovasc Res. 2015;106(1):163–73.

71. Lichtenegger M, Tiapko O, Svobodova B, Stockner T, Glasnov TN, Schreibmayer W, et al. An optically controlled probe identifies lipid-gating fenestrations within the TRPC3 channel. Nat Chem Biol. 2018 Mar 19;14(4):396–404.

72. Svobodova B, Lichtenegger M, Platzer D, Di Giuro CML, de la Cruz GG, Glasnov T, et al. A single point mutation in the TRPC3 lipid-recognition window generates supersensitivity to benzimidazole channel activators. Cell Calcium. 2019;79:27–34.

73. Sierra-Valdez F, Azumaya CM, Romero LO, Nakagawa T, Cordero-Morales

JF. Structure–function analyses of the ion channel TRPC3 reveal that its cytoplasmic domain allosterically modulates channel gating. J Biol Chem. 2018 Oct 12;293(41):16102–14.

74. Guedes de la Cruz G, Svobodova B, Lichtenegger M, Tiapko O, Groschner K, Glasnov T. Intensified Microwave-Assisted N-Acylation Procedure – Synthesis and Activity Evaluation of TRPC3 Channel Agonists with a 1,3-Dihydro-2H-benzo[d]imidazol-2-one Core. Synlett. 2016 Dec 8;28(06):695–700.
75. Tiapko O, Shrestha N, Lindinger S, Guedes de la Cruz G, Graziani A, Klec C, et al. Lipid-independent control of endothelial and neuronal TRPC3 channels by light. Chem Sci. 2019 Mar 7;10(9):2837–42.
76. Fan C, Choi W, Sun W, Du J, Lu W. Structure of the human lipid-gated cation channel TRPC3. Elife. 2018;7.
77. Tang Q, Guo W, Zheng L, Wu J-X, Liu M, Zhou X, et al. Structure of the receptor-activated human TRPC6 and TRPC3 ion channels. Cell Res. 2018 Jul 26;28(7):746–55.
78. Vinayagam D, Mager T, Apelbaum A, Bothe A, Merino F, Hofnagel O, et al. Electron cryo-microscopy structure of the canonical TRPC4 ion channel. Elife. 2018;7.
79. Duan J, Li Z, Li J, Santa-Cruz A, Sanchez-Martinez S, Zhang J, et al. Structure of full-length human TRPM4. Proc Natl Acad Sci U S A. 2018;115(10):2377–82.
80. Paulsen CE, Armache J-P, Gao Y, Cheng Y, Julius D. Structure of the TRPA1 ion channel suggests regulatory mechanisms. Nature. 2015 Sep 22;525(7570):552–552.
81. Cao E, Liao M, Cheng Y, Julius D. TRPV1 structures in distinct conformations reveal activation mechanisms. Nature. 2013;504(7478):113–8.
82. Duan J, Li J, Chen G-L, Zeng B, Xie K, Peng X, et al. Cryo-EM structure of the receptor-activated TRPC5 ion channel at 2.9 angstrom resolution. bioRxiv. 2018 Nov 11;467969.
83. Liu X, Singh BB, Ambudkar IS. TRPC1 is required for functional store-operated Ca2+ channels. Role of acidic amino acid residues in the S5-S6 region. J Biol Chem. 2003 Mar 28;278(13):11337–43.

84. van Rossum DB, Patterson RL, Sharma S, Barrow RK, Kornberg M, Gill DL, et al. Phospholipase Cgamma1 controls surface expression of TRPC3 through an intermolecular PH domain. Nature. 2005;434(7029):99–104.
85. Patterson RL, van Rossum DB, Ford DL, Hurt KJ, Bae SS, Suh PG, et al. Phospholipase C-gamma is required for agonist-induced Ca2+ entry. Cell. 2002;111:529–41.
86. Eder P, Molkentin JD. TRPC channels as effectors of cardiac hypertrophy. Circ Res. 2011 Jan 21;108(2):265–72.
87. Sinkins WG, Goel M, Estacion M, Schilling WP. Association of immunophilins with mammalian TRPC channels. J Biol Chem. 2004 Aug 13;279(33):34521–9.
88. Harikishore A, Sup Yoon H. Immunophilins: Structures, Mechanisms and Ligands. Curr Mol Pharmacol. 2015 Dec 7;9(1):37–47.
89. Liao M, Cao E, Julius D, Cheng Y. Structure of the TRPV1 ion channel determined by electron cryo-microscopy. Nature. 2013 Dec 5;504(7478):107.
90. Lichtenegger M, Stockner T, Poteser M, Schleifer H, Platzer D, Romanin C, et al. A novel homology model of TRPC3 reveals allosteric coupling between gate and selectivity filter. Cell Calcium. 2013 Sep 1;54(3):175–85.
91. Hanson SM, Sansom MSP, Becker EBE. Modeling Suggests TRPC3 Hydrogen Bonding and Not Phosphorylation Contributes to the Ataxia Phenotype of the *Moonwalker* Mouse. Biochemistry. 2015 Jul 7;54(26):4033–41.
92. Becker EBE, Oliver PL, Glitsch MD, Banks GT, Achilli F, Hardy A, et al. A point mutation in TRPC3 causes abnormal Purkinje cell development and cerebellar ataxia in moonwalker mice. Proc Natl Acad Sci U S A. 2009 Apr 21;106(16):6706–11.
93. Becker EBE. The Moonwalker Mouse: New Insights into TRPC3 Function, Cerebellar Development, and Ataxia. 2014;
94. Hanson SM, Sansom MSP, Becker EBE. Modeling Suggests TRPC3 Hydrogen Bonding and Not Phosphorylation Contributes to the Ataxia Phenotype of the Moonwalker Mouse. Biochemistry. 2015;150626072742003.
95. Beck A, Speicher T, Stoerger C, Sell T, Dettmer V, Jusoh SA, et al.

Conserved Gating Elements in TRPC4 and TRPC5 Channels. J Biol Chem. 2013;288(27):19471–83.

96. Gregorio-Teruel L, Valente P, Gonzalez-Ros JM, Fernandez-Ballester G, Ferrer-Montiel A. Mutation of I696 and W697 in the TRP box of vanilloid receptor subtype I modulates allosteric channel activation. J Gen Physiol. 2014;143(3):361–75.
97. Hofmann T, Schaefer M, Schultz G, Gudermann T. Subunit composition of mammalian transient receptor potential channels in living cells. Proc Natl Acad Sci U S A. 2002 May 28;99(11):7461–6.
98. Palovcak E, Delemotte L, Klein ML, Carnevale V. Comparative sequence analysis suggests a conserved gating mechanism for TRP channels. J Gen Physiol. 2015;146(1):37–50.
99. Zhang Z, Tang J, Tikunova S, Johnson JD, Chen Z, Qin N, et al. Activation of Trp3 by inositol 1,4,5-trisphosphate receptors through displacement of inhibitory calmodulin from a common binding domain. Proc Natl Acad Sci U S A. 2001 Mar 13;98(6):3168–73.
100. Kim Y, Wong ACY, Power JM, Tadros SF, Klugmann M, Moorhouse AJ, et al. Alternative Splicing of the TRPC3 Ion Channel Calmodulin/IP3 Receptor-Binding Domain in the Hindbrain Enhances Cation Flux. J Neurosci. 2012 Aug 15;32(33):11414–23.
101. Azumaya CM, Sierra-Valdez F, Cordero-Morales JF, Nakagawa T. Cryo-EM structure of the cytoplasmic domain of murine transient receptor potential cation channel subfamily C member 6 (TRPC6). J Biol Chem. 2018 Jun 29;293(26):10381–91.
102. Ciuraszkiewicz A, Schreibmayer W, Platzer D, Orr-Urtreger A, Scholze P, Huck S. Single-channel properties of α3β4, α3β4α5 and α3β4β2 nicotinic acetylcholine receptors in mice lacking specific nicotinic acetylcholine receptor subunits. J Physiol. 2013 Jul 1;591(13):3271–88.
103. Tsien R., Rink T., Poenie M. Measurement of cytosolic free Ca2+ in individual small cells using fluorescence microscopy with dual excitation wavelengths. Cell Calcium. 1985 Apr 1;6(1–2):145–57.
104. Di Giuro CML, Shrestha N, Malli R, Groschner K, van Breemen C, Fameli N. Na+/Ca2+exchangers and Orai channels jointly refill endoplasmic reticulum (ER) Ca2+via ER nanojunctions in vascular endothelial cells. Pflugers Arch

Eur J Physiol. 2017;469(10):1287–99.

105. Zhao Y, Yarov-Yarovoy V, Scheuer T, Catterall WA. A gating hinge in Na+ channels; a molecular switch for electrical signaling. Neuron. 2004 Mar 25;41(6):859–65.
106. Morales-Lázaro SL, Serrano-Flores B, Llorente I, Hernández-García E, González-Ramírez R, Banerjee S, et al. Structural determinants of the transient receptor potential 1 (TRPV1) channel activation by phospholipid analogs. J Biol Chem. 2014;289(35):24079–90.
107. Ko YJ, Jo WH. Secondary water pore formation for proton transport in a ClC exchanger revealed by an atomistic molecular-dynamics simulation. Biophys J. 2010 May 19;98(10):2163–9.
108. Poteser M, Schleifer H, Lichtenegger M, Schernthaner M, Stockner T, Kappe CO, et al. PKC-dependent coupling of calcium permeation through transient receptor potential canonical 3 (TRPC3) to calcineurin signaling in HL-1 myocytes. Proc Natl Acad Sci U S A. 2011 Jun 28;108(26):10556–61.
109. Zubcevic L, Le S, Yang H, Lee S-Y. Conformational plasticity in the selectivity filter of the TRPV2 ion channel. Nat Struct Mol Biol. 2018 May 30;25(5):405–15.
110. Banke TG, Chaplan SR, Wickenden AD. Dynamic changes in the TRPA1 selectivity filter lead to progressive but reversible pore dilation. Am J Physiol Physiol. 2010 Jun;298(6):C1457–68.
111. Steinberg X, Kasimova MA, Cabezas-Bratesco D, Galpin JD, Ladron-de-Guevara E, Villa F, et al. Conformational dynamics in TRPV1 channels reported by an encoded coumarin amino acid. Elife. 2017;6:1–18.
112. Barad BA, Echols N, Wang RY, Cheng Y, DiMaio F, Adams PD FJ. 3J9J: Structure of the capsaicin receptor, TRPV1, determined by single particle electron cryo-microscopy. Nat Methods. 2015;12:943–6.
113. Afonine P V, Klaholz BP, Moriarty NW, Poon BK, Sobolev O V, Terwilliger TC, et al. New tools for the analysis and validation of cryo-EM maps and atomic models. Acta Crystallogr Sect D, Struct Biol. 2018 Sep 1;74(Pt 9):814–40.
114. Brohawn SG, Campbell EB, MacKinnon R. Physical mechanism for gating and mechanosensitivity of the human TRAAK K+ channel. Nature. 2014 Dec 4;516(7529):126–30.

115. Hou X, Burstein SR, Long SB. Structures reveal opening of the store-operated calcium channel Orai. Elife. 2018 Aug 30;7.
116. Hamada K, Miyatake H, Terauchi A, Mikoshiba K. IP3-mediated gating mechanism of the IP3 receptor revealed by mutagenesis and X-ray crystallography. Proc Natl Acad Sci U S A. 2017;114(18):4661.

10. Appendix

Figure 1: Full length multiple sequence alignment of various TRP channels next to exemplary K^+ and Na^+ voltage-gated channels

```
TRPV1      MKKWSSTDLGAAADPLQKDTCPDPLDGDPNSRPPPAKPQLSTAKSRTRLFGKGDSEEAFP     60
Kv1.2      ------------------------------------------------------------     0
NavAB      ------------------------------------------------------------     0
TRPC6      -------------------MSQSPAFGPRRGSSPRGAAGAAA--------RRNESQDYLL     33
TRPC3      ------------------------------------------------------------     0
TRPC7      ------------------------------------------------------------     0
TRPC1      ------------------------------------------------------------     0
TRPC4      ------------------------------------------------------------     0
TRPC5      ------------------------------------------------------------     0

TRPV1      VDCPHEEGELDSCPTITVSPVITIQRPGDGPTGARLLSQDSVAASTEKTLRLYDRRSIFE     120
Kv1.2      ------------------------------------------------------------     0
NavAB      ------------------------------------------------------------     0
TRPC6      MD---SELGEDGCPQAPLPCYGYYPCFRGSDNRLAHRR---QTVLREKGRRLANRGPAY-     86
TRPC3      ----------------------------MEGSPSLRR---MTVMREKGRRQAVRGPAF-     27
TRPC7      -------------------------MLRNSTFKNMQRR---HTTLREKGRRQAIRGPAY-     31
TRPC1      -----------------MMAALYPSTDLSGASSSSLPS-------SPSSSSPNEVMALK-     35
TRPC4      ------------------MAQFYYKRNVNAPYRD--------------------RIPLR-     21
TRPC5      ------------------MAQLYYKKVNYSPYRD--------------------RIPLQ-     21

TRPV1      AVAQNNCQDLESLLLFLQKSKKHLT--DNEF-KDPETGKTCLLKAMLNLHDGQNTTIPLL     177
Kv1.2      ------------------------------------------------------------     0
NavAB      ------------------------------------------------------------     0
TRPC6      -------------MFSD-RSTSLSIEEERFLDAAEYGNIPVVRKMLEEC----------     121
TRPC3      -------------MFND-RGTSLTAEEERFLDAAEYGNIPVVRKMLEES----------     62
TRPC7      -------------MFNE-KGTSLTPEEERFLDSAEYGNIPVVRKMLEES----------     66
TRPC1      -------------DVRE-VKEENTLNEKLFLLACDKGDYYMVKKILEEN----------     70
TRPC4      -------------I-VR-AESELSPSEKAYLNAVEKGDYASVKKSLEEA----------     55
TRPC5      -------------I-VR-AETELSAEEKAFLNAVEKGDYATVKQALQEA----------     55

TRPV1      LEIARQTDSLKELVNASYTDSYYKGQTALHIAIERRNMALVTLLVENGADVQ--------     229
Kv1.2      ------------------------------------------------------------     0
NavAB      ------------------------------------------------------------     0
TRPC6      ----H---------SLNVNCVDYMGQNALQLAVANEHLEITELLLKKENLSRVGDALLLA     168
TRPC3      ----K---------TLNVNCVDYMGQNALQLAVGNEHLEVTELLLKKENLARIGDALLLA     109
TRPC7      ----K---------TLNFNCVDYMGQNALQLAVGNEHLEVTELLLKKENLARVGDALLLA     113
TRPC1      ----S-------SGDLNINCVDVLGRNAVTITIENENLDILQLLLDYG--CQSADALLVA     117
TRPC4      ----E------IYFKININCIDPLGRTALLIAIENENLELIELLLSFN--VYVGDALLHA     103
TRPC5      ----E------IYYNVNINCMDPLGRSALLIAIENENLEIMELLLNHS--VYVGDALLYA     103

TRPV1      -------------------------------AAAHGDFFKKTKGRPGFYFGELPLSLAAC     258
Kv1.2      ------------------------------------------------------------     0
NavAB      ------------------------------------------------------------     0
TRPC6      ISKGYVRIVEAILSHPAFAEGKRLATSPSQSELQQDDFYAYDEDGTRFSHDVTPIILAAH     228
TRPC3      ISKGYVRIVEAILNHPGFAASKRLTLSPCEQELQDDDFYAYDEDGTRFSPDITPIILAAH     169
TRPC7      ISKGYVRIVEAILNHPAFAQGQRLTLSPLEQELRDDDFYAYDEDGTRFSHDITPIILAAH     173
TRPC1      IDSEVVGAVDILLNHRPKRSSRPTIVKL----MERIQ-----NPEYSTTMDVAPVILAAH     168
```

```
TRPC4      IRKEVVGAVELLLNHKKPSGEKQVPP-I----LLDKQ-----FS--EFTPDITPIILAAH     151
TRPC5      IRKEVVGAVELLLSYRRPSGEKQVPT-L----MMDTQ-----FS--EFTPDITPIMLAAH     151

TRPV1      TNQLGIVKFLLQNSWQTADISARDSVGNTVLHALVEVADNTADNTKFVTSMYNE----IL     314
Kv1.2      ------------------------------------------------------------     0
NavAB      ------------------------------------------------------------     0
TRPC6      CQEYEIVHTLLRKGARIERPH---DYFCKCNDCNQKQKHDSFSHSRSRINAYKGLASPAY     285
TRPC3      CQKYEVVHMLLMKGARIERPH---DYFCKCGDCMEKQRHDSFSHSRSRINAYKGLASPAY     226
TRPC7      CQEYEIVHILLLKGARIERPH---DYFCKCNECTEKQRKDSFSHSRSRMNAYKGLASAAY     230
TRPC1      RNNYEILTMLLKQDVSLPKPH---AVGCECTLCSAKNKKDSLRHSRFRLDIYRCLASPAL     225
TRPC4      TNNYEIIKLLVQKGVSVPRPH---EVRCNCVECVSSSDVDSLRHSRSRLNIYKALASPSL     208
TRPC5      TNNYEIIKLLVQKRVTIPRPH---QIRCNCVECVSSSEVDSLRHSRSRLNIYKALASPSL     208

TRPV1      MLGAKLHPTLKLEELTNKKG--MTPLA---------LA-AG---TGKIGVLAYILQREIQ     359
Kv1.2      MTVATGDPADEAAALPGHPQDTYDPEADHECCERVVINISGLRFETQLKTLAQFPET--L     58
NavAB      ------------------------------------------------------------     0
TRPC6      LSLSSEDPVMTALEL----------------------------SNELAVLANIEKE--F     314
TRPC3      LSLSSEDPVLTALEL----------------------------SNELAKLANIEKE--F     255
TRPC7      LSLSSEDPVLTALEL----------------------------SNELARLANIETE--F     259
TRPC1      IMLTEEDPILRAFEL----------------------------SADLKELSLVEVE--F     254
TRPC4      IALSSEDPFLTAFQL----------------------------SWELQELSKVENE--F     237
TRPC5      IALSSEDPILTAFRL----------------------------GWELKELSKVENE--F     237

TRPV1      EPECRHLSRKFTEWAYGPVHSSLYDLSCIDTCEKNSVLEVIAYSSSETPN----------     409
Kv1.2      LGDPKKRMRYF-DPLR----------NEYFFDRNRPSFDAILYYYQSGGRLRRPVNVPLD     107
NavAB      ------------------------------------------------------------     0
TRPC6      KNDYKKLSMQCKDFVV----------GLLDLCRNTEEVEAILNGDVETLQ----------     354
TRPC3      KNDYRKLSMQCKDFVV----------GVLDLCRDSEEVEAILNGDLESAE-------PL-     297
TRPC7      KNDYRKLSMQCKDFVV----------GVLDLCRDTEEVEAILNGDVNFQV----------     299
TRPC1      RNDYEELARQCKMFAK----------DLLAQARNSRELEVILNHTSSDEP-------LD-     296
TRPC4      KSEYEELSRQCKQFAK----------DLLDQTRSSRELEIILNYRDDNSL--------I-     278
TRPC5      KAEYEELSQQCKLFAK----------DLLDQARSSRELEIILNHRDDHSE-------EL-     279

TRPV1      ----------------------------------------RHDMLL----------------     415
Kv1.2      IFSEEIRFYELGEEAMEMFREDEGYIKEEERPLPENEFQRQVWLLFEYPESSGPARIIAI     167
NavAB      ------------------------------------------------------------     0
TRPC6      -------S--GDHGRPNLSRL-KLAIKYEVKKFVAHPNCQQQLLSIWYENLSGLRQQTMA     404
TRPC3      -------E--VHRHKASLSRV-KLAIKYEVKKFVAHPNCQQQLLTIWYENLSGLREQTIA     347
TRPC7      -------W--SDHHRPSLSRI-KLAIKYEVKKFVAHPNCQQQLLTMWYENLSGLRQQSIA     349
TRPC1      -----KRG--LLEERMNLSRL-KLAIKYNQKEFVSQSNCQQFLNTVWFGQMSGYRRKPTC     348
TRPC4      ----------EEQSGNDLARL-KLAIKYRQKEFVAQPNCQQLLASRWYDEFPGWRRRHWA     327
TRPC5      ----------DPQKYHDLAKL-KVAIKYHQKEFVAQPNCQQLLATLWYDGFPGWRRKHWV     328

TRPV1      ------------------------VEPLNRLLQDKWDRFVKRIFYFNFLVYCLYMIIFTM     451
Kv1.2      VSVMVI-----LISIVSFCLETLP------IFRDENEDMHGSGVTFHT--Y-SNS-----     208
NavAB      ------------------------------------------------------------     0
TRPC6      VKFLVVLAVAIGLPFLALIYWFAPCSKMGKIMRGPFMKFVAHAASFTI--F-LGLLVMNA     461
TRPC3      IKCLVVLVVALGLPFLAIGYWIAPCSRLGKILRSPFMKFVAHAASFII--F-LGLLVFNA     404
TRPC7      VKFLAVFGVSIGLPFLAIAYWIAPCSKLGRTLRSPFMKFVAHAVSFTI--F-LGLLVVNA     406
TRPC1      KKIMTVLTVGIFWPVLSLCYLIAPKSQFGRIIHTPFMKFIIHGASYFT--F-LLLLNLYS     405
TRPC4      VKMVTCFIIGLLFPVFSVCYLIAPKSPLGLFIRKPFIKFICHTASYLT--F-LFLLLLAS     384
TRPC5      VKLLTCMTIGFLFPMLSIAYLISPRSNLGLFIKKPFIKFICHTASYLT--F-LFMLLLAS     385

TRPV1      AAYYRPVDGLPPF--------KMEKTGDYFRVT-GEILS-VLGGVYFFFRGIQYFLQRRP     501
Kv1.2      --------TIGYQ--------QSTSFTDPFFIVETL------CIIW--------------     232
```

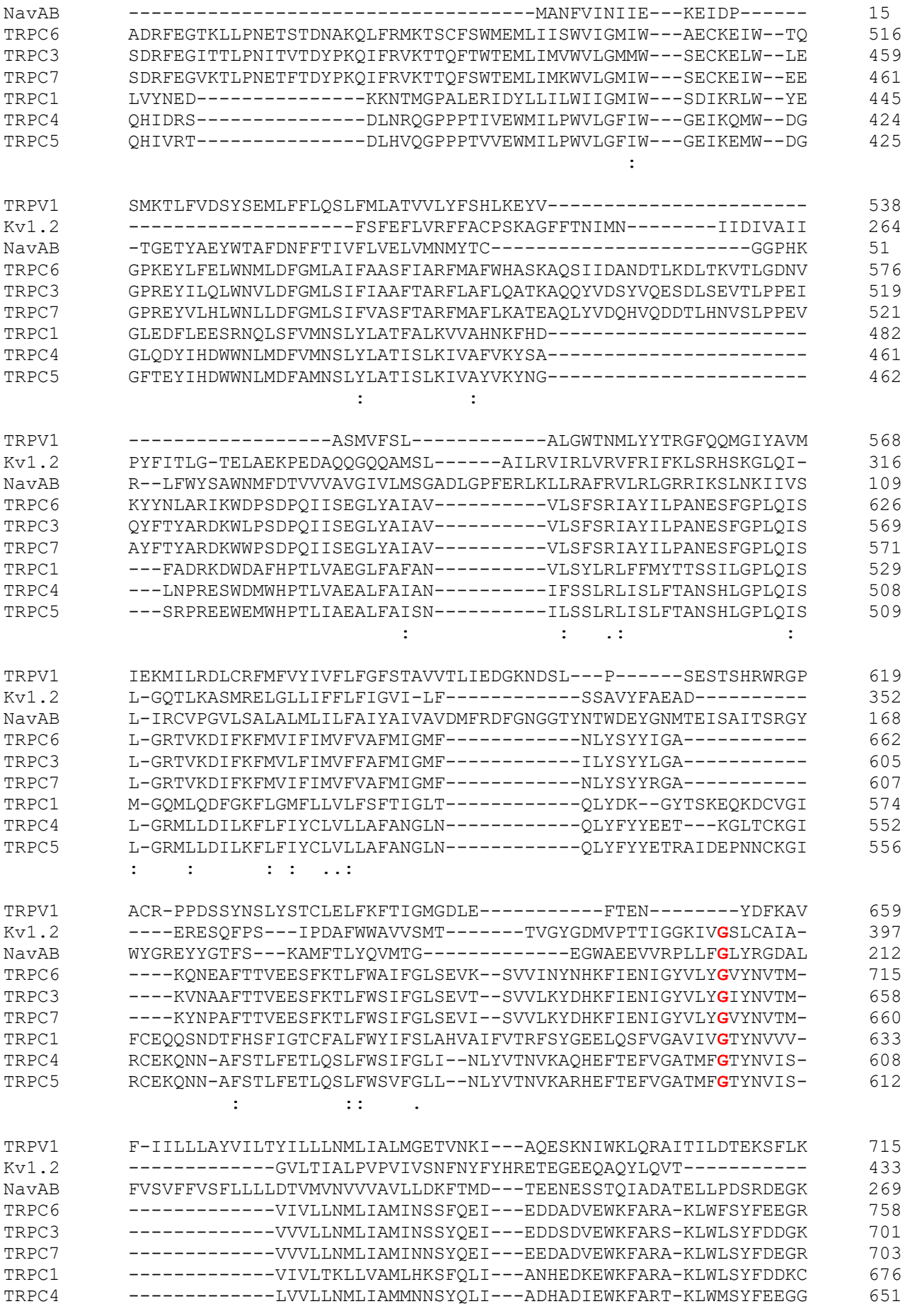
NavAB ----------MANFVINIIE---KEIDP------ 15
TRPC6 ADRFEGTKLLPNETSTDNAKQLFRMKTSCFSWMEMLIISWVIGMIW---AECKEIW--TQ 516
TRPC3 SDRFEGITTLPNITVTDYPKQIFRVKTTQFTWTEMLIMVWVLGMMW---SECKELW--LE 459
TRPC7 SDRFEGVKTLPNETFTDYPKQIFRVKTTQFSWTEMLIMKWVLGMIW---SECKEIW--EE 461
TRPC1 LVYNED---------------KKNTMGPALERIDYLLILWIIGMIW---SDIKRLW--YE 445
TRPC4 QHIDRS---------------DLNRQGPPPTIVEWMILPWVLGFIW---GEIKQMW--DG 424
TRPC5 QHIVRT---------------DLHVQGPPPTVVEWMILPWVLGFIW---GEIKEMW--DG 425
TRPV1 SMKTLFVDSYSEMLFFLQSLFMLATVVLYFSHLKEYV---------- 538
Kv1.2 ----------FSFEFLVRFFACPSKAGFFTNIMN--------IIDIVAII 264
NavAB -TGETYAEYWTAFDNFFTIVFLVELVMNMYTC----------GGPHK 51
TRPC6 GPKEYLFELWNMLDFGMLAIFAASFIARFMAFWHASKAQSIIDANDTLKDLTKVTLGDNV 576
TRPC3 GPREYILQLWNVLDFGMLSIFIAAFTARFLAFLQATKAQQYVDSYVQESDLSEVTLPPEI 519
TRPC7 GPREYVLHLWNLLDFGMLSIFVASFTARFMAFLKATEAQLYVDQHVQDDTLHNVSLPPEV 521
TRPC1 GLEDFLEESRNQLSFVMNSLYLATFALKVVAHNKFHD---------- 482
TRPC4 GLQDYIHDWWNLMDFVMNSLYLATISLKIVAFVKYSA---------- 461
TRPC5 GFTEYIHDWWNLMDFAMNSLYLATISLKIVAYVKYNG---------- 462
TRPV1 ----------ASMVFSL----------ALGWTNMLYYTRGFQQMGIYAVM 568
Kv1.2 PYFITLG-TELAEKPEDAQQGQQAMSL------AILRVIRLVRVFRIFKLSRHSKGLQI- 316
NavAB R--LFWYSAWNMFDTVVVAVGIVLMSGADLGPFERLKLLRAFRVLRLGRRIKSLNKIIVS 109
TRPC6 KYYNLARIKWDPSDPQIISEGLYAIAV----------VLSFSRIAYILPANESFGPLQIS 626
TRPC3 QYFTYARDKWLPSDPQIISEGLYAIAV----------VLSFSRIAYILPANESFGPLQIS 569
TRPC7 AYFTYARDKWWPSDPQIISEGLYAIAV----------VLSFSRIAYILPANESFGPLQIS 571
TRPC1 ---FADRKDWDAFHPTLVAEGLFAFAN----------VLSYLRLFFMYTTSSILGPLQIS 529
TRPC4 ---LNPRESWDMWHPTLVAEALFAIAN----------IFSSLRLISLFTANSHLGPLQIS 508
TRPC5 ---SRPREEWEMWHPTLIAEALFAISN----------ILSSLRLISLFTANSHLGPLQIS 509
TRPV1 IEKMILRDLCRFMFVYIVFLFGFSTAVVTLIEDGKNDSL---P------SESTSHRWRGP 619
Kv1.2 L-GQTLKASMRELGLLIFFLFIGVI-LF----------SSAVYFAEAD---------- 352
NavAB L-IRCVPGVLSALALMLILFAIYAIVAVDMFRDFGNGGTYNTWDEYGNMTEISAITSRGY 168
TRPC6 L-GRTVKDIFKFMVIFIMVFVAFMIGMF----------NLYSYYIGA---------- 662
TRPC3 L-GRTVKDIFKFMVLFIMVFFAFMIGMF----------ILYSYYLGA---------- 605
TRPC7 L-GRTVKDIFKFMVIFIMVFVAFMIGMF----------NLYSYYRGA---------- 607
TRPC1 M-GQMLQDFGKFLGMFLLVLFSFTIGLT----------QLYDK--GYTSKEQKDCVGI 574
TRPC4 L-GRMLLDILKFLFIYCLVLLAFANGLN----------QLYFYYEET---KGLTCKGI 552
TRPC5 L-GRMLLDILKFLFIYCLVLLAFANGLN----------QLYFYYETRAIDEPNNCKGI 556
TRPV1 ACR-PPDSSYNSLYSTCLELFKFTIGMGDLE----------FTEN--------YDFKAV 659
Kv1.2 ----ERESQFPS---IPDAFWWAVVSMT-------TVGYGDMVPTTIGGKIVGSLCAIA- 397
NavAB WYGREYYGTFS---KAMFTLYQVMTG----------EGWAEEVVRPLLFGLYRGDAL 212
TRPC6 ----KQNEAFTTVEESFKTLFWAIFGLSEVK--SVVINYNHKFIENIGYVLYGVYNVTM- 715
TRPC3 ----KVNAAFTTVEESFKTLFWSIFGLSEVT--SVVLKYDHKFIENIGYVLYGIYNVTM- 658
TRPC7 ----KYNPAFTTVEESFKTLFWSIFGLSEVI--SVVLKYDHKFIENIGYVLYGVYNVTM- 660
TRPC1 FCEQQSNDTFHSFIGTCFALFWYIFSLAHVAIFVTRFSYGEELQSFVGAVIVGTYNVVV- 633
TRPC4 RCEKQNN-AFSTLFETLQSLFWSIFGLI--NLYVTNVKAQHEFTEFVGATMFGTYNVIS- 608
TRPC5 RCEKQNN-AFSTLFETLQSLFWSVFGLL--NLYVTNVKARHEFTEFVGATMFGTYNVIS- 612
TRPV1 F-IILLLAYVILTYILLLNMLIALMGETVNKI---AQESKNIWKLQRAITILDTEKSFLK 715
Kv1.2 ----------GVLTIALPVPVIVSNFNYFYHRETEGEEQAQYLQVT---------- 433
NavAB FVSVFFVSFLLLLDTVMVNVVVAVLLDKFTMD---TEENESSTQIADATELLPDSRDEGK 269
TRPC6 ----------VIVLLNMLIAMINSSFQEI---EDDADVEWKFARA-KLWFSYFEEGR 758
TRPC3 ----------VVVLLNMLIAMINSSYQEI---EDDSDVEWKFARS-KLWLSYFDDGK 701
TRPC7 ----------VVVLLNMLIAMINNSYQEI---EEDADVEWKFARA-KLWLSYFDEGR 703
TRPC1 ----------VIVLTKLLVAMLHKSFQLI---ANHEDKEWKFARA-KLWLSYFDDKC 676
TRPC4 ----------LVVLLNMLIAMMNNSYQLI---ADHADIEWKFART-KLWMSYFEEGG 651

```
TRPC5      -------------LVVLLNMLIAMMNNSYQLI---ADHADIEWKFART-KLWMSYFDEGG     655
                        :   : : :: ..         . .   :

TRPV1      CMRKAFRSGKLLQVGYTPDGKDDY--RWCFRVDEVNWTTWNT-----------NVGIINE     762
Kv1.2      -------SCPKI---PSSPDLKKSRSAST----IS-------KSDYMEIQ----EGVNN-     467
NavAB      GRPG---ATEMFQIGQEPPVLKMPTRQPTIGSTIGNDFSLHAK-----------------     309
TRPC6      TLPV---PFNLV---PSPKSL------FYLLLKLKKWISELFQGHKKGFQEDAEMNKINE     806
TRPC3      TLPP---PFSLV---PSPKSF------VYFIMRIVN----FPKCRRRRLQKDIEMGMGNS     745
TRPC7      TLPA---PFNLV---PSPKSF------YYLIMRIKMCLIKLCKSKAKSCENDLEMGMLNS     751
TRPC1      TLPP---PFNII---PSPKTI------CYMISSLSKWICSHTSKGKVKRQ----------     714
TRPC4      TLPT---PFNVI---PSPKSL------WYLIKWIWTHLCKKKM---RRKP----------     686
TRPC5      TLPP---PFNII---PSPKSF------LYLGNWFNNTFCPKRDPDGRRRR----------     693
                     .

TRPV1      DPG-----NCEGVK-------RTLSFSLRSSRVSGRHWKNFALVP----------LLREA     800
Kv1.2      --------SNEDFR-------------EENLK------TANCTLANTNYVNITKMLTDV-     499
NavAB      ------------------------------------LDQLLQRDEWMMQHMKKLQE--     329
TRPC6      EKKLGILGSHEDLSKLSLDKKQVGHNKQPSIRSSEDFHLNSFNNPPRQYQKIMKRLIKRY     866
TRPC3      KSRLN-------------------LFTQSNSRVFESHSFNSILNQPTRYQQIMKRLIKRY     786
TRPC7      KFKKT-------------------RYQ-AGMRNSENLTANNTLSKPTRYQKIMKRLIKRY     791
TRPC1      ----------------------------NSLKE----WRNLKQKRDENYQKVMCCLVHRY     742
TRPC4      ----------------------------ESFGTIG-RRAADNLRRHHQYQEVMRNLVKRY     717
TRPC5      ----------------------------RNLRSFT-ERNADSLIQNQHYQEVIRNLVKRY     724
                                                                    *

TRPV1      ---SARD-RQSAQPEEVYLRQFSGSLKPEDAEVFKSP-----------AASGEK------     839
Kv1.2      ------------------------------------------------------------     499
NavAB      ----------------QMDAFGQRLPTSRLFM----------------------------     345
TRPC6      VLQAQID-KESDEVNEGELKEIKQDISSLRYELLEEKSQNTEDLAELIRELGEKLSMEPN     925
TRPC3      VLKAQVD-KENDEVNEGELKEIKQDISSLRYELLEDKSQATEELAILIHKLSEKLNPSML     845
TRPC7      VLKAQVD-RENDEVNEGELKEIKQDISSLRYELLEEKSQATGELADLIQQLSEKFGKNLN     850
TRPC1      LTSMRQKMQSTDQATVENLNELRQDLSKFRNEIRDLLGFRTSKYAMFYPRN---------     793
TRPC4      VAAMIRDAKTEEGLTEENFKELKQDISSFRFEVLGLLRGSKLSTIQSANASKES-SNSAD     776
TRPC5      VAAMIRNSKTHEGLTEENFKELKQDISSFRYEVLDLLGNRKHPRSFSTSSTEL-----SQ     779


TRPV1      ------------------------------------------------------------     839
Kv1.2      ------------------------------------------------------------     499
NavAB      ------------------------------------------------------------     345
TRPC6      QEETNR--------------------------------------------------------     931
TRPC3      RCE-----------------------------------------------------------     848
TRPC7      KDHLRVNKGK------DI--------------------------------------------     862
TRPC1      ------------------------------------------------------------     793
TRPC4      SDEKSDSEGNSKDKKKNFSLFDLTTLIHPRSAAIASERHNISNGSALVVQEPP-------     829
TRPC5      RDDNNDGSGGARAKSKSVS-FNLGCK------------KKTCHGPPLIRTMPRSSGAQGK     826


TRPV1      ------------------------------------------------------------     839
Kv1.2      ------------------------------------------------------------     499
NavAB      ------------------------------------------------------------     345
TRPC6      ------------------------------------------------------------     931
TRPC3      ------------------------------------------------------------     848
TRPC7      ------------------------------------------------------------     862
TRPC1      ------------------------------------------------------------     793
TRPC4      ---REKQRKVNFVTDIKNFGLFHRRSKQNAAEQNANQIFSVSEEVARQQAAGPLERNIQL     886
TRPC5      SKAESSSKRSFMGPSLKKLGLLFSKFNGHMSEPSSEPMYTISDGIVQQHCMWQDIRYSQM     886


TRPV1      ------------------------------------------------------------     839
Kv1.2      ------------------------------------------------------------     499
NavAB      ------------------------------------------------------------     345
```

```
TRPC6      ------------------------------------------------------------     931
TRPC3      ------------------------------------------------------------     848
TRPC7      ------------------------------------------------------------     862
TRPC1      ------------------------------------------------------------     793
TRPC4      ESRGL--AS----------RGDLSIPGLSEQCVLVDHRERNTDTLGLQVGKRVCPFKSEK     934
TRPC5      EKGKAEACSQSEINLSEVELGEVQGAAQSSECPLACS-------SSLHCASSICSSNSKL     939

TRPV1      ------------------------------------------      839
Kv1.2      ------------------------------------------      499
NavAB      ------------------------------------------      345
TRPC6      ------------------------------------------      931
TRPC3      ------------------------------------------      848
TRPC7      ------------------------------------------      862
TRPC1      ------------------------------------------      793
TRPC4      VVVEDTVPIIPKEKHAKEEDSSIDYDLNLP-DTVTHEDYVTTRL     977
TRPC5      LDSSED--VFET--------WGEACDLLMHKWGDGQEEQVTTRL     973
```

Full length multiple sequence alignment of TRPC1 (Uniprot ID: P48995), TRPC3 (Uniprot ID: Q13507-3), TRPC4 (Uniprot ID: Q9UBN4), TRPC5 (Uniprot ID: Q9UL62), TRPC6 (Uniprot ID: Q9Y210), TRPC7 (Uniprot ID: Q9HCX4), TRPV1 (Uniprot ID: Q8NER1), $K_v1.2$ (Uniprot ID: P16389), Na_vAB (Uniprot ID: A0A0M0JVU2) generated using online sequence alignment tool Clustal Omega (1.2.4). All sequences are of human origin except for the Na_vAB ion channel sequence from *Chrysochromulina sp.* Conserved glycine residues corresponding to G652 in TRPC3 sequence (human isoform 3) are highlighted in red.

Figure 2: Space-filling model of TRPC6 ion channel complex structure from cryo-EM imaging

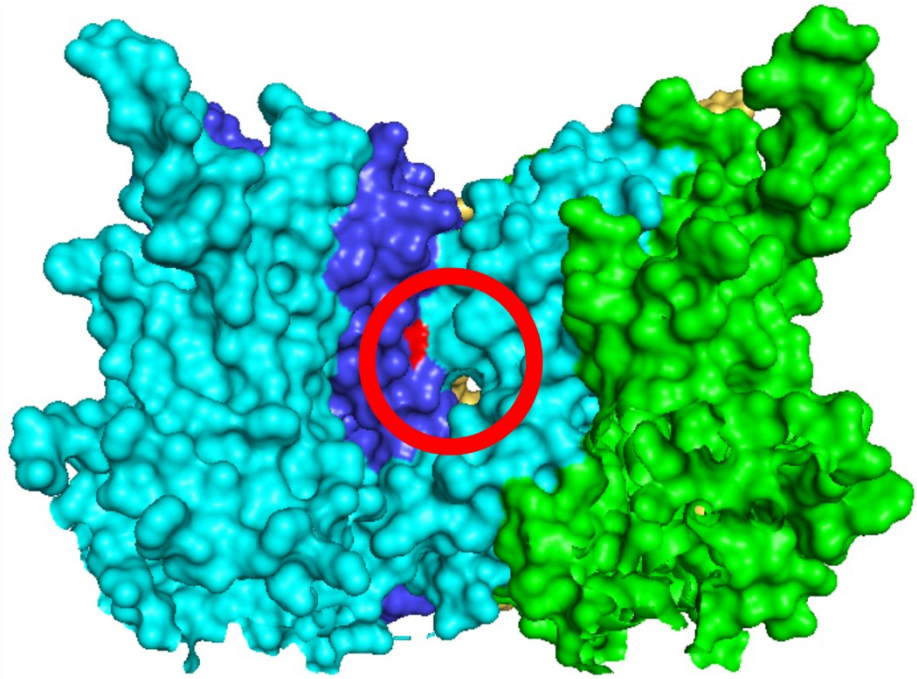

Cryo-EM structure of TRPC6 tetramer published by Tang et al. (PDB ID: 5YX9; (77)) was used to construct the space-filling 3D model of the channel's architecture. Colour coding of the individual channel subunits is identical to Figure 4 and 22. For easier comparison with the TRPC3 homology model in Figure 21 the ECD, CD and the pre-S1 elbow of TRPC6 are omitted here. G709 localized in the 'lipid window' is highlighted in red.